論文 / 著書情報
Article / Book Information

題目(和文)	カーボンナノウォールの表面改質と電気化学センサーへの応用
Title(English)	Study on surface modification of carbon nanowalls and their application to electrochemical sensors
著者(和文)	BOHLOOLIFatemeh
Author(English)	Fatemeh Bohlooli
出典(和文)	学位:博士（工学）, 学位授与機関:東京工業大学, 報告番号:甲第12203号, 授与年月日:2022年9月22日, 学位の種別:課程博士, 審査員:森 伸介,関口 秀俊,伊原 学,多湖 輝興,谷口 泉
Citation(English)	Degree:Doctor (Engineering), Conferring organization: Tokyo Institute of Technology, Report number:甲第12203号, Conferred date:2022/9/22, Degree Type:Course doctor, Examiner:,,,,
学位種別(和文)	博士論文
Type(English)	Doctoral Thesis

Doctoral dissertation

Study on surface modification of carbon nanowalls and their application to electrochemical sensors

Fatemeh Bohlooli

Academic supervisor: Assoc. Prof. Shinsuke Mori

Department of Chemical Science and Engineering
School of Materials and Chemical technology
Tokyo Institute of Technology

2022

Abstract

Two-dimensional (2D) graphene-like carbon nanostructures have recently attracted a lot of practical interest due to their unique physical, electrical, and optical properties. Carbon nanowalls (CNW) belong to this category of functional materials that can be described as an open network of interconnected two-dimensional graphene sheets standing vertically on a substrate. Owing to the large surface area, highly active graphene edges, and fabricating without the use of catalysts, CNW has shown its fascinating application as electrode material for different electrochemical systems such as electrodes for batteries and supercapacitors, fuel cells supports, oxygen reduction, and most recently electrochemical sensors and biosensors. Higher electrolyte permeability and reduction in ion resistance can be promoted by the opened structure of a CNW film. However, the functional properties of CNW can also be greatly influenced by the presence of structural defects and attached functional groups.

In this study, we propose two different approaches for modifying CNW surface for their potential applications in electrochemical sensing and biosensing field; Firstly, coating of CNW surface by transitional metal oxide (MnO_x) via anodic deposition technique and secondly, post plasma treatment of CNW with O_2/Ar plasma and introducing novel inter-synthesis sequential treatment method. At first step (chapter 2), synthesizing of CNW at different deposition times and their characterization was discussed. Plasma enhanced chemical vapor deposition in a CO/H_2 microwave discharge system was performed for fabricating CNW. Subsequent to this, synthesis of MnO_x/CNW was considered. Potentiostatic anodic deposition technique was applied for depositing of manganese oxides (MnO_x) onto the CNW surface at different deposition times**.** It was shown that when deposition time is very short, the film has mostly original CNW structure with some nucleation spots of MnO_x. By increasing deposition time, the accumulation of MnO_x around the walls can be clearly confirmed. While, by further increase in deposition time, it is difficult to distinguish the border between CNW and MnO_x, which indicates that MnO_x can slightly infiltrate into the gaps between the walls. The average manganese oxidation state for the prepared electrodes was calculated based on deconvoluted O1s spectra and multiple splitting of Mn3s core level spectrum. As observed, electrodeposited MnO_x coatings exhibit mixed Mn valance states, where by increasing deposition time, the oxidation state of Mn increases.

Cyclic voltammetry (CV) and amperometry techniques were performed to evaluate the sensor performance of MnO_x/CNW towards detecting H_2O_2 (chapter 3). The prepared nanocomposite electrode exhibited high electrochemical activity for oxidation of hydrogen peroxide (H_2O_2) in phosphate buffer solution at an applied potential of +0.7V, showing a linear dependence on the concentration of H_2O_2 from 40µM to 10230µM, a high sensitivity (698.6 µA mM^{-1} cm^{-2}), and a detection limit of 0.55µM (signal/noise=3). The proposed hybrid CNW structure combined with the transitional metal oxide MnO_x demonstrated a great potential of CNW based composite electrodes in non-enzymatic electrochemical sensor application.

To further improve CNW performance as a metal-free electrochemical sensor through its intrinsic modification, O_2/Ar plasma with different O_2 flow ratios were applied to modify the surface of CNW (chapter 4). Our results revealed that the CNW treated in low oxygen flow rate (O_2/Ar: 0.1/10sccm) exhibited the highest concentration of incorporated oxygen on its structure, which consequently resulted in conversion of intrinsic hydrophobicity of CNW to hydrophilicity. Interestingly, however, further increase in oxygen flow rate did not increase the oxygen content of CNW structure, but instead it resulted in an increment in the defect and contributing less oxygen on CNW surface. We assume that when low density of oxygen species exists in the plasma treatment gas mixture, the amorphous carbon structures that exist on the surface of as-grown CNW are selectively etched and the potential active oxygen species are stabilized to the produced defect sites, therefore formation of oxygen functional groups occurs favorably. However, the higher density of reactive oxygen species can result in higher etching rate, which can consequently lead to increase the etch rate from both amorphous and sp^2 structures and prevent the stabilization of oxygen in the defect positions, hence contributing less oxygen functional groups on the CNW structure. Subsequent to finding the surface characteristic of CNW at different O_2/Ar plasma treatment condition, novel inter-synthesis sequential treatment method was introduced to synthesize CNW with oxygen functional groups not only on top surface but also on the deep parts of the walls. Layer by layer and highly branched structure was observed by SEM cross-section images.

Electrochemical measurements revealed that the most hydrophilic CNW surface does not exhibit the highest electrochemical activity for the oxidation of H_2O_2 (chapter 5). The highest amperometric response is observed for the CNW sample treated with O_2/Ar: 1.0/10sccm, which

has lower oxygen content than CNW treated with O_2/Ar: 0.1/10sccm but still possessing hydrophilic characteristic and also owning more defective structure. These results can suggest the importance of both defects and oxygen-containing functional groups in electrochemical behavior of the electrodes as both defects and oxygen-containing functional groups can act as potential active sites for electrochemical reactions and oxygen-containing functional groups can enhance the hydrophilicity and surface area wetted by the electrolyte. The modified CNW in O_2/Ar: 1.0/10sccm plasma displayed wide linear response range for oxidation H_2O_2 from 50μM to 28000μM, low LOD, and sensitivity of 126.6μA/mM.cm^2. This study demonstrates that intrinsic modification of CNW by O_2/Ar plasma can result in enhancing CNW performance in electrochemical sensing systems as a metal-free electrode.

Finally, overall summary obtained in this study and future works were described at chapter 6.

Contents

Chapter 1. Introduction

1.1. Background

In recent years, carbon-based nanomaterials have attracted a lot of practical interest due to their significant optical, electronic, mechanical, chemical properties and structural diversity. [1]. The carbon is the element in periodic table that shows an organization in different allotropic forms. Elemental carbon exists in two natural allotropes; diamond with sp^3 hybridization and graphite with sp^2 hybridization, both displaying unique physical properties such as hardness, thermal conductivity, and electrical conductivity. Diamond and graphite are the two widely known allotropic forms of carbon for a long time. However, the advent of fullerenes in 1985 by Kroto et al. marked the beginning of an era of synthetic carbon allotropes. Fullerene, which belongs to a zero-dimensional (0D) carbon nanostructures, was reported first, followed by one-dimensional carbon nanotubes (CNTs) in 1991 and then rediscovery of 2D graphene in 2004 [2].

Among these three families of carbon allotropes, graphene has the most uniform structure where the differences can be seen only in the sheet extensions and the nature of edges. Furthermore, graphene is considered as the structural element of some other carbon allotropes as it can be wrapped up, rolled up cylindrically or stacked up to form 0D fullerenes, 1D carbon nanotubes and 3D graphite [3].

Although to compare with fullerenes and carbon nanotubes, chemical modification of graphene is still in its earliest infancy, graphene-based technology is considered to have the greatest potential for applications [2]. Over the last two decades, research on graphene has greatly increased, and various excellent properties have been observed by researchers.

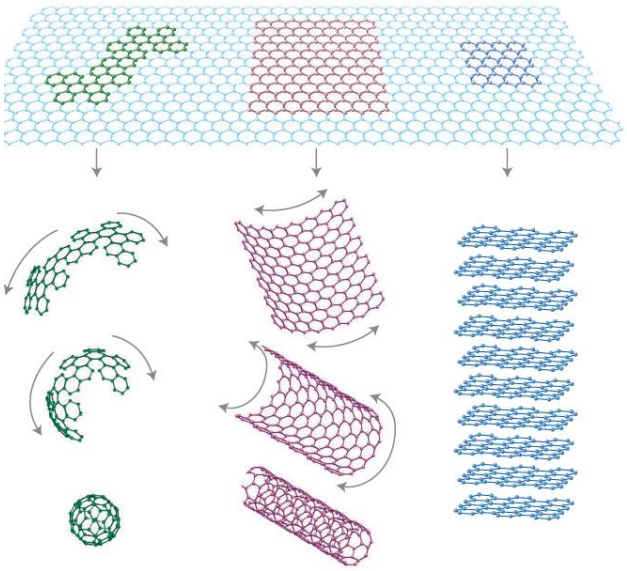

Figure 1.1. Graphene as building material for carbon materials of all other dimensions [3]

Due to easy surface functionalization, extremely large surface area, superior 2-D electrical conductivity, and chemical purity, graphene can be considered as an ideal electrode material. In addition, it displays remarkable electrochemical properties including low charge-transfer resistance, large potential window, excellent electrochemical activity, and fast electron transfer rate [4].

Graphene and its derivatives such as graphene oxide (GO) and reduced graphene oxide (rGO) have been widely applied to develop improved chemical and biological electrochemical sensors. This is because of better and unique electrochemical properties of graphene materials as well as the ease of functionalizing the graphene surfaces with specific elements of interest.

A large number of works have been dedicated to the application of graphene and graphene related materials for the analysis of DNA, protein, cell, and important biomarkers such as glucose, β nicotinamide adenine dinucleotide and its reduced form (NAD+/NADH), dopamine (DA), ascorbic acid (AA), uric acid (UA), and hydrogen peroxide (H_2O_2) [5].

Much of the electrochemical sensor and biosensor development research regarding applying graphene has focused on graphene oxide and its reduced form. Another form of graphene that has recently gained a lot of research interest is vertical graphene multilayers, also known as carbon nanowalls (CNW). CNW can be described as an open network of interconnected two- dimensional

graphene sheets standing vertically on a substrate, which are separated with an interlayer spacing of several nanometers.

Owing to the large surface area, highly active graphene edges, and fabricating without the use of catalysts, CNW has been already suggested as electrode material for different electrochemical systems such as electrodes for batteries and supercapacitors [6–8], fuel cells supports [9,10], oxygen reduction [11], and most recently electrochemical sensors and biosensors [12,13].

Higher electrolyte permeability and reduction in ion resistance can be promoted by the opened structure of a CNW film. However, the functional properties of CNW can also be greatly influenced by the presence of structural defects and attached functional groups [14].

This thesis focuses on further improving surface characteristics of CNW films for their potential application in electrochemical sensing and biosensing field. Two different approaches were utilized to enhance CNW performance in electrochemical systems; (I) electrodeposition of transitional metal oxide on CNW and (II) plasma surface treatment of CNW for their potential application as electrochemical sensors towards H_2O_2 detection. Furthermore, novel inter-synthesis sequential treatment method was introduced in order to prepare CNW with oxygen functional groups not only on the top surface but also in deep parts of the walls.

A comprehensive review of the current literature covering the use of manganese oxide/carbon nanomaterials composite and post plasma treatment of carbon nanomaterials in H_2O_2 sensing will be presented in the following sections.

A brief introduction about CNW, its synthesis methods and growth mechanism will be first reviewed. Subsequent to this, post plasma treatment of carbon nanomaterials will be considered. This will comprise the introduction about the mechanism of plasma treatment on carbon nanomaterials, its effect on the surface morphology and chemistry of carbon nanostructures, and then plasma treatment of CNW with different gases will be discussed. Then, introduction to electrochemical sensing techniques including voltammetry and amperometry methods will be reviewed. Finally, the introduction about existing H_2O_2 sensing techniques, the materials used for electrochemical sensing of H_2O_2, and review of manganese oxides/carbon nanomaterials composites applied for H_2O_2 electrochemical sensing will be discussed.

1.2. Introduction to Carbon nanowalls and its synthesis method

Carbon nanowalls (CNW) are an open network of interconnected two-dimensional graphene sheets standing vertically on a substrate, which are separated with an interlayer spacing of several nanometers. As displayed in figure 1.2, the sheets form a self-supported network of wall structures with the height in the range of 1-2μm and the thickness in the order of several nanometers [15].

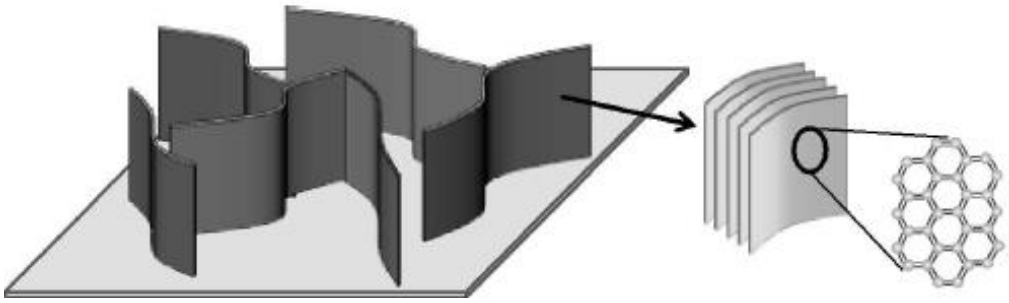

Figure 1.2. Schematic illustration of carbon nanowalls [15]

It is characterized by high surface to volume ratio, high aspect ratio, and good thermal and electrical properties with a high mechanical stability. In addition, unlike CNT, CNW is grown without the use of metallic catalyst and therefore does not require further purification steps before final utilization and application [16].

The first synthesis of CNW was reported by Wu et al in 2002, when the growth of CNW was found during synthesis of carbon nanotubes in a microwave plasma enhanced chemical vapor deposition system (MPECVD) [17]. Since then, various PECVD methods has been utilized to synthesize CNW.

PECVD method is a system with typically low pressure, in which the purity of the deposition can be controlled. It mainly consists of three major parts including plasma generator, gas (precursor and etchants), and vacuum heating chamber that usually made of a quartz tube (to place the substrate for plasma interactions on for CNW deposition) [18]. Based on the plasma sources, PECVD systems are classified into microwave (MW) plasma sources, radio frequency (RF), inductively coupled plasma (ICP), RF capacitively coupled plasma (CCP), direct current (DC)

plasma, and electron cyclotron resonance (ECR) plasma. DC plasma sources have the simplest form, containing two parallel plate electrodes fixed in the vacuum chamber. In this technique, one of the electrodes is connected to a DC power and the other one is earthed and plasma is activated in the interspace between these two electrodes. RF-PECVD can be sorted as capacitively coupled plasma (CCP) and inductively coupled plasma (ICP). A higher plasma density, lower damage to substrate, and freedom from inner electrode contamination are the main advantages of the ICP mode. Microwave plasma (MP) source is another popular method of PECVD in CNW synthesis [19]. It is a high-frequency plasma system with a MW generator with a frequency of approximately 2.45GHz. The generated MW is coupled to the vacuum heating chamber either via a traverse rectangular cavity guide or an external antenna, producing a higher electric field effect inside the chamber with the wave propagation mode of TE (transverse electric mode). The electromagnetic waves in the waveguide interact with the plasma discharge to form a standing wave. The waveguide length is controlled by an external tuner to attain the maximum electric field in the growth region. The maximum electric field is attained in low dimension (wavelength) of the MW and results in an increase in the electron-neutral collision and produces radicals for the deposition process [18].

Generally, in PECVD techniques, CNW growth is performed by gas phase deposition process. Firstly, the carbon source gas is introduced into the plasma. Plasma is generated by applying a strong electromagnetic field to accelerate electrons to collide with the neutral gas. This collision results in dissociation, ionization, and excitation, which in turn numerous species-more electrons, ions, photons, and radicals, as well as excited background gas are formed. Each of plasma particles play a significant role when the plasma is applied for material synthesis. For instance, energetic ions can cause sputtering of material, elevate the substrate temperature, and increase surface diffusion. Electrons can supply activation energy for chemical reactions. The generated photons during the de-excitation of the plasma molecules, atoms, and ions can heat the substrate and participate in the photochemical reactions. Highly reactive radicals react with the substrate and deposit or chemically etch the sample. The undissociated source gas is also engaged in chemical reactions on the surface. To compare with thermal CVD, much lower temperatures are required for growing CNW by PECVD systems. The most reported temperature for CNW synthesis is in the range of 400^{o}C to 800^{o}C, which corresponds to CNT growth temperature. However, there are several experiments that declare growing of CNW by PECVD at lower temperatures, some even

at 320^{o}C [20]. It is to say that because in-site temperature measurement of substrate is difficult, most of the measurements are done via thermocouple under the substrate holder or beside the heater. In addition, plasma itself can heat the substrate as well, which can result in inaccurate measurements. This is more sever when higher plasma density systems such as MPCVD and ICP are utilized. It has been reported by Teo et al. that a significant high temperature of 700^{o}C was induced by plasma with 66W input without using other heaters [21]. Different substrate temperatures can vary the deposited film properties. Raman spectra of the CNW films prepared in different temperatures showed that low temperatures bring more defects than higher temperatures as I_D/I_G ratio increases at lower temperatures [19,22].

Furthermore, since many chemical reactions and depositions can occur at much lower temperatures to compare with thermal CVD, a wide range of substrates can be selected [18]. Substrates including metals, crystals, and other materials with or without catalytic property such as Ni [23], Cu [20], Al [20], Si [24], quartz [24], etc. has been selected so far to grow CNW. The effect of substrate on CNW growth is limited to the initial stage when carbon cluster nucleation starts and it fades as CNW grows thicker.

Different effects of substrate such as lattice matching with graphite or not, formation stable carbide compound or not, and carbon solubility of the substrate can influence the CNW growth. The growth process for Ni and other metals with high carbon solubility may be more complex and not clear yet. It has been shown that higher crystalline degree and growth rate can be achieved with Fe metal compared to Cu and Si [19]. For different substrates of silicon, quartz, and platinum, the evolution process is different. In the case of using quartz as the substrate, a large lattice mismatch exists between the substrate and graphene, which lead to formation of amorphous carbon as buffer. By utilizing silicon as the substrate, carbide is formed at the interface. While no formation of amorphous carbon or carbide is reported while utilizing platinum as the substrate due to good crystal matching [19,25].

1.2.1. Growth mechanism of CNW in PECVD system

As it mentioned earlier, CNW is deposited by PECVD systems, in which carbon-containing gas is partially atomized and ionized upon plasma conditions. The resultant radicals are then transported to the substrate and condensate on its surface to form nanostructured CNW. The schematic growth mechanism for CNW is illustrated in figure 1.3 and can be summarized as follows:

1. Formation of defects on the substrate surface by ion stimulated plasma-surface interaction
2. Migration of carbon species to the substrate surface and attaching to the produced defects on the surface by dangling bonds
3. Formation of thin layer of carbon film on the substrate called a buffer layer, composed of both graphitic and amorphous carbon
4. Attaching more carbon species to thin film layer in the form of carbon nanoislands and initiating nucleation
5. Nucleation of small graphene nanosheets on dangling bonds followed by a two-dimensional growth
6. Generation of strong local electric field perpendicular to the substrate, leading to curling the edges of top layer sheets vertically along with the direction of the electric field
7. Bonding of reactive carbon species to the edges of graphene sheets, and fast vertically growing of sheets and shadowing low-lying graphene sheets
8. Eventually, increasing the height of graphene sheets with the growth rate rather than the thickness, resulting in the formation of nanowall

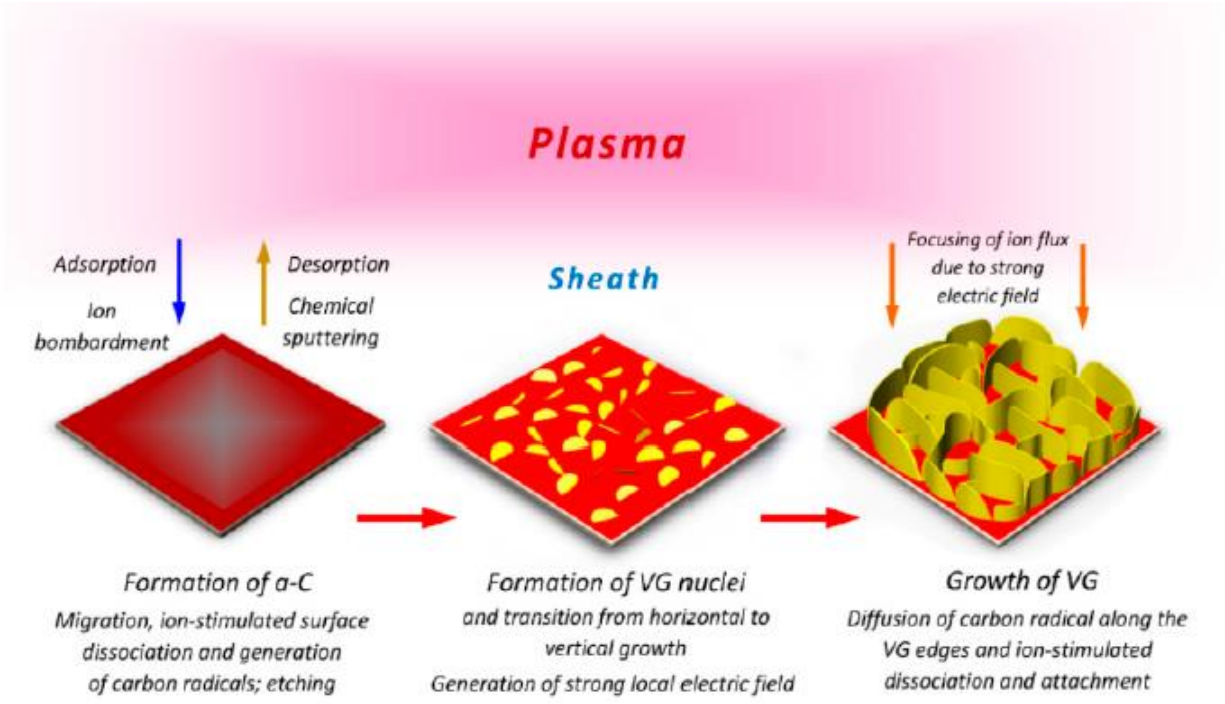

Figure 1.3. Schematic representation of plasma-enhanced deposition of CNW [18]

1.2.2. Effect of plasma parameters on CNW growth

It has been found that reactive gas species play a significant role in the growth of high-quality CNW. The gaseous species for CNW growth can be categorized in three different groups: (i) carbon-containing precursor gases to produce carbon radicals for growing CNW (ii) etchant gases (H_2, Ar, O_2) for removal of amorphous carbon and help growing high crystalline CNW, and (iii) dopant gases (N_2, NH_3).

The HC (hydrocarbon) gases are widely used as the carbon source for CNW growth alongside with other etchant gases such as H_2, O_2, and Ar. The presence of H atoms in the plasma system assists in enhancing migration of carbon precursors and nucleation of carbon radicals. It is also more reactive with amorphous carbon atoms than sp^2 and sp^3 carbon structures, therefore it helps with etching and removing amorphous carbon and greatly improving the quality of CNW. Addition of neutral gases such as Ar can control the density of nanoislands in the initial stage of growth and consequently the density of CNW. It can also provide high quality CNW by increasing plasma stability and moderating the growth rate. The presence of O radicals can reduce the defects and

suppress the carbon nucleation and hinder the formation of interface layer. Therefore, the vertical growth of CNW from the nuclei can be promoted by removing this horizontal interface layer [18,26]. CNW can be also formed by applying CF gases such as C_2F_6 in a mixture with H_2 and O_2 [27]. Another gas source to synthesize CNW is a CO/H_2 mixture, where CNW can be observed only if H_2 was added [28]. Recently, other precursors like p-xylene[10], ethanol or hexane[29,30], aluminum acetylacetonate [31] have been employed to synthesize CNW as well.

In addition to the mixture of source gases, the proportion and flow rate of gas into the plasma system also has an important role in the growth of CNW. For instance, the study on the influence of concentration of CH_4/H_2 mixture in various flow rates (0-100%) on CNW growth was reported by Wang et al. It was shown that density of CNW sheets was highly influenced by CH_4 concentration, which is in charge for nucleation of carbon radicals and initial growth. Higher precursor concentration (40-100%) resulted in higher nucleation rate with small lateral size [32]. In another experiment by Wu et al. the effect of flow rate of gas mixtures on the growth mechanism of CNW was evaluated by varying flow rate of CH_4/H_2 mixture from 30, 10, 6, 4, to 1sccm. Amorphous carbon with column structures was observed for flow rate of 30sccm. Decreasing flow rate resulted in appearing tube-like carbon structures. While high quality CNW was observed at a flow rate between 4-8sccm. Further decrease in flow rate led to formation of amorphous carbon on substrate [33]. These results demonstrate that different gas flow rates in even same discharge conditions can highly affect the morphology of the final product.

The growth mechanism of CNW can also be influenced by flow rate of etchant gases. The effect of H_2 gas flow rate on the nucleation and growth of CNW was investigated by Kondo et al. [34]. The synthesis of CNW was studied in various H_2 flow rates (0, 3, 5, 7, and 10sccm). Without any H radical, a thin layer of carbon was formed on the substrate. At flow rate of 3sccm, deposition carbon nanoparticles were initiated. Further increase to 5sccm and 7sccm resulted in producing CNW with an interlayer spacing of 10-20 nm and sheet thickness of less than 5 nm. Variation in H radical flow rate influenced the height of CNW as well and showed the maximum value at the flow rate of 5sccm, meaning that the optimum density of H radical inside the system highly influenced the vertical growth of CNW.

Since varying flow rates results in changing the pressure inside the system, it can be concluded that growth of CNW can also be influenced by the operating pressure. In low pressure systems,

the flow rate of inserted gases controls the total pressure inside the chamber. When the total pressure is low, low flow of gas species through the system exists, which consequently results in lower growth rate. However, this slow growth rate can provide high quality CNW to compare with the CNW prepared in higher pressures due to effectively removal of a-C from the surfaces. The curling up of nanosheets to a vertical form can also be influenced by plasma power. It has been described by Zhu et al. that increasing the power from 500W to 1200W increases the growth rate of CNW [35]. At high plasma power, a high electric field is induced on the plasma sheath above the substrate, which causes elevation of the temperature of substrate. This forces the nanosheet to curl up to a vertical form (same as electric field direction) and increases the growth rate.

Although, plasma parameters can influence the growth mechanism and properties of CNW, further plasma treatment after the growth can modify the properties of CNW, which is one of main advantages of plasma-assisted techniques.

1.3. Plasma assisted surface modification

Plasma-based techniques have recently gained considerable attention as a versatile and biocompatible technique for modifying and inducing changes in the characteristic of nanomaterials. It can help improve the physical and chemical properties, such as wettability, metal adhesion, dyability, refractive index, hardness, chemical inertness, lubricity, and biocompatibility of materials surfaces in a short time. Furthermore, nanostructures have a larger surface area than bulk materials, which make this method more suitable for nanomaterials processing [36].

In plasma treatment, high-energy active species (HASs), including free radicals, excited molecules or atoms, positive ions, and electrons, attack and interact with the carbon materials surface aiming π bonds/C=C bonds. The next step of treatment strongly depends on the applied gas type. In the case of inert gas, rebinding of free radicals or macromolecular fragments on the carbon material (CM) surfaces can occur, which results in a network of cross-linked surface structures, and consequently improving mechanical performance of CM. On the other hand, when reactive gases such as O_2, N_2, NH_3, and CO_2 are introduced for treating the CM surfaces, formation of various functional groups on the surface occurs favorably. The generated dangling bonds at the first step display strong ability to chemisorb other species, such as activated atoms or free radicals. Additionally, the HASs can react with atoms or molecules on the surface of materials and produce

some volatile substances, resulting in etching the surface. The combined action of etching and grafting functional groups can control the physical structure and chemical properties of CM surfaces. Figure 1.4 Shows different surface modification processes by plasma treatment [37].

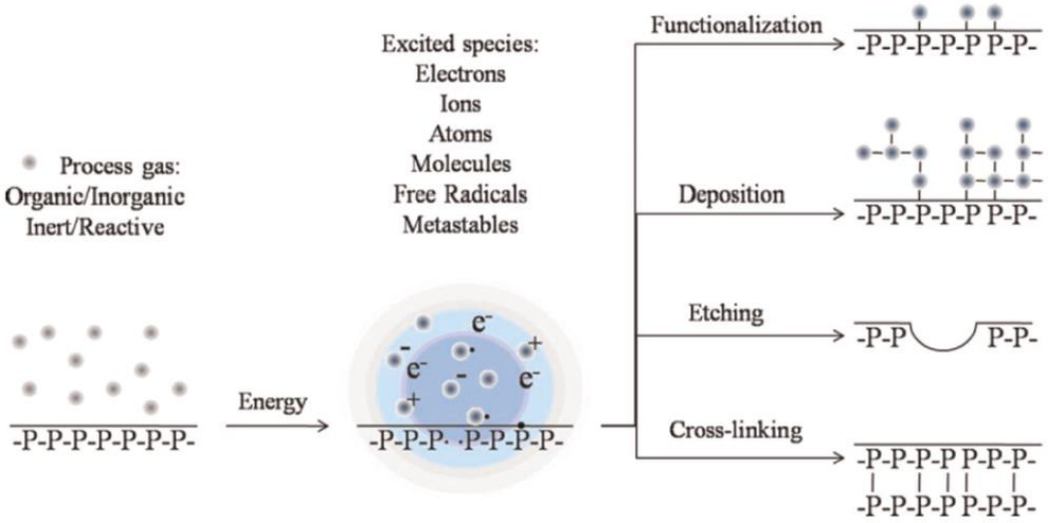

Figure 1.4. Various surface modification processes that can be achieved using plasma technology [38]

1.3.1. Effect of plasma treatment on the surface morphology and chemistry of CMs

Plasma treatment is regarded as a "destructive" surface modification method. It has been reported that the external surface morphologies of CMs including ACs and ACFs are affected by etching effect of non-thermal plasma treatment (NPT). While the interior surfaces can be left without any damage as HASs do not reach the smallest micropores of CMs, limiting the reaction between HASs and internal carbon atoms [39,40]. Therefore, the bulk properties of CMs do not alter by plasma treatment. In addition to surface structure, the surface chemistry can be also altered by plasma treatment. Depending on the feed gas applied for the treatment, different functional groups on CM surfaces can be formed by insertion or by substitution of the previous functional groups [41]. Generally, presence of heteroatoms such as nitrogen, halogens, and especially oxygen determine the surface chemistry properties of CMs. Among all feed gases, O_2 has become a common gas for forming non-thermal plasma due to its strong influence on the surface characteristics. Oxygen radicals can react with carbon atoms on external surface of CMs and OFGs with basic, neutral,

and /or acidic characteristics are formed [42]. It has been reported that the breakage of C=C bonds can create active sites to bind oxygen functional groups [43,44]. Different parameters such as modification time and output voltage can influence the concentration of OFGs on the surface structure. Furthermore, it has been shown that formation of oxygen functional groups can reach its saturation state, meaning that by further increasing modification time, the surface cannot continue to accept new oxygen groups [45]. And instead longer modification can damage the previously produced OFGs and reconvert them to the O_2 [46]. The effect of discharge power and treatment time on modifying MWCNTs by LTOP reported by Wang et al. revealed that oxygen reaches its maximum quantity at certain power of 15W and treatment time of 40min. While further increase in discharge power and treatment time did not result in increasing the surface oxygen ratio due to overetching [47].

Applying other feed gases such as N_2, NH_3, air, H_2S, etc. results in different functional groups on CM surfaces. For instance, Applying N_2 or NH_3 results in grafting NFGs including C-N, C-NO_2, C-NH_2 on CMs surfaces [45,48]. SFGs can be formed on the surface of CMs by using H_2S as treatment gas [49]. In the case of treating the surface with air, mixed oxygen and nitrogen functional groups can be generated [50]. To sum up, different types of functional groups can be grafted on surface of carbon materials by applying different gaseous media.

1.3.2. Plasma treatment of CNW

Post deposition exposure under different plasma medium such as hydrogen, oxygen, nitrogen, argon, and fluorine have been applied to tune CNW characteristics and mostly to switch their wettability. Exposing the CNW samples to hydrogen, oxygen, nitrogen, and argon mostly results in hydrophilic nature, while the fluorination makes the CNW surface superhydrophobic [51,52].

In the case of hydrogen, the surface can be modified through strong etching and formation a roughened layer on the CNW surface. Moreover, the surface wettability can be controlled by forming H-bonds on the edges. It has also been reported that hydrogen plasma treatment can remove the absorbed oxygen atoms in the nanowall surface and in turn enhance CNW adsorption capabilities [53]. Hybridization of sp^2 bonded carbon atoms can also be changed to sp^3 through hydrogen plasma treatment, which further results in the transformation of band structure from semimetal to insulators [54].

Post plasma treatment of CNW with oxygen can influence both the edges and the interstitial sites of the CNW to form different functional groups. The wettability of the CNW treated with oxygen plasma is improved due to the presence of O-terminated carbon structure, which can also increase the penetration of aqueous solutions into the gaps between the walls [55] as well as enhance the capability of CNW to interact with electrolyte rapidly [56]. It has also been reported that photoluminescent (PL) properties of graphene can be modified by oxygen plasma treatment [57,58].

Nitrogen plasma can be used for doping and grafting of the amino functional groups into the CNW structure and consequently enhance its electrical conduction and improve the electron field emission. The nitrogen plasma post-treatment can improve carrier concentration and carrier mobility by attaching N atoms to the graphene edges while keeping the morphology and edges of CNW intact [59]. Enhancement of electrochemical properties of N-doped CNW as a supercapacitor has been reported by Chi et al. and Yen et al [60,61].

Argon plasma can influence both electronic and surface properties of CNW [51,62]. It is usually used to enhance the removal of a-C. The prolonged Ar treatment on the edges of carbon nanowalls results in thinning of the edges and creating several defects, which these defects can act as the additional emission sites, resulting in the enhanced electronic properties and field emission characteristics [63,64]. Post plasma treatment of CNW with Ar at atmospheric conditions leads to the formation of H/O-terminated CNW by incorporation of oxygen into the lattice through the dissociation of oxygen molecules in the air, making the CNW surface superhydrophilic. In contrast to hydrogen, nitrogen, oxygen, and Ar plasma treatments, fluorine-containing plasma post-treatment results in the hydrophobic nature of the surface by forming F-terminated bonds on CNW [51,65].

In addition, the effect of plasma treatment by N_2 and O_2 on physical properties of CNW such as specific surface area and pore size and electrochemical properties such as specific capacitance has been reported by Evlashin et al. It was revealed by BET study that after plasma modification, the specific surface area of CNW decreases from $S_{CNW}=1203 m^2g^{-1}$ for untreated CNW to $S_{NCNW}=919 m^2g^{-1}$, and $S_{OCNW}=658 m^2g^{-1}$ for CNW films treated with N_2 and O_2, respectively. Furthermore, due to facilitating in etching, plasma treatment decreases the porosity, where the pore size of 1.5nm, 1.7nm, and 2nm was reported for unmodified CNW, NCNW, and OCNW, respectively. The unmodified CNW displayed the specific capacitance of 1.3 Fcm^{-3}, while NCNW

and OCNW showed the specific capacitance of 4.4 Fcm^{-3}, and 8.9 Fcm^{-3}, respectively. The authors reported that experimental dependence of capacitance should be proportional to the BET specific surface area, N_{groups} the number of functional groups, and $n_{def} \sim 1/L^2$ the number of defects ($S_{BET}N_{O+N}/n_{def}$) [66].

To sum up, post plasma treatment can result in formation of functional groups, increase in the defect density, or doping the impurities into graphene lattice. By modifying the properties of CNW through plasma-surface treatment, the CNW can be utilized for specific applications. For instance, CNW with high crystalline nature and sharp edges can be used for field emission application. Fluorinated CNW films with superhydrophobic nature are suitable for hydrophobic coatings. N-doped CNW films with improved electrical properties and capacitance are useful for various electrical and electrochemical applications. Surface functionalization with oxygen can enhance the hydrophilic properties of CNW, which can in turn improve the interaction between the electrolyte and electrode and promote its application in electrochemical systems such as energy storage devices, catalytic reactions, sensors and biosensors [18].

1.4. Electrochemical sensing techniques

Electrochemistry concerns the interplay between electricity and chemistry, meaning that the measurements of electrical quantities, such as current, potential, or charge and their relationship to chemical parameters are studied. The electrochemical interaction takes place at the electrode-solution interface.

The type of electrical signal used for the quantitation depends on electroanalytical techniques. Generally, there are two principle sorts of electroanalytical measurements including potentiometric and potentiostatic. Potentiometric measurements are based on static (zero current) situation in which the information about the changes in the activity or concentration of the analyte is obtained from the measurement of the potential established across a membrane.

In potentiostatic (controlled-potential) techniques, which are based on dynamic (non-zero current) situations, the charge transfer processes at the electrode-solution interface are studied. In this method, the constant potential is applied to working electrode to drive an electron transfer reaction and the resultant current, which reflects the rate at which electrons move across the electrode-

solution interface is measured. Thus, any chemical species that is electroactive can be measured by potentiostatic techniques [67].

Different operating methods are often employed for the study of electroactive substances. The voltammetry and amperometry methods are the most adopted techniques in the development of electrochemical sensing systems because of their low-cost instrumentation, simplicity, and high sensitivity [5].

Commonly, electrochemical measurement is conducted using three electrode system comprises of working electrode, a counter electrode, and a reference electrode, which all are immersed in a solution with a supporting electrolyte to assure the conductivity in the solution. The counter electrode is usually made from platinum and has a significantly larger surface area than working electrode in order to reduce the current resistance. The reference electrode has a stable and well-known potential against which other electrodes in the system can be controlled and measured. They often consist of a saturated calomel electrode (SCE) or silver-silver chloride electrode (Ag/AgCl). The working electrodes are typically constructed from stable materials such as carbon (graphite or glassy carbon) or metals (mercury, platinum or gold). It is the most important part of the electrochemical cell where the reaction of interest occurs on its surface. The mentioned three electrodes are connected to a potentiostat, where the applied potential to working electrode is controlled by and then results are recorded by a computer [68]. Figure 1.5 illustrates the schematic representation of an electrochemical cell with three electrode system.

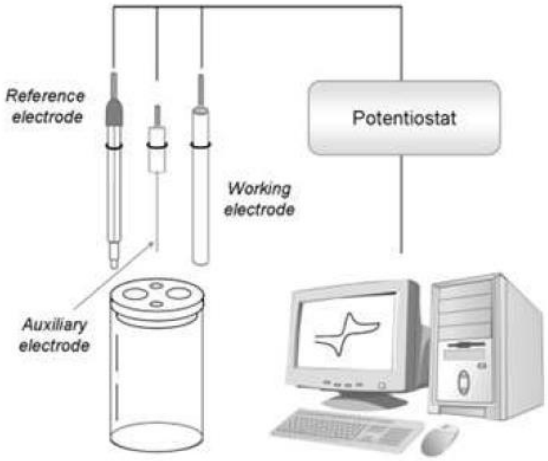

Figure 1.5. Schematic representation of an electrochemical cell with three electrode system [68]

1.4.1. Voltammetry method

In voltammetry technique, a range of potential is applied onto the working electrode and the changes in the current are measured. Based on the applied potential, the analyte is oxidized or reduced at the electrode surface and produce the current, while the bulk solution remains unchanged. In these measurements, the potential is related to the qualitative properties of the analyte and the measured current provides the information about the quantity of the analyte. The analytical data are recorded in the form of the voltamograms, which produced current by the analyte is plotted versus the potential of the working electrode [68]. Several voltammetry techniques have been developed so far, including differential pulse voltammetry, linear sweep voltammetry, square-wave voltammetry, and cyclic voltammetry [69].

Cyclic voltammetry (CV) is the most commonly applied technique for determination of redox potential and electrochemical reaction rates of analyte solution. Different factors including electrode surface, stability of reduced/oxidized analyte, electrochemical reversibility of the analyte and so on can determine the general shape of voltammogram [70]. Figure 1.6 displays a classical cyclic voltammogram for the following reversible reaction

$$Fe(CN)_6^{3-} + e^- \rightleftharpoons Fe(CN)_6^{4-}$$

and introduces the main parameters.

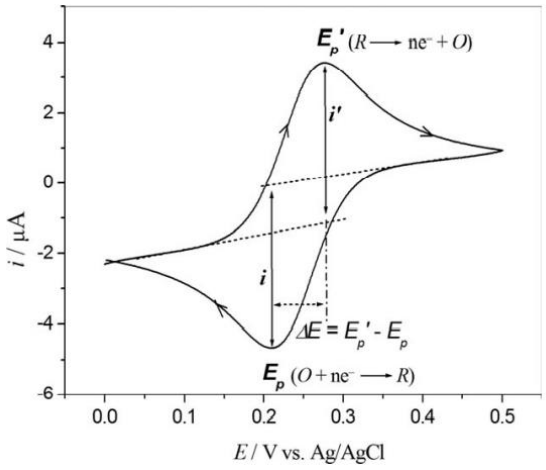

Figure 1.6. The cyclic voltammogram showing the important parameters [71]

1.4.2. Amperometry method

In amperometry technique, a constant potential is applied at the working electrode with respect to the reference electrode. The electric current is generated from the electrochemical oxidation or reduction of an electroactive species on the electrodes 'surface, therefore providing specific information related to the quantity of analyte present. The potential is set at a desired value or it is stepped to the selected values before injecting the sample. This method relays on the concentration of the target analyte. Because biocatalytic reaction rates are often first-order dependent on the bulk analyte concentration, such steady-state currents are usually proportional to the bulk analyte concentration [72]. Figure 1.7 shows typical amperometric response of H_2O_2 at VACNTs (Vertical aligned multiwalled carbon nanotube) and MnO_2/VACNTs [73].

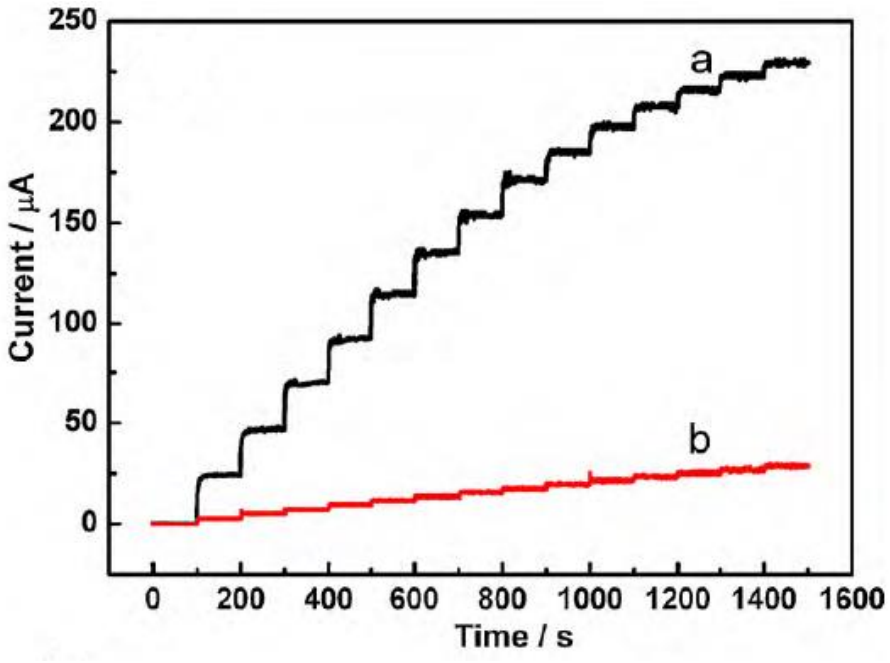

Figure 1.7. A sample amperometric response at MnO_2/VACNTs (a) and VACNTs (b) by adding 0.2mM H_2O_2 at each step

1.4.3. Sensitivity and limit of detection

To determine the sensitivity and limit of detection (LOD) of a sensor, a calibration plot is used. The calibration curves are constructed by plotting measured steady state current (I) versus concentration (C) of the analyte derived from the ampermetric responses [70].

The sensitivity (S) of a sensor is defined as the slop of the calibration curve divided by the area of the electrode. The LOD is the lowest concentration of an analyte that can be consistently detected with a specific level of confident using following equation

$$LOD = k\frac{Stblank}{B}$$

where St_{blank} is the standard deviation of the blank solution and B is the slope of the calibration curve. In the determination of the LOD**,** the confidence level parameter is set as k = 3 [74].

According to the LOD and sensitivity definition, the LOD can be increased if the current in the working electrode of the sensor can be adjusted in a way that less noise is observed (smaller St_{blank}).

And the sensitivity can be increased if the analyte interaction with the working electrode produces a larger response.

Considering the large surface areas and high conductivity of carbon nanomaterials, their application in biosensors can be both advantageous and disadvantageous in tuning the LOD and sensitivity. In general, a larger surface area provides more reactive sites for electrochemical reactions, which can result in an increased total current response for an analyte in solution. However, an increase in background current offsets the increase in current response, which consequently limits the sensitivity and raises the LOD. Pure carbon nanomaterial sensors display this effect in a larger degree, which require active sites (nonreduced carbon or oxygenated sites) for sensing since extensive reduction of the carbon surface leads to an increased background current. This necessitates modification of the carbon surface, that is, functionalization of the carbon surface and/or attachments of metal NPs, biomolecules, etc., in order to detect trace amount of the analyte reproducibly. By these modifications of the carbon electrode surface, the sensitivity and LOD can be improved by enhancing electron transfer between analyte and electrode [70].

Among all biomarkers, H_2O_2 is particularly important for the development of efficient sensors and biosensors, since it is an enzymatic product of oxidases, an important mediator in clinical and pharmaceutical analyses, food controlling, and environmental protection.

1.5. Hydrogen peroxide sensors

Hydrogen peroxide (H_2O_2) is a very simple molecule in nature but it has a great significance in pharmaceutical, clinical, environmental, food manufacturing and chemical industries [75]. It is one of the reactive oxygen species (ROS) that plays an important role as a marker for oxidative stress [72,76]. Oxidative stress is believed to be an important cause for many different kinds of disorders in body such as atherosclerosis [77], Parkinson's disease [78], diabetes [79], and cancer [80]. H_2O_2 is also a by-product generated from some biochemical reactions catalyzed by most of the oxidase enzymes, such as glucose oxidase (GOD), cholesterol oxidase (ChoOx), glutamate oxidase (GlOx), oxalate oxidase (OxaOx), and lactate oxidase (LOx) [72,81,82]. Therefore, accurate detection of H_2O_2 is of great importance in biomedical, industrial, and environmental applications.

Various analytical methods have been reported for the detection and quantification of H_2O_2 such as titrimetry [83,84], chromatography [85], colorimetric [86], chemiluminence [87],

spectrophotometric [88], fluorescence [89], and electrochemical analyses [73,90]. Among these methods, electrochemical technique has attracted extensive attention due to its advantages of high sensitivity, low cost, and simple operation.

In electrochemical sensors, H_2O_2 can be either oxidized or reduced on the surface of an electrode. However, slow electrode kinetics and high overpotential of such electrodes can restrict the analytical applications of these redox reactions. Furthermore, other existing electroactive species can be reduced or oxidized from a matrix so that the simultaneous detection in the same sample is possible only when two species possess redox potentials sufficiently separated. Therefore, recent studies focused on modifying the electrode surfaces for decreasing the overpotential, increasing the electron transfer kinetic and the selectivity [91].

A wide range of materials such as redox proteins [92], noble metals [93,94], and transitional metals [95–97] have been employed for electrochemical sensing of H_2O_2.

Recently, nanomaterials have attracted an increasing interest in sensing and biosensing application due to their unique chemical, physical, and electronic properties that are different from those of bulk counterparts. In addition, easy tailoring the properties of nanomaterials for designing new sensing platforms to enhance the sensing performance has made them a feasible alternative to chemical sensors and biosensors [75].

1.5.1. Materials used for electrocatalytic sensing of hydrogen peroxide

Electrochemical sensors for detection of H_2O_2 are generally classified into two major types including enzymatic and non-enzymatic sensors [98].

1.5.1.1. Enzymatic H_2O_2 biosensors

Generally, an electrochemical biosensor can convert a biological response into an electrical signal using different electrochemical strategies. Since 1990s, redox protein-based biosensors have been extensively employed for clinical diagnosis and bioassay [99]. Heme proteins such as horseradish peroxidase (HRP), hemoglobin (Hb), microperoxidase (MP), and myoglobin (Mb) have been paid substantial attentions to be used in construction of H_2O_2 biosensors because of their intrinsic redox capability. The heme proteins contain the iron that can easily undergo oxidation and reduction over a wide range of potentials [75]. Heme protein-based H_2O_2 biosensors can be divided into two

categories according to the different ways of electronic transfer: mediated-free biosensors and mediated biosensors.

The mediated biosensors utilize various electron-shuttling mediators such as ferrocene, hexacyanoferrates, and thionine to facilitate the electron transfer between the electrode and the enzyme (redox protein). But they can also speed up the electron transfer between the electrode and various interfering reactions. While, mediated-free biosensors are based on direct electron transfer between the protein and the electrode without mediation. These types of biosensors are able to operate in a potential range closer to the redox potential of the protein itself, therefore fewer interfering reactions can occur. Mediated free biosensors have high selectivity, sensitivity, and conveniences. However, the main challenge to construct these biosensors is that the redox centers of heme proteins are always embedded in protein structure, which make the electron transfer distance so long so that the realization of direct electrochemistry is often difficult [75,99].

Electrochemical biosensors based on the electrocatalysis of immobilized enzymes toward H_2O_2 are highly selective and exhibit low detection limit. However, they display several limitations such as complex fabrication procedures, limited life time, high cost, and poor stability. Therefore, much effort has been devoted to the development of enzyme-free H_2O_2 sensors with low detection limit and wide response range [100].

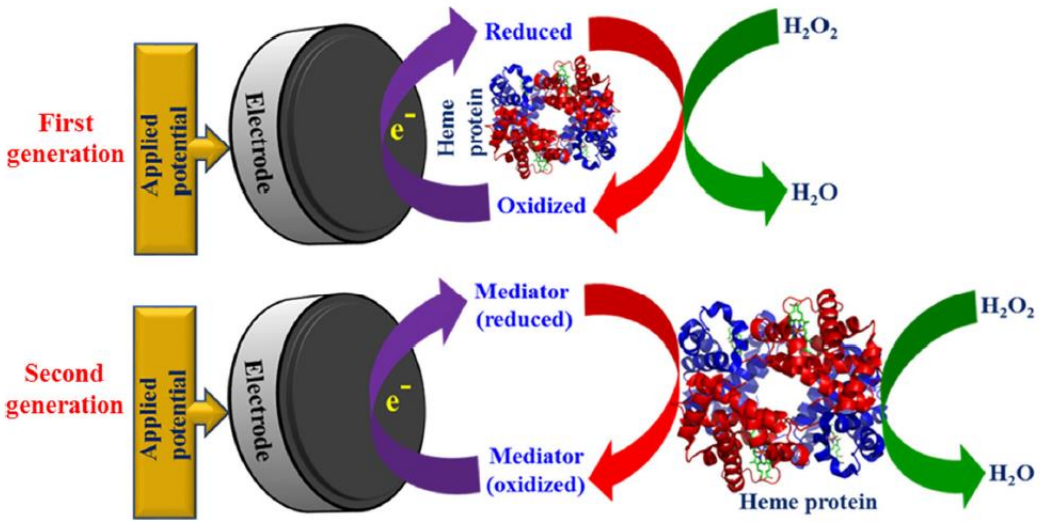

Figure 1.8 Schematic representation of mediated and mediated-free H_2O_2 sensors [72]

1.5.1.2. Nonenzymatic H_2O_2 sensing

There are many advantages of utilizing enzyme-free electrochemical methods for the detection of H_2O_2 such as stability, simplicity, reproducibility, and low cost. To obtain highly efficient enzyme-free sensors, modification of the electrode surface with suitable materials, which enhance the electron transfer between electrode and analyte (H_2O_2) becomes increasingly important [101].

For this purpose, noble metal catalysts such as Au, Pt, Pd, Ag and their alloys have been successfully applied to improve the electron transfer kinetics [93,94,102,103]. However, the noble metal-based sensor has some disadvantages such as low sensitivity, surface poisoning, high cost and limited availability of precious noble metals. Therefore, developing of low-cost, highly sensitive and selective non-enzymatic H_2O_2 sensors without applying noble metals is of great interest [101,104].

Recently, a number of studies have been carried out to synthesize new nanocomposite catalysts using transition metals, their oxides or complexes. Transition metals are known as good catalysts because they are capable to have multiple oxidation states and also, they can absorb other substances onto their surfaces and activate them in the process. Transition metal oxides such as cobalt oxide [105], copper oxide [106], nickel oxide [107], manganese oxide [108], and iron oxide [95] have been reported to improve the electrochemical response to H_2O_2. As an important transition metal oxide, manganese oxides nanomaterials have drawn attention in electrochemical sensing of H_2O_2, due to its low cost, abundant resources, environment friendliness, and catalytic activity which can promote H_2O_2 decomposition [74,109]. Recently, a comprehensive research has been focused on combining nanostructured manganese oxides with an electrically conductive carbon frame to improve their analytic functioning.

Due to high surface-to-volume ratio, high electrical conductivity, chemical stability, and extraordinary mechanical strength, carbon-based nanomaterials have received enormous attention to be used in the field of sensors and biosensors. Increasing the electroactive surface area, enhancing electron transfer, and promoting adsorption of molecules make the carbon nanomaterials especially advantageous for electrochemical sensors [110]. Carbon nanotubes (CNTs) and graphene are the most widely used carbon nanomaterials in the electrochemical sensing field. This is because of their intrinsic electronic, optical and magnetic properties and their performance as a chemically stable platform. Unlike the many other nanomaterials that their stability can be compromised by factors such as temperature, high ionic strength, and pH, CNTs

and graphene are chemically robust. The oxidation and reduction mechanisms of H_2O_2 on carbon nanohybrid-modified electrodes is presented in figure 1.9 [72].

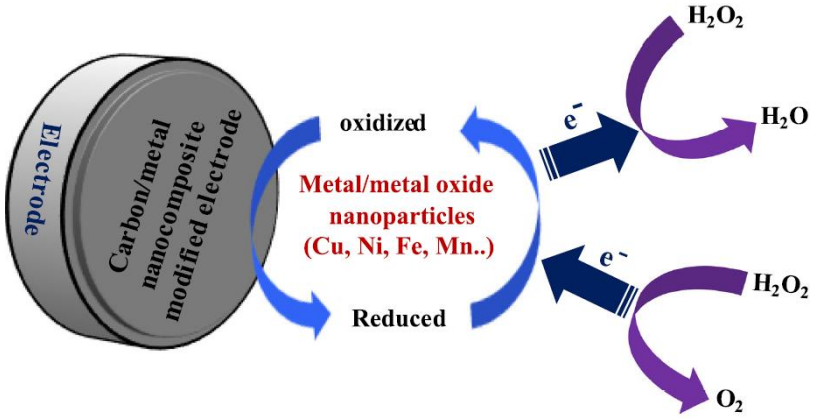

Figure 1.9. Schematic representation of oxidation and reduction reaction of H_2O_2 on carbon nanohybrid-modified electrodes [72]

1.5.1.2.1. Manganese oxide/carbon nanotube composites

The unique properties of CNT including high surface area, excellent electrical conductivity, strong mechanical strength and high stability, have been exploited to develop a wide range of biosensors. Several molecules such as glucose, acetaminophen, dopamine, ascorbic acid and various organic vapors, have been detected by functionalized CNT and modified electrodes [72]. Manganese oxides/CNTs composites have shown their high electrocatalytic activity in the reduction and oxidation of H_2O_2. Xu et al. reported a highly sensitive amperometric sensor based on MnO_2-modified vertically aligned multiwalled carbon nanotubes (MnO_2/VACNTs) towards the oxidation of H_2O_2 [73]. A δ-MnO_2/CNTs nanocomposite fabricated by hydrothermal process was introduced by Begum et al. for reduction of H_2O_2 [74]. In addition, combination MnO_2/CNTs with other metals and carbon materials such as Ag [111], Ta [112], and graphene [98] as electrochemical sensors for detecting H_2O_2 have been reported.

1.5.1.2.2. Manganese oxide/ graphene composite

In the carbon material family, graphene, a 2D carbon material, has attracted intense interests due to its remarkable physicochemical properties such as large theoretical specific surface area, extraordinary electronic properties and electron transport capabilities, strong mechanical strength and excellent thermal and electrical conductivities [99]. Besides this unique properties, having various derivatives such as graphene oxide (GO) and reduced graphene oxide (rGO), increases its functionalization capability and broadens its applications [113]. In addition, the chemically obtained graphene brings about remarkable structural defects (vacancies, holes) and surface functional groups (hydroxy, epoxy, carbonyl, phenol, etc.), which can act as active sites for immobilizing various species via covalent bonds for designing sensitive sensors [99]. The advantages of utilizing graphene and its derivatives in manganese oxide/ graphene composite in reduction and oxidation of H_2O_2 have been demonstrated in several studies. Li et al. reported MnO_2/GO hybrid structure for non-enzymatic detection of H_2O_2 [114]. Mn_3O_4-MnO_2 hetero-nanorods/graphene nanocomposite fabricated by combining a hydrothermal (for MnO_x nanorods), a wet chemical process (for composites) and thermal treatment for (hetero-structure) was proposed by Zeng et al [115]. In another study by Li et al., graphene oxide/manganese dioxide nanowires (GO/MnO_2 NWs) composite was used as an electrode material for non-enzymatic detection of H_2O_2 [97]. Rice-like MnO_x nanorods covered by nanographene is another nanocomposite of manganese which is introduced for determination H_2O_2 by Pan et al [116]. Utilizing reduced graphene oxide (rGO) in combination with manganese dioxide was also studied by Wang et al. and Zhang et al. [108,117]. Manganese dioxide based ternary nanocomposite containing Au and Ag for nonenzymatic sensing of H_2O_2 was introduced by Wang et al. and Zhang et al., respectively [108,117].

Although, there are many studies devoted to the composite of manganese dioxide and graphene/ its derivatives for electrochemical sensing of H_2O_2, there has not been any report to utilize carbon nanowall as another type of two-dimensional (2D) graphene-like carbon nanostructures in combination with manganese oxides for detecting H_2O_2. The first utilization of CNW as a platform for electrochemical sensing of H_2O_2 was investigated by Tomatsu et al. [12]. However, the sensor performance is based on the utilizing high cost noble metal Pt. The combination of CNW with manganese oxides as an electrochemical sensor towards H_2O_2 was investigated in this thesis.

1.6. The Objective of this study

The aim of this study is development of novel electrochemical sensors based on carbon nanowalls. For this purpose, two different surface modifications were applied to enhance CNW performance in electrochemical systems. Firstly, the application of CNW as a base material with high conductivity and large surface area is investigated by introducing a hybrid structure of CNW and transitional metal oxide MnO_x as an efficient non-enzymatic H_2O_2 sensor. Then the direct application of CNW as a metal-free electrode in electrochemical systems is investigated by improving electrochemical sensor performance of CNW through its intrinsic modification by O_2/Ar plasma. Furthermore, novel inter-synthesis sequential treatment method was introduced in order to provide CNW with more defective edge planes and conformal oxygen functional groups to further improve selective electrocatalysis property of CNW.

1.7. Structure of this dissertation

This dissertation contains 6 chapters.

In Chapter 1, the research background and motivation are introduced, which followed by a comprehensive review on CNW, its synthesis method and growth mechanism, post plasma treatment on carbon nanomaterials and especially CNW, an introduction on existing H_2O_2 sensing techniques and the materials used for electrochemical sensing of H_2O_2.

Transitional metal oxides and especially manganese oxides have been considered attractive for detecting H_2O_2 since they have catalytic activity towards H_2O_2 decomposition. For this reason, hybrid MnO_x/CNW nanocomposite electrode was firstly introduced as electrochemical sensor for H_2O_2. Chapter 2 discusses the synthesis and characterization of CNW films, which followed by coating CNW samples with manganese oxides at different deposition times. The effect of different electrodeposition times on manganese oxidation state was thoroughly investigated.

Chapter 3 discusses the electrochemical performance of MnO_x/CNW nanocomposite electrode towards decomposition of H_2O_2. Linear range, limit of detection, and sensitivity of the hybrid electrode was determined and mechanism for oxidation and reduction of H_2O_2 was proposed.

In this hybrid structure, CNW was mainly used as a base material with high conductivity and large surface area combined with excellent electrocatalytic ability of MnO_x toward H_2O_2 decomposition and little attention has been paid for direct application of CNW as a metal-free electrode in electrochemical systems through its intrinsic electrochemical ability due to the highly active graphene edges.

Chapter 4 introduces plasma surface treatment of CNW by O_2/Ar plasma in order to functionalize CNW with defects and oxygen functional groups and increase its electrochemical performance. Effect of different oxygen flow rates in plasma treatment gas mixture on characteristics of CNW was investigated in detail. In addition, novel inter-synthesis sequential treatment method was introduced to deposit CNW film with more defective edge planes and conformal oxygen functional groups.

Chapter 5 discusses the electrochemical performance of CNW samples treated in different O_2/Ar plasma conditions and propose a reaction model based on the surface and electrochemical characteristics of the samples. In addition, the selective electrocatalysis properties of CNW was investigated.

Chapter 6 presents a summary of this dissertation and future work.

Chapter 2. Synthesis of CNW and its hybrid composite with manganese oxides and their characterization

2.1. Background of the chapter

In recent years, the electrochemical measurements of H_2O_2 with electrodes made of carbon nanotubes (CNTs) or graphene have been widely studied [73,74,98,100]. Carbon nanowalls (CNW) are another type of carbon nanomaterial that can be a useful platform for electrochemical applications as they consist of stacks of graphene sheets standing vertically on a substrate. In addition, in contrast to other CVD-grown materials like CNT, CNW can be fabricated without the use of catalysts, making them especially attractive to investigate basic electrochemical phenomena. The excellent electrocatalytic activity and biosensing properties of multilayer graphene nanoflakes in simultaneous determining dopamine, ascorbic acid, and uric acid in phosphate buffer solution was demonstrated by Shang et al [13]. The performance of CNW as a platform for electrochemical sensing of H_2O_2 was investigated by Tomatsu et al, which shows excellent electrocatalytic activity for the reduction of H_2O_2 [12]. However, the sensor performance is based on the utilizing high cost noble metal Pt. In this study, for the first time, we propose a nanocomposite electrode based on the large surface area and high conductivity of CNW and catalytic activity of MnO_x in the absence of any noble metals for electrochemical sensing of H_2O_2. The purpose of this chapter is to fabricate MnO_x/CNW nanocomposite electrode in different deposition times, characterize them, and estimate Mn oxidation state based on the XPS data.

2.2. Synthesis of CNW films and their characterization

2.2.1. Experimental

The production of CNW was carried out by a microwave plasma-enhanced chemical vapor deposition (MPECVD) with CO/H_2 microwave discharge system as shown in figure 2.1. The applied MPECVD system in this study was composed by 2.45 GHz microwave generator (APPLIED SCIENCE AND TECHNOLOGY, INC AX 2000). Silicon plate (9×9×0.5mm) and carbon rod (ϕ3 × 10mm) were employed as the substrates for characterization and electrochemical measurements, respectively.

Firstly, substrate was placed into the reactor chamber and the chamber was pumped down to 1Pa. Then CO and H_2 gases were simultaneously introduced at a constant flow rates at 23 and 2 Standard

Cubic Centimeter per Minute (SCCM), respectively and the chamber pressure was kept at 250Pa. This pressure was maintained throughout the whole reaction process. The microwave was tuned to output of 100W and CO and H_2 plasma was created for 30s, 60s, and 120s to prepare different CNW samples. Finally, the substrates were taken out of the chamber to characterize and also employ anodic deposition of MnO_x on CNW samples.

The deposited CNW films were observed using scanning electron microscope (JSM – 7500 F) operated at accelerating voltage of 15.0kV and beam current of 10μA without metal coating. For evaluating the hydrophilicity of CNW films, the contact angle of deionized water was measured on the surface of the electrode through the sessile drop method using a digital microscope (aigo, DMS012). The composition analysis of the fabricated CNW samples was carried out on an X-ray photoelectron spectroscopy (XPS, ESCA 5500 MT) with $Mg_{K\alpha}$ X-ray radiation as the source of excitation.

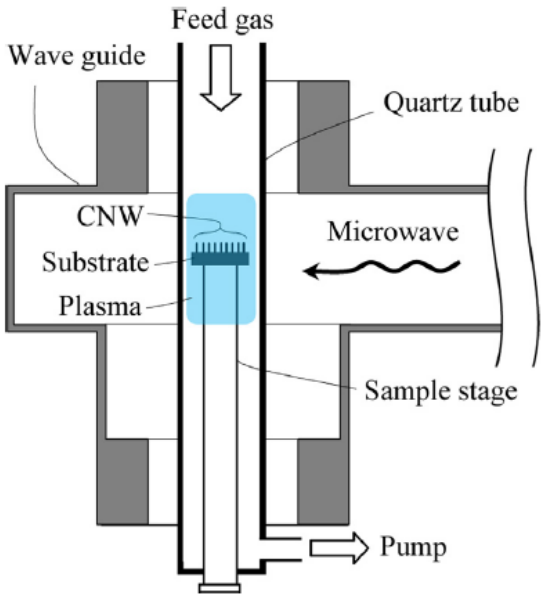

Figure 2.1. schematic representation of MPECVD system [118]

2.2.2. Result and discussion

Figure 2.2 shows the SEM images of the surface and cross section of CNW films deposited at different deposition times (30s, 60s, and 120s). Growing of CNW perpendicularly to the substrate can be revealed by cross section images. It also displays that by increasing deposition time, CNW earn more branches and consequently the gaps between the walls get narrower. These results suggest that increasing deposition time can lead in an increase in the surface area of CNW. In addition, in this study, the growth rate of 3μm / min was obtained, which is much higher than our previous result (1μm/min), because the plasma input power increased to 100W over the previous condition where the plasma input power was set at 60W [28].

The water contact angle measurements of CNW films synthesized in different deposition times showed a decrease in contact angle by increasing deposition time from 149° to 125°, and 120° for CNW samples deposited in 30s, 60s, and 120s, respectively and consequently improved the wettability. To evaluate the elemental percentages of CNW samples prepared at different deposition times, XPS analysis performed and the percentage of elements were calculated based on the peak area shown in figure 2.3 and collected in table 2.1. As can be observed from table 2.1, there is negligible change in the elemental percentage by increasing deposition time, indicating that improvement in CNW hydrophilicity is irrelevant to the oxygen content on the CNW surface in this work. Based on the SEM observation, this can be associated to the highly branched structure of CNW in longer deposition times. This is because in branched structure, CNW is more densely formed which may inhibit the lotus effect and there are more edges, where the number of defects increases and wettability improves consequently.

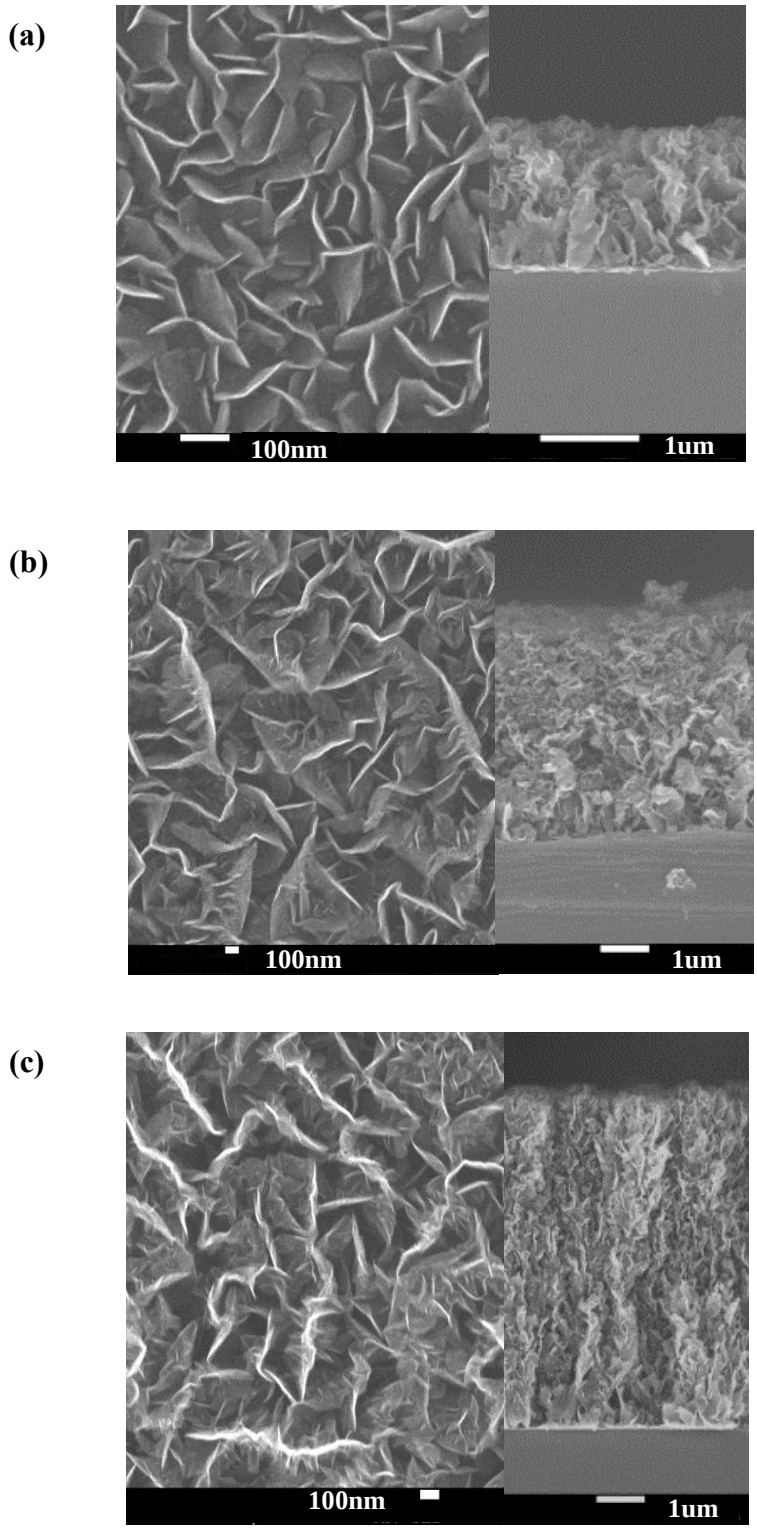

Figure 2.2. SEM images of deposited CNW on Si substrate for 30s (a), 60s (b), and 120s (c)

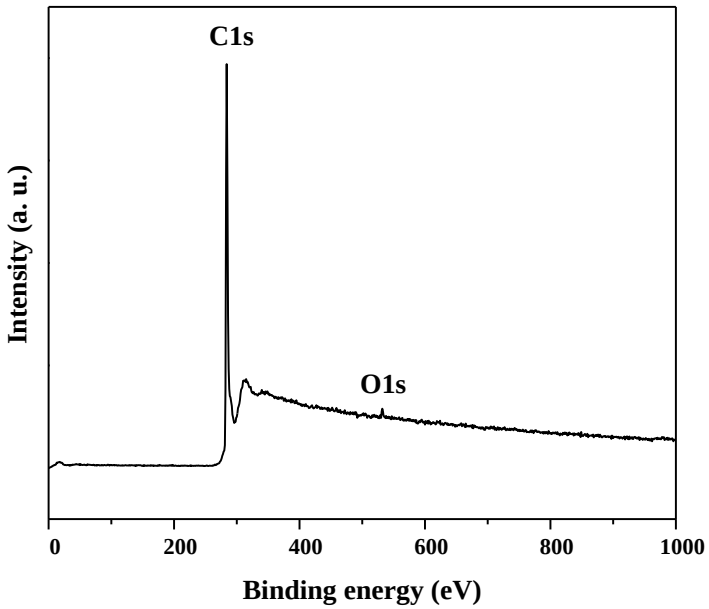

Figure 2.3. XPS spectrum for CNW prepared in 60s

Table 2.1. Elemental percentages for CNW samples prepared in different deposition times

Synthesis time (s)	C%	O%
30	99.2	0.8
60	99.4	0.6
120	99.3	0.7

According to the XPS and water contact angle analyses, in the next section, CNs prepared in 60s was selected to deposit MnO_x on its surface as the result showed very negligible differences in the characteristic of CNW films prepared in 60s and 120s.

For a detailed analysis of the surface chemistry of CNW prepared in 60s, XPS spectra in the region of the C1s peak (282-294eV) was recordered and displayed in figure 2.4. The C1s peak was decomposed into 4 components. The two major peaks at 284.4 and 285.0 corresponds to the sp^2

C=C and sp3 C-C, respectively. The peak situated at 286.6 can be attributed to C-O (oxygen in alcohol or ether), while the peaks situated at 291.8eV can be ascribed to π-π* transition.

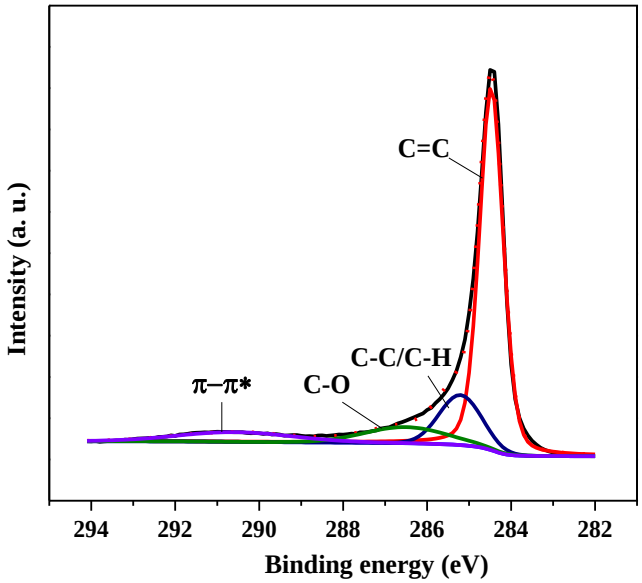

Figure 2.4. C1s spectra for CNW synthesized in 60s

Raman spectroscopy was further applied to understand the structural characteristic of the CNW sample. As disclosed in figure 2.5, the sample shows a typical spectrum for CNW with clear characteristic graphitic D, G, and D'. The D peak of the samples which is associated with the defects in sp^2 structures, was approximately shown at 1350cm^{-1}. The G band is related to the sp^2 structure, showing the degree of graphite-like domains in CNW was observed at 1580cm^{-1}. A weak band observed at around 1620cm^{-1} corresponds to D' that emerges with D band indicating disorder in the finite-sized sp^2 crystal and it is typical for graphene edges [119]. The ratio between the intensity of D and G bands (I_D/I_G) is used as the quantitative analysis technique to estimate the degree of disorder in graphene lattice [120]. The CNW sample showed the I_D/I_G ratios of 1.65, which can be related to its defective edge structures.

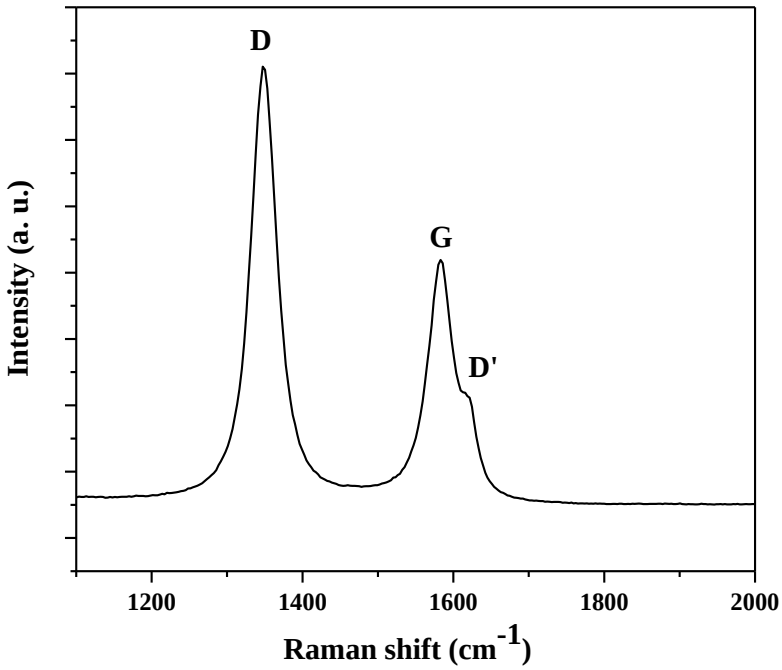

Figure 2.5. Raman spectra of CNW film prepared in 60s

2.3. Synthesis of MnO_x/CNW and their characterization

2.3.1. Experimental

Manganese (II) acetate tetrahydrate (Mn $(CH_3COO)_2.4H_2O$) was purchased from FUJIFILM Wako Pure Chemical Corporation, and deionized water was used throughout the experiment.

After synthesizing CNW samples, the electrochemical deposition of manganese oxides on CNW surfaces was carried out for 5s, 30s, and 60s in 0.25 M $(CH_3COO)_2Mn.4H_2O$ electrolyte using a three-electrode system composed of carbon rod and silicon as working electrodes, an Ag/AgCl (NaCl saturated) electrode as reference electrode and platinum wire as counter electrode (figure 2.6). The applied potential was controlled at 1.0V (Ag/AgCl) using versa STAT 3 (Princeton Applied Research).

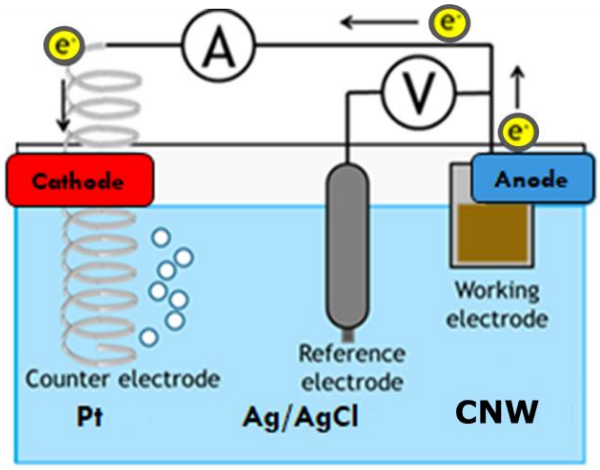

Figure 2.6. schematic representation of three electrode system for anodic deposition

The morphology of MnO_x/CNW nanocomposite films were observed using scanning electron microscope (JSM – 7500 F) operated at accelerating voltage of 15.0kV and beam current of 10µA. The composition analysis of the fabricated electrodes was carried out on an X-ray photoelectron spectroscopy (XPS, ESCA 5500 MT) with $Mg_{K\alpha}$ X-ray radiation as the source of excitation.

2.3.2. Result and discussion

Figure 2.7 shows SEM images of CNW/MnO_x composite films, where MnO_x was deposited electrochemically on CNW for 5s, 30s, and 60s. As it was observed, when the deposition time is very short, the film has mostly original CNW structure with some nucleation spots of MnO_x. By increasing deposition time to 30s, the accumulating of manganese oxides around the walls can be clearly confirmed. While in the case of 60s, it is difficult to distinguish the border between CNW and manganese oxide, which indicates that MnO_x can slightly infiltrate into the gaps between the walls.

XPS analysis is used to evaluate the chemical composition and oxidation state of the as-synthesized manganese oxides. The wide XPS spectrum of MnO_x/CNW displayed in figure 2.8

shows the peaks attributed to the core level of Mn 2p, Mn 3s, O1s and C1s. Based on the areas under these peaks, the elemental ratios of manganese oxides prepared in different deposition times were estimated and the results were collected in table 2.2. It can be seen that when deposition time is 5s, the ratio of C/Mn is much higher than those for longer deposition times, indicating partial formation of manganese oxides on CNW. Increasing deposition time from 30s to 60s showed a slight change in the elemental ratios that means there is negligible change in the thickness of the film while infiltrating of manganese oxide into the gaps of CNW occurs, as confirmed by the SEM observations.

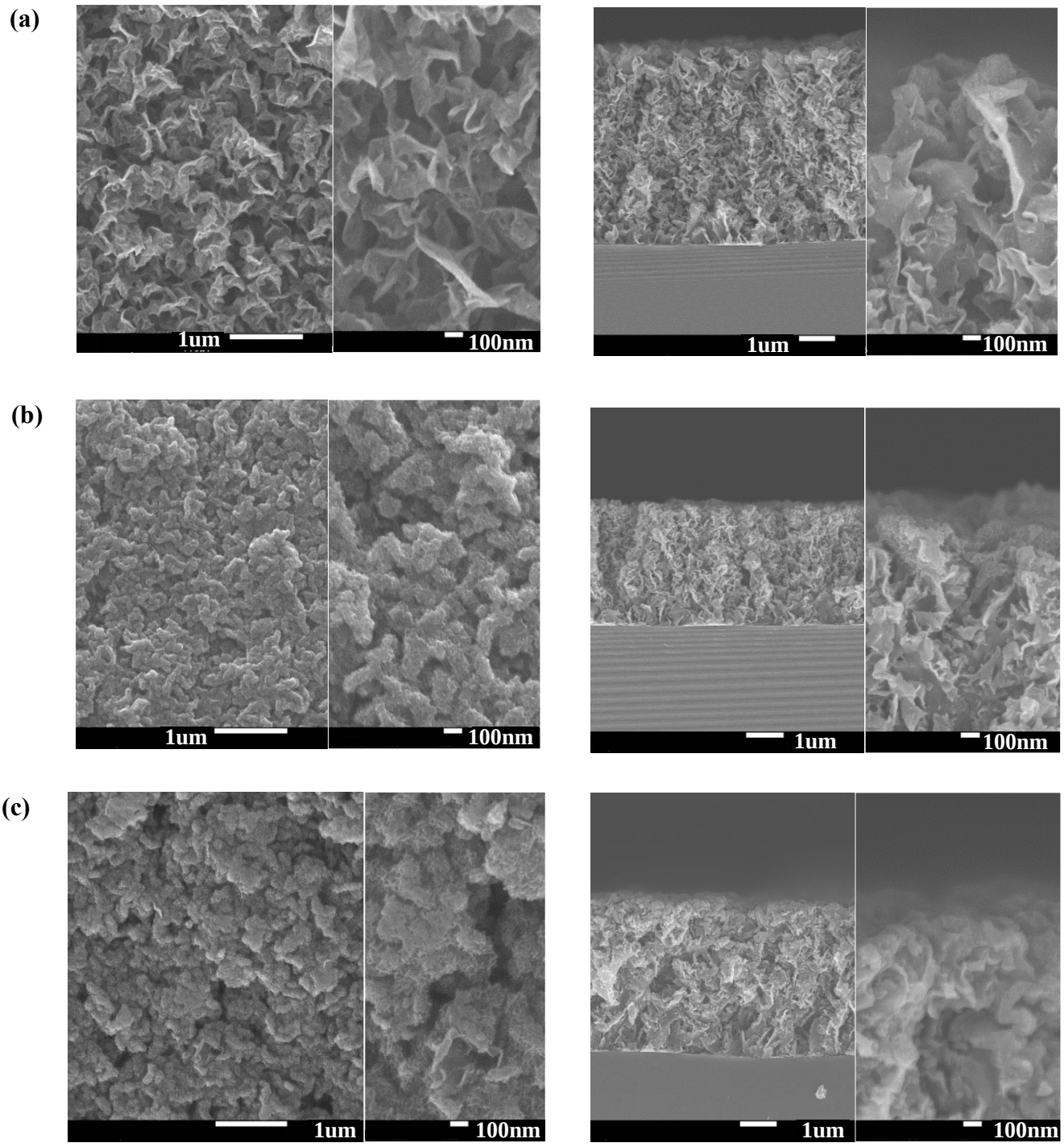

Figure 2.7. SEM top images of MnO_x/CNW and their cross sections prepared in 5s (a), 30s (b), and 60s (c)

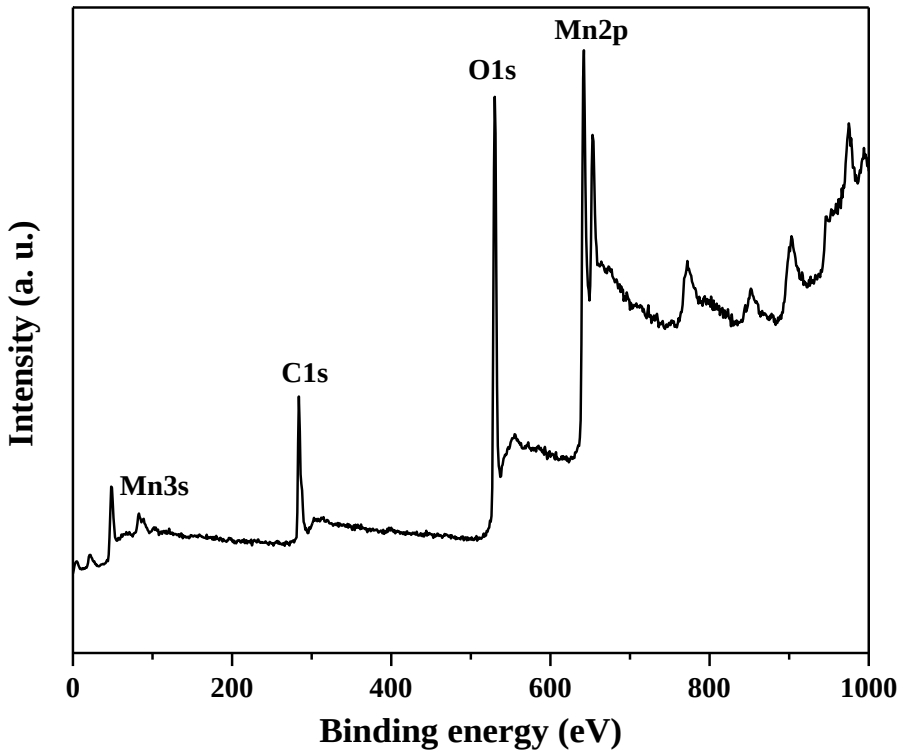

Figure 2.8. XPS survey spectra for MnO_x/CNW prepared in 60s

Table 2.2. Elemental percentages and ratios for MnO_x/CNW prepared in different deposition times

Deposition time (s)	C%	O%	Mn%	C/Mn	O/Mn
5	74.7	12.4	12.9	5.79	0.96
30	49	30.5	20.5	2.39	1.49
60	45.6	33.8	20.6	2.21	1.64

Because, the electrochemical sensing characteristics are correlated with the manganese oxidation state, the manganese average oxidation state for each sample was further analyzed by the deconvoluted O1s spectra and the multiple splitting of Mn3s core level spectrum. As exhibited in figure 2.9 and table 2.3, the O1s spectra could be deconvoluted into three constituents corresponding to various oxygen containing chemical bonds including water molecule (H-O-H), hydroxide (Mn-OH), and oxide (Mn-O-Mn). It is observed that percentage of Mn-OH for the film prepared in 5s is much higher than the coatings fabricated in longer deposition times. This can be due to the partial formation of MnO_x on CNW as a nucleation spots that attend only on the top surface of CNW, mostly creating hydroxy group. While increasing deposition time resulted in higher lattice oxygen content rather than hydroxy group, having the highest amount for MnO_x prepared in 60s, although increasing deposition time from 30s to 60s showed a slight change. This tendency agrees with that of C/Mn elemental ratio and can be attributed to the fact that with increasing deposition time, thickness of film increases initially but saturates in longer deposition time while infiltrating of manganese oxide into the gaps of CNW occurs. Therefore, oxygen does not take part more in surface hydroxide group but participates as lattice oxygen that results in higher oxidation state for manganese in MnO_x prepared in longer deposition time.

The average manganese oxidation state for the prepared electrodes can be calculated from the intensities of the Mn-O-Mn and Mn-OH components according to Eq. (2.1),

$$\text{Ox. State} = \frac{4\,(S_{\text{Mn-O-Mn}} - S_{\text{Mn-OH}}) + 3\,(S_{\text{Mn-OH}})}{S_{(\text{Mn-O-Mn})}} \qquad (2.1)$$

where *S* is signal of the different components of the O1s spectra [121]. Based on O1s data, the average oxidation of 1.5, 3.3, and 3.5 were obtained for the nanocomposite films prepared for 5s, 30s, and 60s, respectively, revealing same tendency with those estimated from O/Mn elemental ratios reported in table 2.2.

The Mn3s splitting energies were also used for determining oxidation state of Mn. As shown in figure 2.9 and table 2.3, the Mn3s spectra shows a peak splitting caused by the parallel spin coupling of the 3s electron with the 3d electron upon photoelectron ejection. This energy separation between the two peaks is described in terms of exchange interaction energy as in Eq. (2.2),

$$\Delta E = (2S+1)\,K[3s, 3d] \qquad (2.2)$$

where *S* stands for the total spin of unpaired electrons in the 3s and 3d levels in the final states and *K*[3s, 3d] is the exchange integral between 3s-3d energy levels [122]. Since in lower Mn valances, there are more unpaired electrons in the 3d orbital, more interaction can occur upon photoelectron ejection, increasing the splitting of the 3s peaks. A graphical representation of the separation of peak energies (*ΔE*) as a function of the manganese oxidation is displayed in ref [123] as shown below.

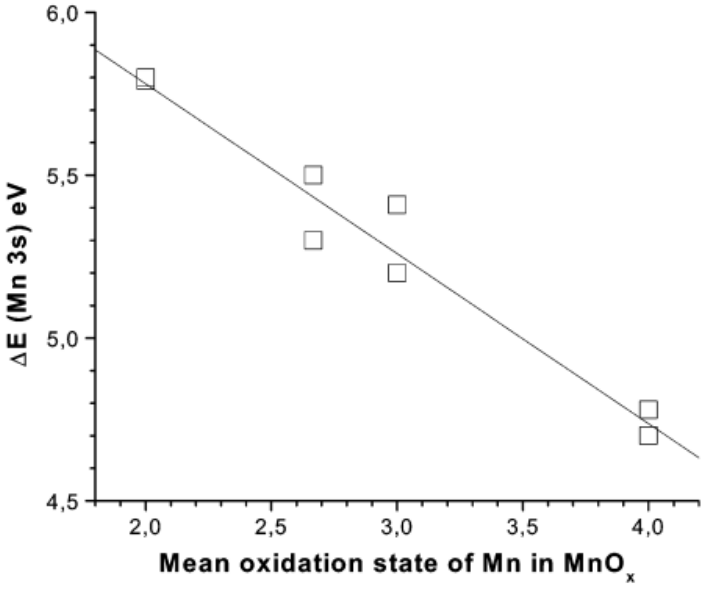

Fig.4 in Ref. [123]. Separation of peak energies ΔE representative of the Mn 3s multiple splitting as a function of the mean manganese oxidation state according to Eq. (2.2).

For the prepared nanocomposite electrodes in 5s, 30s, and 60s, the peak splitting of the doublet of Mn3s core level spectra were obtained 5.93, 5.32 and 5.01eV, respectively, resulting in the oxidation state of 2.1, 3.1, and 3.5 [Fig.4 in Ref. [123]. These results are in good agreement with O1s data and O/Mn elemental ratios.

According to the obtained results, it can be concluded that electrodeposited MnO_x coatings except the coating prepared in 5s, exhibit a mixed Mn valance states, where by increasing deposition time, the oxidation state of Mn increases.

The possible electrodeposition mechanism can be proposed as Ref. [124] that in initial step, two Mn^{2+} aqua complexes participate in one-electron, one proton equilibrium to form two Mn^{3+} species in solution as following equilibriums:

$$2Mn^{II}(H_2O)_6^{2+} \rightleftharpoons 2Mn^{III}(H_2O)_5(OH)^{2+} + 2H^{+} + 2e^{-} \quad (2.3)$$

$$2Mn^{III}(H_2O)_5(OH)^{2+} \longrightarrow Mn^{II}(H_2O)_6^{2+} + Mn^{IV}(H_2O)_4(OH)_2^{2+} \quad (2.4)$$

These Mn^{3+} species disproportion and reform Mn^{2+} aqua and a Mn^{4+} species which can add to the MnO_x surface. The Mn^{4+} formed at newly deposited edge sites may subsequently react with solution Mn^{2+} to form Mn^{3+} on the surface of MnO_x [Fig. 10 in Ref 124].

In this work, according to the XPS and SEM results, we selected 60s as the optimum condition and electrochemical measurements were performed applying MnO_x/CNW prepared in 60s in the next chapter.

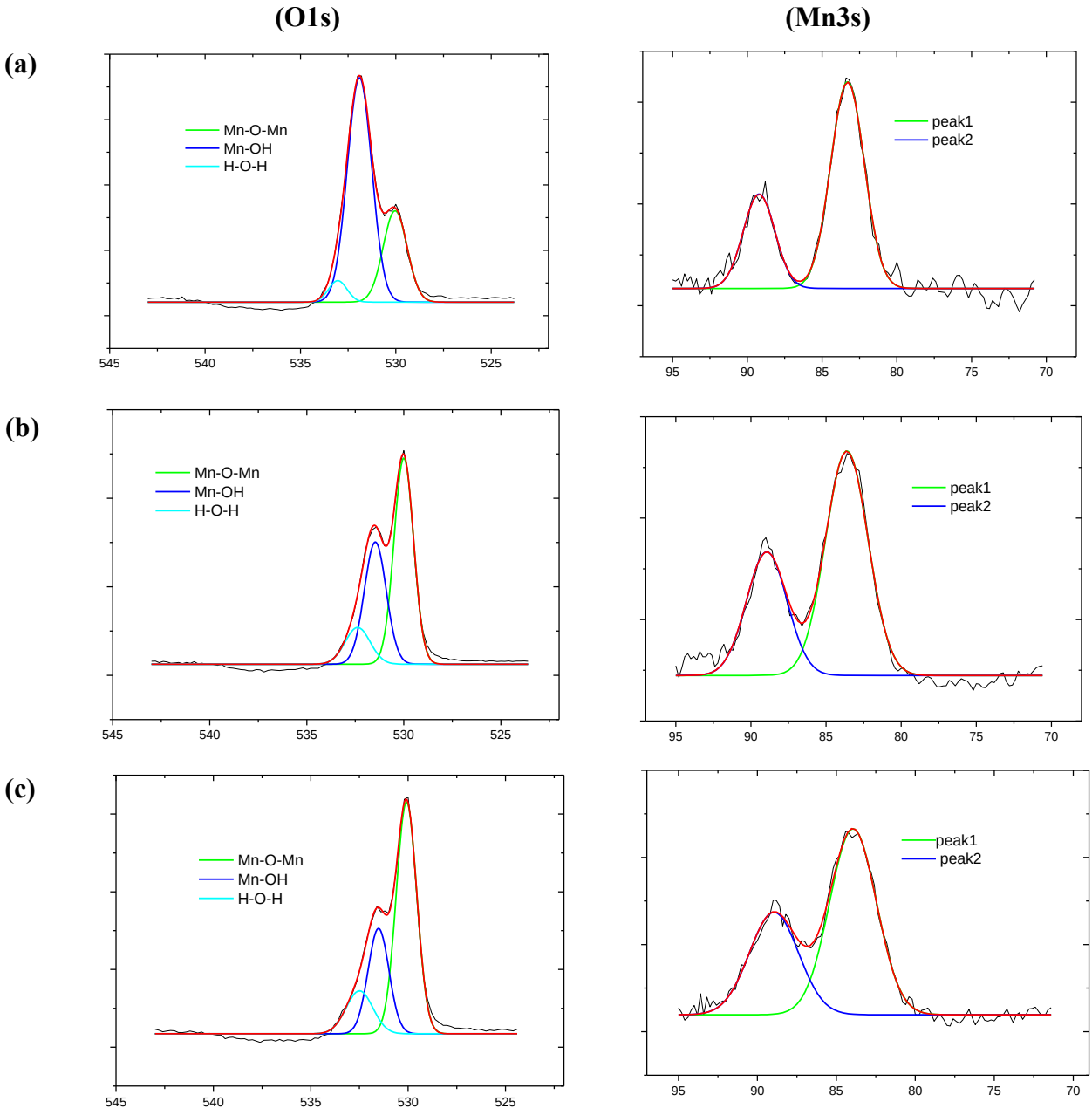

Figure 2.9. XPS spectra of MnO_x films prepared in 5s (a), 30s (b), and 60s (c) in O1s and Mn3s regions

Table 2.3. Data obtained from XPS spectra

Deposition time (s)	Mn3s			O1s			Mn oxidation state derived from Mn3s/O1s
	Eb(1)/eV	Eb(2)/eV	ΔE/eV	Eb/eV		Area%	
5	83.29	89.22	5.93	Mn-O-Mn	530.04	27.14	2.1/1.5
				Mn-OH	531.90	67.96	
				H-O-H	533.04	4.89	
30	83.62	88.94	5.32	Mn-O-Mn	530.0	52.62	3.1/3.3
				Mn-OH	531.47	35.13	
				H-O-H	532.38	12.04	
60	83.94	88.95	5.01	Mn-O-Mn	530.08	58.71	3.5/3.5
				Mn-OH	531.52	27.12	
				H-O-H	532.50	14.17	

2.4. Summary of the chapter

In this chapter, we investigated fabricating of CNW in different deposition times and select the sample prepared in optimum condition to further deposit MnO_x on. Electrochemical anodic deposition technique was applied to synthesize MnO_x film on CNW applying different deposition times. SEM and XPS results confirmed that in the beginning, the deposition is fast while it saturates in longer deposition times. One of the possible explanations for this self-limiting deposition mechanism can be attributed to the very low electric conductivity of MnO_x as compared with that of CNW. Furthermore, it was observed that electrodeposited MnO_x coatings except the coating prepared in 5s, exhibit mixed Mn valance states, where by increasing deposition time, the oxidation state of Mn increases.

Chapter 3. Evaluating electrochemical sensor performance of MnO_x/CNW nanocomposite electrode towards H_2O_2

3.1. Background of the chapter

Accurate detection of hydrogen peroxide (H_2O_2) is of great significance because of its wide application in many industrial and environmental processes, and also serving as an essential intermediate in biochemical, food, pharmaceutical, and clinical analysis [125–127]. Various techniques such as titrimetry [83,84], chromatography [128], fluorescence [89,129], chemiluminescence [87], and electrochemistry [73,90,114] have been employed for the quantitative determination of H_2O_2. Among these methods, electrochemical technique has attracted extensive attention due to its high sensitivity and selectivity, low cost, and simple operation.

Electrochemical sensors for detecting of H_2O_2 are generally classified into two major types including enzymatic and non-enzymatic sensors [98]. Although, electrochemical biosensors based on the electrocatalysis of immobilized enzymes toward H_2O_2 possess good sensitivity and selectivity, they exhibit several limitations such as complex fabrication procedures, limited lifetime, high cost, and poor stability. Therefore, much effort has been devoted to the development of enzyme-free H_2O_2 sensors with low detection limit and wide response range [100].

To obtain highly efficient enzyme-free sensors, modification of the electrode surface with suitable materials, which enhance the electron transfer between electrode and analyte (H_2O_2) becomes increasingly important.

For this purpose, noble metal catalysts such as Au, Pt, Pd, Ag and their alloys have been successfully applied to improve the electron transfer kinetics [93,94,102,103]. However, the noble metal-based sensor has some disadvantages such as low sensitivity, surface poisoning, high cost and limited availability of precious noble metals. Therefore, developing of low-cost, highly sensitive and selective non-enzymatic H_2O_2 sensors without applying noble metals is of great interest [101,104].

Recently, a number of studies have been carried out to synthesize new nanocomposite catalysts using transition metals, their oxides or complexes to improve the electrochemical response to H_2O_2. As an important transition metal oxide, manganese oxides nanomaterials have drawn attention in electrochemical sensing of H_2O_2, due to its low cost, abundant resources, environment friendliness, and catalytic activity which can promote H_2O_2 decomposition [74,109]. But the main disadvantage

of these materials that encounter many challenges with their practical application is low electronic conductivity, low ion diffusion constant and Mn dissolution into electrolyte [130,131]. To overcome these problems, combining nanostructured manganese oxides with an electrically conductive carbon frame can be an important consideration.

The purpose of this chapter is evaluating the electrochemical performance of MnO_x/CNW nanocomposite electrode by cyclic voltammetry (CV) and amperometry measurements and introduce a novel non-enzymatic electrochemical sensor for H_2O_2 detection.

3.2. Experimental

Hydrogen peroxide (H_2O_2), Uric acid ($C_5H_4N_4O_3$), Citric acid ($C_6H_8O_7$), and Ascorbic acid ($C_6H_8O_6$) were purchased from FUJIFILM Wako Pure Chemical Corporation. Phosphate buffer solution was purchased from Hayashi Pure Chemical Ind. Ltd. All chemicals were of analytical grade and deionized water was used throughout the experiment.

Cyclic voltammetry (CV) and amperometry measurements were performed at the same three electrode system used for depositing MnO_x (figure 2.2) to evaluate the sensor performance of the fabricated electrodes. 0.25 M phosphate buffer solution (pH 7.2) was used as the supporting electrolyte. The potential range of -1 to +1 V and a scan rate of $10mVs^{-1}$ were applied for performing CV measurements. The phosphate buffer solution was pulsed with high purity nitrogen for 10 min prior to experiments. Amperometry measurements were done at applied potentials of +0.7V and -0.5V under the stirring and pulsing with N_2 throughout the experiment (Princeton Applied Research Versa STAT 3).

3.3. Result and discussion

3.3.1. Electrochemical properties of MnO_x/CNW/carbon rod nanocomposite electrode

Figure 3.1a illustrates the cyclic voltammograms (CVs) of bare carbon rod, CNW/carbon rod, MnO_x/carbon rod, and MnO_x/CNW/carbon rod electrodes in N_2-saturated 0.25M phosphate buffer solution at a scan rate of 10mV/s. The CV curve without H_2O_2 exhibits no distinct redox peaks for carbon rod, CNW/carbon rod, and MnO_x/carbon rod. However, modified carbon rod electrode with

MnO_x/CNW shows a redox peak between 0 to 0.5V which is assignable to the reduction of Mn species in the absence of H_2O_2, and also it displays higher background current than those of other electrodes, indicating that MnO_x/CNW improves the electroactive surface area.

In order to investigate catalytic activity of fabricated electrode toward H_2O_2, CVs were recorded in the presence of 5mM H_2O_2 (figure 3.1b). As shown in figure 3.1b, there is no obvious redox peak on the bare carbon rod. However, a couple of small oxidation and reduction peaks were observed on the CNW, which may be brought by the excellent electronic conductivity and limited catalytic activity of carbon materials. In the case of MnO_x coating carbon rod, higher redox currents than CNW was observed, demonstrating the electrocatalytic activity of manganese oxides toward H_2O_2 decomposition. The best electrochemical response was displayed with MnO_x/CNW/carbon rod system. The enhanced anodic and cathodic peak currents at the MnO_x/CNW/carbon rod indicated the excellent electrocatalytic activity of MnO_x/CNW composite for the oxidation as well as reduction of H_2O_2. The superior electrochemical behavior of MnO_x/CNW composite toward H_2O_2 can be mainly attributed to the excellent electrocatalytic activity of manganese oxides combined with high surface area and great electroconductivity of CNW.

(a)

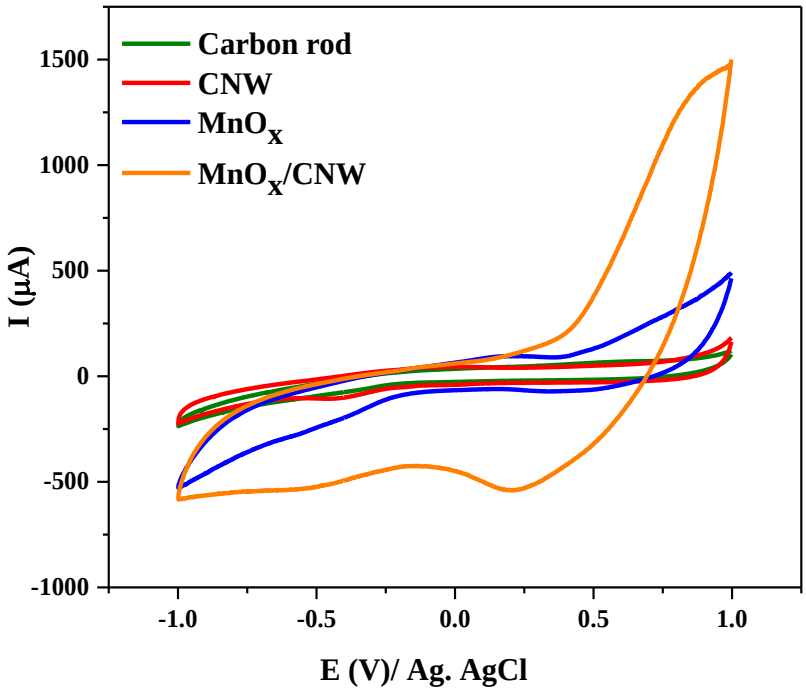

(b)

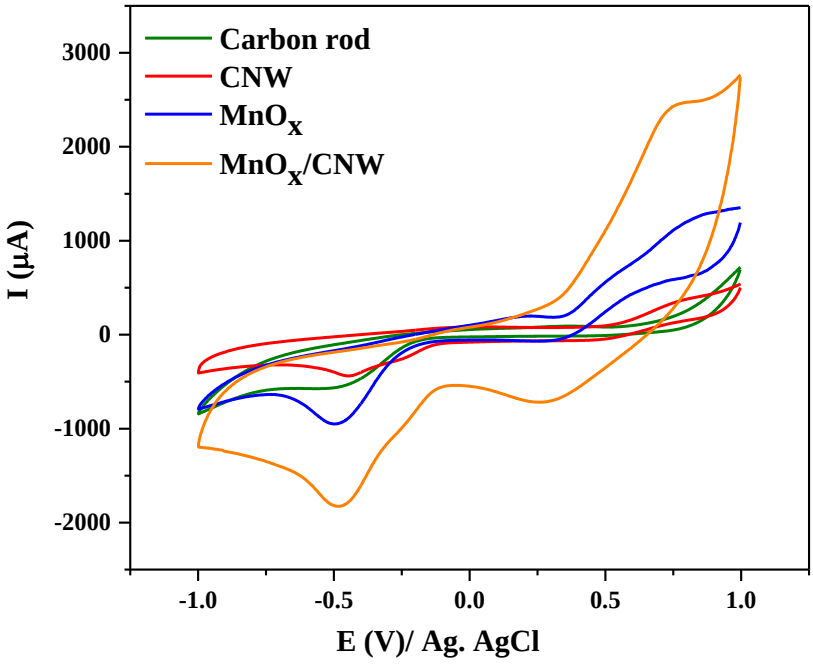

Figure 3.1. Cyclic voltammograms obtained using bare carbon rod, CNW, MnO_x, MnO_x/CNW in the absence of H_2O_2 (a) and in the presence of 5mM H_2O_2 (b)

The electrocatalytic response of MnO_x/CNW to H_2O_2 was further investigated by amperometric technique. Figure 3.2a shows the typical amperometric response of MnO_x/CNW upon the successive addition of H_2O_2 every 60s into the phosphate buffer solution under stirring and pulsing N_2 at +0.7V. The related calibration plot of steady-state currents of MnO_x/CNW electrode against H_2O_2 concentration is depicted in figure 3.2b. The current increased linearly with increasing H_2O_2 concentration and exhibited a wide linear range from 40-10230µM. The regression equation, I (µA)= 438.73C_{H2O2} (mM) + 200.66 with correlation coefficient of 0.9957 was obtained. The limit of detection (LOD) for H_2O_2 detection was estimated to be 0.55µM (S/N=3), using the following equation:

$$\text{LOD} = 3\frac{\text{Stblank}}{\text{B}} \qquad (3.1)$$

where St_{blank} is the standard deviation of the blank solution and B is the slope of the calibration curve in figure 3.2b. The sensitivity was obtained to be 698.6µA. mM^{-1}. cm^{-2}, which is higher than most of those other Mn/carbon nanomaterials-based sensors (table 3.2).

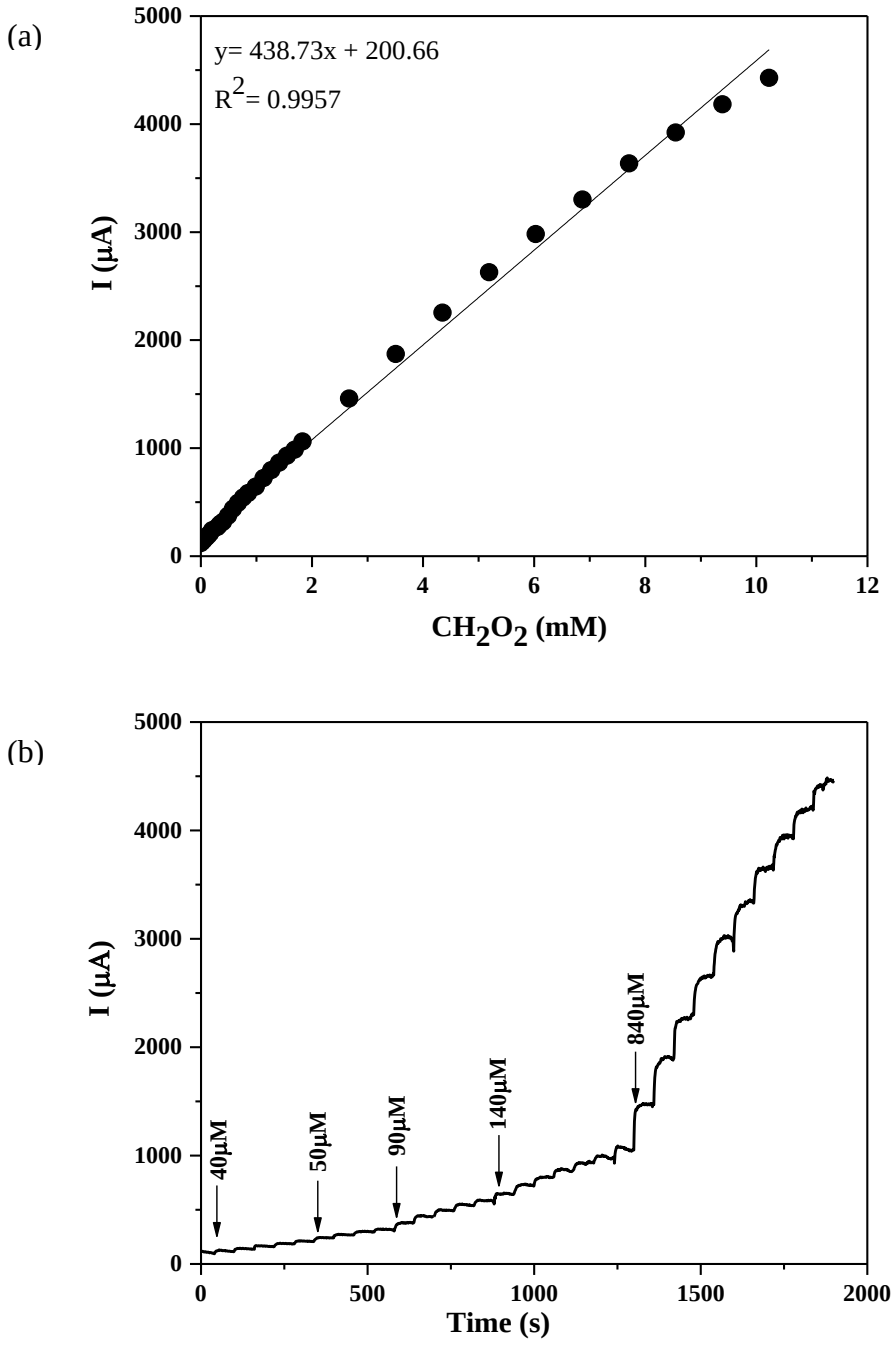

Figure 3.2. Amperometric responses of MnO_x/CNW with increasing H_2O_2 concentration in 0.25M phosphate buffer solution at an applied potential of +0.7V (a), the calibration curve of MnO_x/CNW amperometric responses as a function of H_2O_2 concentration (b)

The amperometric response was also evaluated for the reduction reaction at an applied potential of -0.5V and the result was displayed in figure 3.3. As it was observed in figure 3.3a, a deviation occurs at higher H_2O_2 concentration, which can be related to the high ratio of H_2O_2 to MnO_x. Figure 3.3b shows the calibration curve for H_2O_2 sensor at an applied potential of -0.5V with the linear concentration range of 150-11500µM.

The obtained regression equation was I (µA)= -13.21C_{H2O2}(mM) – 84.44 with a correlation coefficient of 0.9948 and a sensitivity of 21.03 µA mM^{-1} cm^{-2}, which is around 37 times less than the sensitivity obtained at the potential of +0.7V. These results suggest that although MnO_x/CNW electrode has the potential to detect H_2O_2 at both +0.7V and -0.5V, it is highly sensitive to detect H_2O_2 at oxidation potential.

The possible mechanism can be proposed as follows. Firstly, H_2O_2 is adsorbed on MnO_2/CNW active sites. Secondly, the chemical reaction between H_2O_2 and MnO_2/CNW occurs, reducing MnO_2 to the lower state of Mn, which by applying oxidation potential are electro-oxidized back to MnO_2/CNW (Eqs. (3.2) and (3.3)). On the other hand, in the reduction side, some of these reduced Mn species (Eq. (3.2)) can react with H_2O_2 and chemically oxidized to MnO_2/CNW (Eq. (3.4)), which finally by applying the reduction potential are electro-reduced to $Mn(OH)_2$ (or Mn_2O_3/CNW) (Eq. (3.5)).

Because, the sensor contains more Mn (IV) sites than lower states of Mn in its structure, the reaction 3.2 predominates. Therefore, applying oxidation potential leads to higher response current (Eq. 3.3) to compare with the applying reduction potential (Eq. 3.5). This can explain the obtained high sensitivity at the oxidation potential (+0.7V) in comparison to the sensitivity at the reduction potential (-0.5V).

$$MnO_2/CNW\ (s) + H_2O_2\ (aq) \longrightarrow Mn(OH)_2\ (\text{or } Mn_2O_3/CNW)\ (s) + O_2\ (g) \quad (3.2)$$

$$Mn(OH)_2\ (\text{or } Mn_2O_3/CNW)\ (s) + 2OH^-\ (aq) \longrightarrow MnO_2/CNW\ (s) + 2H_2O\ (l) + 2e^- \quad (3.3)$$

$$Mn(OH)_2\ (\text{or } Mn_2O_3/CNW)\ (s) + H_2O_2\ (aq) \longrightarrow MnO_2/CNW\ (s) + 2H_2O \quad (3.4)$$

$$MnO_2/CNW + 2H_2O + 2e^- \longrightarrow Mn\ (OH)_2\ (\text{or } Mn_2O_3/CNW)\ (s) + 2OH^- \quad (3.5)$$

According to the achieved excellent amperometric response at oxidation potential, other sensor performance evaluations were performed at the potential of +0.7V.

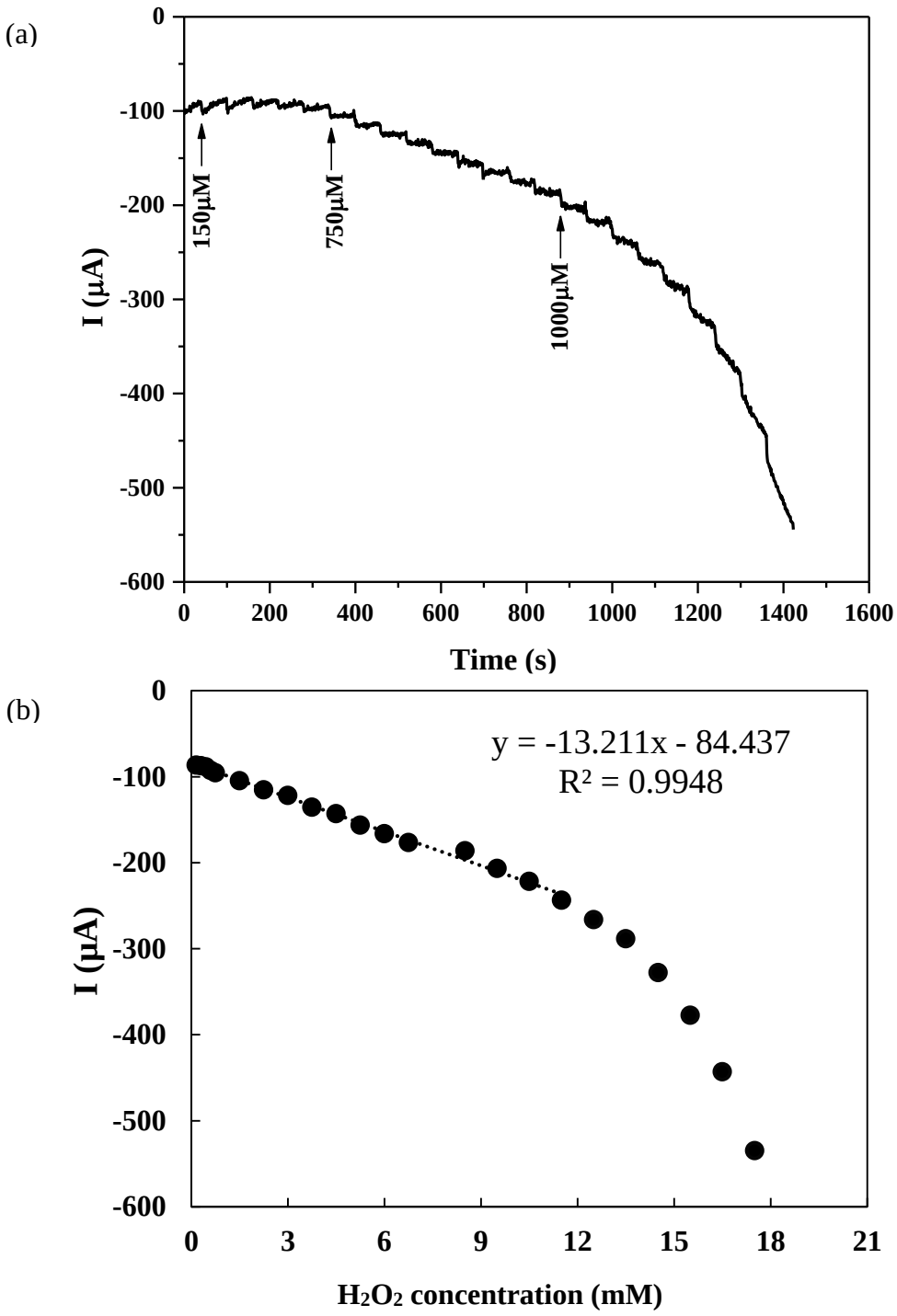

Figure 3.3. Amperometric responses of MnO_x/CNW with increasing H_2O_2 concentration in 0.25M phosphate buffer solution at an applied potential of -0.5V (a), the calibration curve of MnO_x/CNW amperometric responses as a function of H_2O_2 concentration (b)

3.3.2. Reproducibility, stability, and selectivity of MnO_x/CNW/Carbon rod nanocomposite electrode

The reproducibility and stability of the sensor was investigated by measuring the current response of the electrode upon 0.5mM of H_2O_2 in 0.25M phosphate buffer solution at +0.7V. In a series of 5 sensors prepared in a same way, the relative standard deviation (R.S.D) was 3.29%. For one MnO_x/CNW electrode, the R.S.D was found to be 2.34% in 5 successive measurements. The long-term stability of the sensor was also evaluated. The average current response of the electrode remained 92% of its initial value after three weeks of storing in an ambient condition. These results indicate a good reproducibility and stability for the proposed sensor. The selectivity of the electrode was evaluated by an amperometric (i-t) curve upon successive addition of 0.5mM H_2O_2 and 2mM ascorbic acid (AA), uric acid (UA), and citric acid (CA), respectively. As shown in figure 3.4, there is an obvious current response to H_2O_2, while others show negligible response, indicating that the electrode shows high selectivity for H_2O_2 detection.

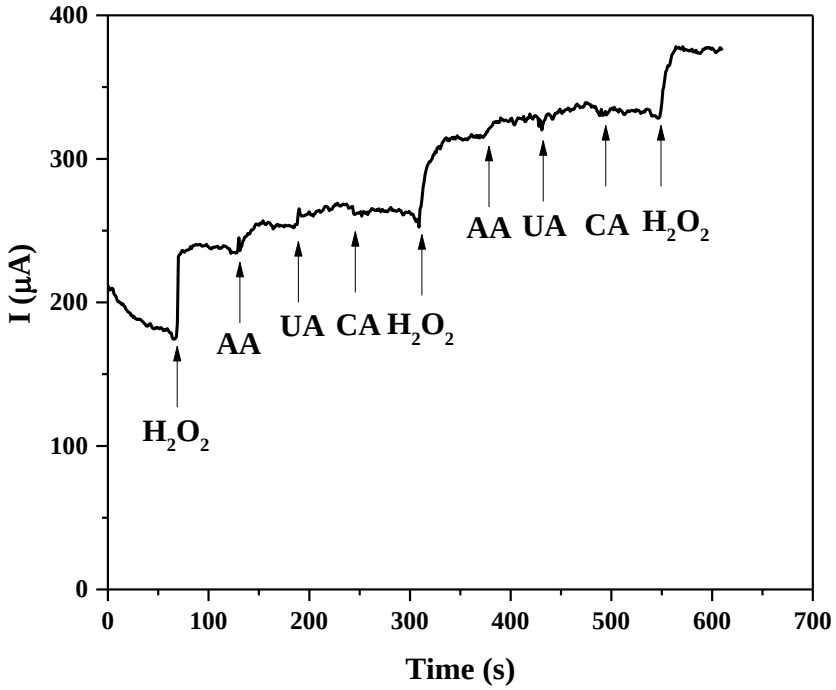

Figure 3.4. Amperometric i-t curve for MnO_x/CNW toward the successive addition of 0.5mM H_2O_2 and 2mM of interferential compounds

The reliability of the fabricated electrode was evaluated by a recovery test. 0.5mM H_2O_2 were added into 0.25M phosphate buffer solution and the current response was measured under the applied potential of +0.7V. Each sample was assayed three times and the converted concentrations and the average recoveries were listed in table 3.1. The recovery rates indicate that the proposed sensor can be a promising candidate for quantitative detection of H_2O_2.

Table 3.1. The detection of H_2O_2 concentration in test samples

sample	added (mM)	found	Recovery (%)
1	0.5	0.5197	103.9
2	0.5	0.5121	102.4
3	0.5	0.4971	99.42

The electrocatalytic performance of MnO_x/CNW electrode was compared to the previously reported Mn/Carbon based electrodes and summarized in table 3.2. The excellent sensor performance of the proposed electrode can be attributed to the edge-plane-based CNW platform with the high surface area which increases the electrocatalytic active area responsible for the fast electron transfer kinetic between MnO_x and CNW. In addition, the main advantages of the proposed electrode are the low cost of fabrication due to using of carbon rod as the substrate and not applying the noble metals in its structure and also, very short synthesis time which takes only 2 minutes (60s for synthesizing CNW, and 60s for depositing MnO_x).

Table 3.2. The comparison of electrocatalytic performance of MnO_x/CNW electrode with previously reported Mn/Carbon based sensors for H_2O_2

Electrode	Sensitivity (μA mM^{-1} cm^{-2})	LOD (μM)	Linear range (μM)	Reference
MnO_2/VACNTs	1080	0.8	1.2 - 1800	[73]
GO/MnO_2	38.2	0.8	5-600	[114]
MnO_2/rGONRs/GCE	-	0.071	0.25-2455	[100]
GO/MnO_2/GCE	191	0.48	4.9-4500	[97]
Au-MnO_2-rGO	980/ 101.6	0.05	0.1-22/22-12600	[108]
δ-MnO_2/CNTs/GCE	243.9	1	50-22000	[74]
Ag-MnO_2-MWCNTs/GCE	82.5	1.7	5-10400	[111]
GOD/PDDA-RGO/MnO_2/AuNPs	83.7	1.8	-	[132]
MnO_2/MWCNTs/Ta	83.3	0.04	3-3025	[112]
MnO_2NPs-CNFs/GCE	71	1.1	10-1500	[133]
MM-HNRS/GS/GCE	1443/642/239	0.16	1-200/200-1200/1200-7440	[115]
MNRS@NG/GS	707.9/229.2	0.2	2-240/240-4440	[116]
MnO_2/graphene nanocomposite	-	2	10-90/200-900	[134]
PANI-MnO_2/GCE	403.3/152.1	0.8	5-50/50-10000	[135]
MnO_2/OMC/GCE	806.8	0.07	0.5-600	[136]
MnO_2/RGO/p25	297.2	0.3	1-4000	[137]
Ag/MnO_2/GO/GCE	105.4	0.7	3 -7000	[117]
MnO_x/CNW	698.6	0.55	40-10230	this work

3.4. Summary of the chapter

In this chapter, the electrochemical sensing performance of MnO_x/CNW/carbon rod electrode towards H_2O_2 was evaluated. Compared to the bare CNW and MnO_x electrodes, the MnO_x/CNW nanocomposite electrode displays high electrocatalytic activity towards the oxidation and reduction of H_2O_2. This can be attributed to the combination of high conductivity and large surface area of CNW with excellent electrocatalytic ability of MnO_x towards H_2O_2 decomposition. The performance of this sensor is satisfactory due to its low LOD, wide linear range, and excellent sensitivity, also displaying good stability, reproducibility and negligible interferences from AA, UA, and CA. This study demonstrates a new pathway for the application of carbon nanowalls in electrochemical sensing.

Chapter 4. Plasma surface treatment of CNW

4.1. Background of the chapter

Owing to the large surface area, highly active graphene edges, and fabricating without the use of catalysts, CNW has shown its fascinating application as electrode material for different electrochemical systems such as electrodes for batteries and supercapacitors [6–8], fuel cells supports [14], oxygen reduction [11], and electrochemical sensors [12,138]. In many of those electrochemical studies for CNW applications, hybrid structures such as CNW/metal oxide deposits, CNW/ biocatalyst, and CNW/Pt nanoparticle have been utilized. However, in these hybrid CNW structures, CNW was mainly used as a base material with high conductivity and large surface area and little attention has been paid for direct application of CNW as a metal/enzyme-free electrode in electrochemical systems through its intrinsic electrochemical ability due to the highly active graphene edges.

In previous chapters, we introduced a hybrid CNW structure combined with the transitional metal oxide MnO_x as an efficient non-enzymatic H_2O_2 sensor. In this chapter, we aimed to enhance the electrochemical sensing performance of CNW by intrinsic modification, so that the optimum modified CNW can be utilized as a potential metal-free electrochemical sensor.

Plasma-based techniques have recently gained considerable attention as a versatile and biocompatible technique for modifying and inducing changes in the characteristic of nanomaterials. Various gas mixtures containing H_2, O_2, and N_2 introduced in plasma can be used to induce activation and incorporation of functional groups on CNW surface [52]. For instance, hydrogen plasma treatment is used for etching and producing high quality CNW as well as increasing its surface area [52,139,140]. Nitrogen plasma can be used for doping and grafting of the amino functional groups into the CNW structure and consequently increase its electrical conduction and improve the electron field emission [141,142]. Post synthesis treatment in oxygen plasma can lead to oxidation and formation oxygen-containing functional groups [52,55].

At the same time, the functional properties of CNW can also be greatly influenced by the presence of structural defects [14]. Among the various gas mixtures, oxygen has been found to simultaneously etch and introduce functional groups onto the surface of carbon nanomaterials. It has also been reported that the crystallinity of carbon nanostructures can be destroyed in high energy plasma with a high density of oxygen ions through continuous etching [143]. The article by Shimoeda et al. has demonstrated that taking advantage of utilizing oxygen atoms for the selective etching from the top edges of CNW without etching reaction of the wall surface, which

can be essential for carbon nanoelectronic devices [144]. In addition, there is a report that oxygen plasma treatment of CNW can enhance the aqueous solution penetration into the gaps between the walls [55]. Furthermore, the enhancement of electrochemical capacitor performance of oxygen plasma treated CNW was reported by Sahoo et al [56]. Nevertheless, no specific studies on improving CNW performance as electrochemical sensor through its intrinsic modification by oxygen plasma has been reported so far. In this chapter, we report the modification of CNW with different concentration of oxygen plasma and characterize their structures. Further investigating of their performance in electrocatalysis and sensing applications as a metal-free electrode will be discussed in chapter 5.

4.2. Experimental

CNW was prepared in 60s by the same method reported in chapter 2. A low-pressure plasma functionalization technique using the same apparatus for CNW synthesis was applied to functionalize the CNW. After synthetizing CNW, the chamber was pumped down to 1Pa. Then different concentration of oxygen (from 0.0 to 2.0sccm) admixed to 10sccm Argon were introduced into the chamber and then plasma was ignited at 250 Pa at a microwave power of 100W for 10s. The plasma emission was monitored by a spectrometer (Ocean Optics, HR4000, with a 200 to 1100 nm grating, 5um entrance slit and 3648 pixels CCD) covering the spectral range 200-1100 nm with 0.75 nm spectral resolution. Finally, the substrates were taken out of the chamber for further characterization and applications.

Surface morphology characterization of CNW was carried out using a field emission scanning electron microscopy (JSM-7500F) operated at voltage of 5.0kV and beam current of 10μA for all the samples. Raman spectroscopy was performed to study the structural changes of the samples after plasma treatment using JASCO NRS-4100 at an excitation wavelength of 532nm. The hydrophilicity of the samples was evaluated by measuring the contact angle of deionized water on the surface of CNW samples by sessile drop method, using a digital microscope (aigo, DMS012). The chemical composition and bonds of the samples were analyzed by X-ray photoelectron spectroscopy (XPS, PHI5000 VersaProbe) using a monochromatic Mg K_α X-ray source. The pass energies of 117.4eV and 23.5eV was applied for recording the wide scan and the high-resolution spectra, respectively.

4.3. Result and discussion

4.3.1. Morphology of as-grown CNW and plasma treated CNW samples

To understand the effect of oxygen plasma treatment on CNW morphology, a series of CNW films were treated at different plasma conditions. The change in surface morphology of CNW after each treatment was analyzed by FE-SEM and is presented in figure 4.1a-e. A top view and cross section image showing the morphology of as-grown CNW is presented in figure. 4.1a, while the CNW treated in different oxygen flow rates are displayed in figure. 4.1b-e.

The preservation of morphology after exposing the CNW samples to 10sccm Ar and O_2/Ar: 0.1/10sccm plasma is clearly evident from figure 4.1a-c. As it can be seen, when the oxygen flow rate is very low (0.1sccm), no obvious damage was caused at the edge or the wall structure, but the slight reduction in the height of CNW was observed. Increasing oxygen flow rate from 0.1 to 1.0sccm, resulted in more height reduction as well as etching the edges of CNW. In addition, from figure 4.1d inlet (after treatment), it can be derived that increase in morphological defect results in an increment in the surface roughness as well. Further increase in oxygen flow rate from 1.0 to 2.0sccm resulted in mainly destruction of CNW structure. The CNW was disappeared from the edges of the silicon substrate and only a thin layer of CNW with wider wall-to-wall space was left in the middle part of the substrate which was used for characterization. Figure 4.1e shows the SEM images of the left CNW in the middle of silicon substrate and its destroyed border. From these results, it can be concluded that because at higher oxygen flow rates, the high density of excited species and radicals are produced, strong interaction with the carbon surface can occur which consequently increase the etch rate and create certain defects in the surface structure. The increased etch rate can also result in removing the top layers of CNW surface and decreasing the height of the samples as observed from the cross-section images. For better comparison, the SEM images of all CNW samples before and after treatment with different O_2/Ar plasma condition and their relevant heights are given in figures 4.2 to 4.5. This reduction in the height of CNW can suggest an explanation for the increment in wall-to-wall spacing of CNW by increasing oxygen flow rates in the plasma gas mixture. As the cross-section results display, there is 65% reduction in the height of the CNW film after treating with O_2/Ar: 2.0/10sccm. This means that the top layers which contain small flakes and thinner branches with small wall to wall space are disappeared and the bottom part which has large flakes and less branches with wider wall to wall space are appeared at the top surface [28].

(a)

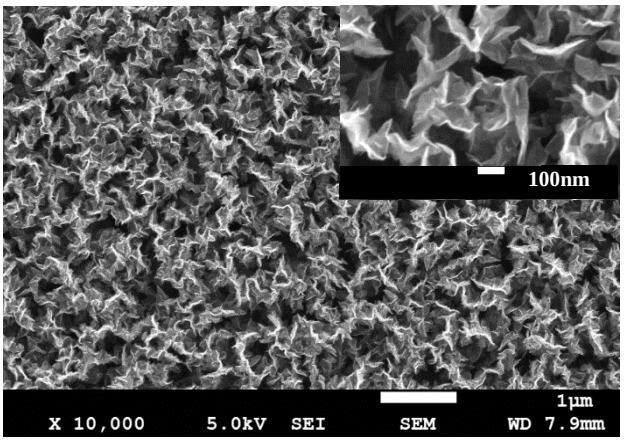
100nm
1µm
X 10,000 5.0kV SEI SEM WD 7.9mm

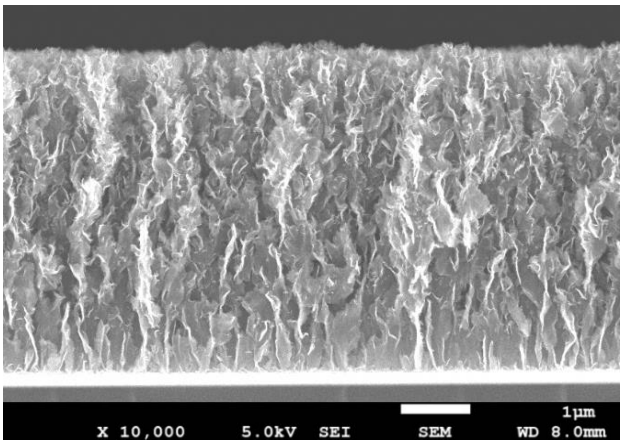
1µm
X 10,000 5.0kV SEI SEM WD 8.0mm

(b)

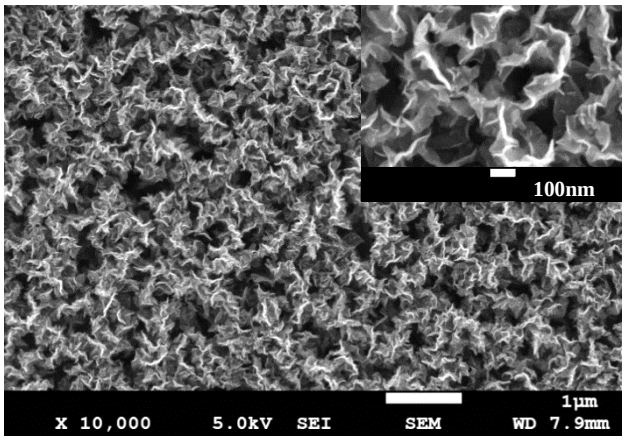
100nm
1µm
X 10,000 5.0kV SEI SEM WD 7.9mm

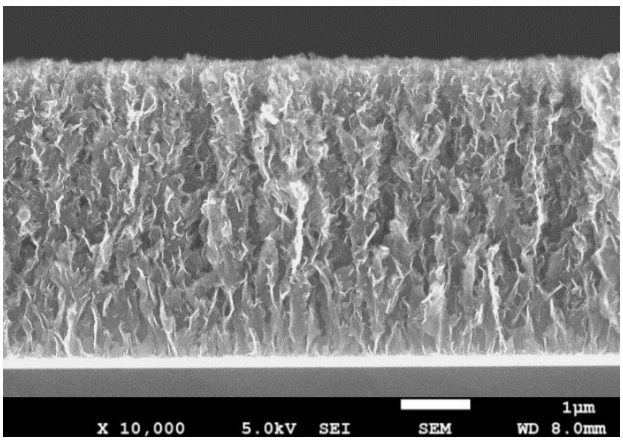
1µm
X 10,000 5.0kV SEI SEM WD 8.0mm

(c)

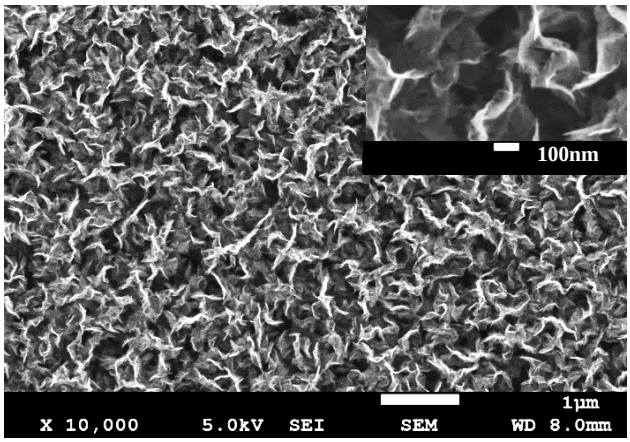
100nm
1µm
X 10,000 5.0kV SEI SEM WD 8.0mm

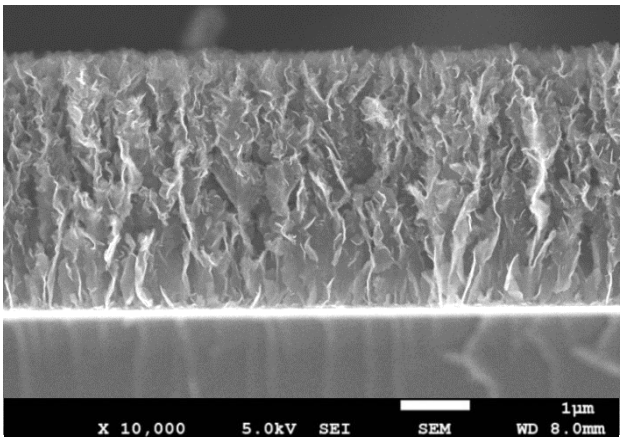
1µm
X 10,000 5.0kV SEI SEM WD 8.0mm

(d)

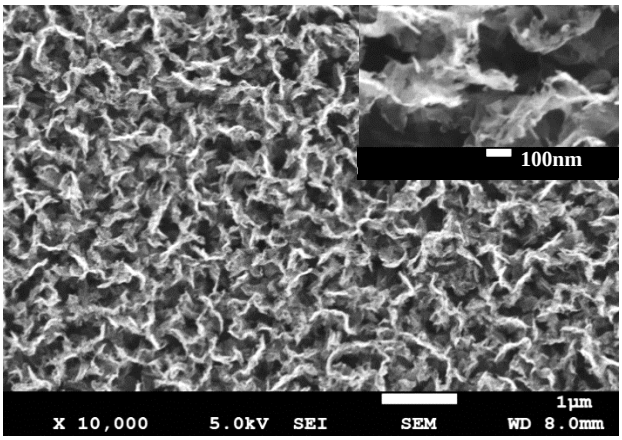

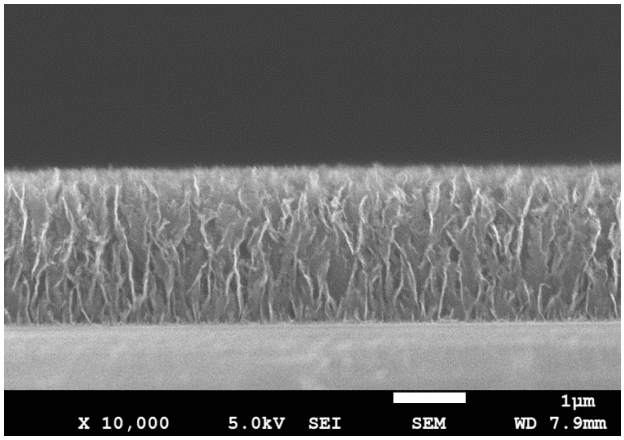

(e)

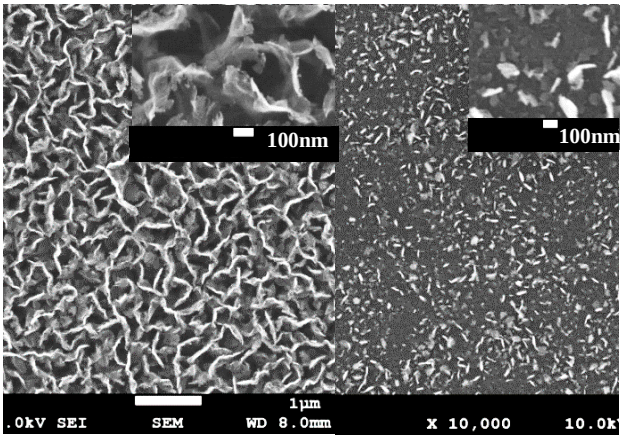

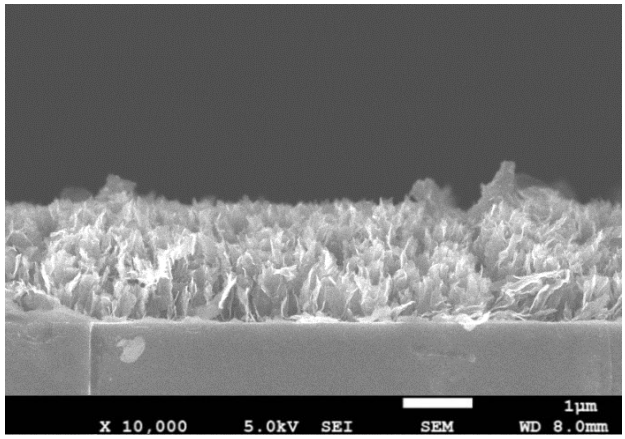

Figure 4.1. FE-SEM images of the CNW without and with plasma treatment; (a) as-grown CNW, (b) O_2/Ar: 0.0/10sccm, (c) O_2/Ar: 0.1/10sccm, (d) O_2/Ar: 1.0/10sccm, and (e) O_2/Ar: 2.0/10sccm

(a)

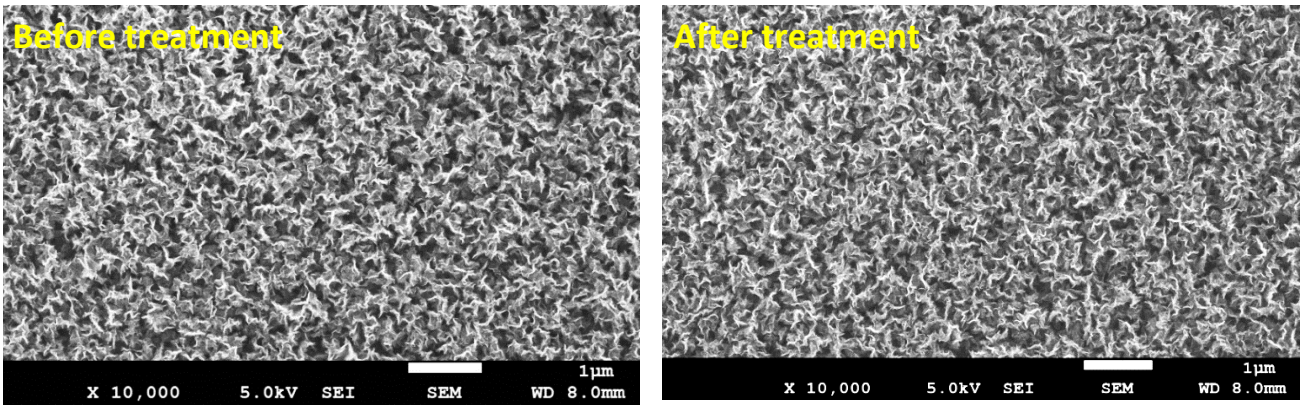

(b)

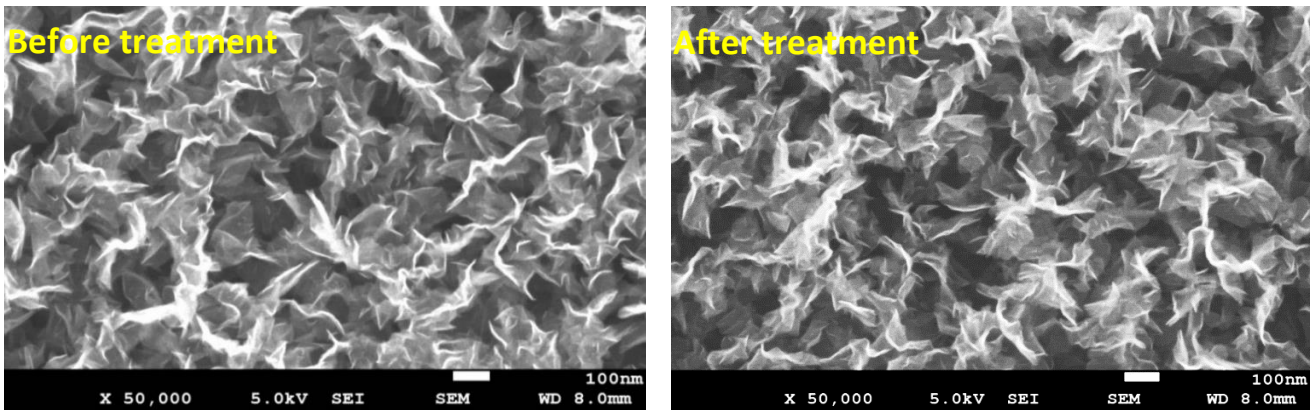

(c)

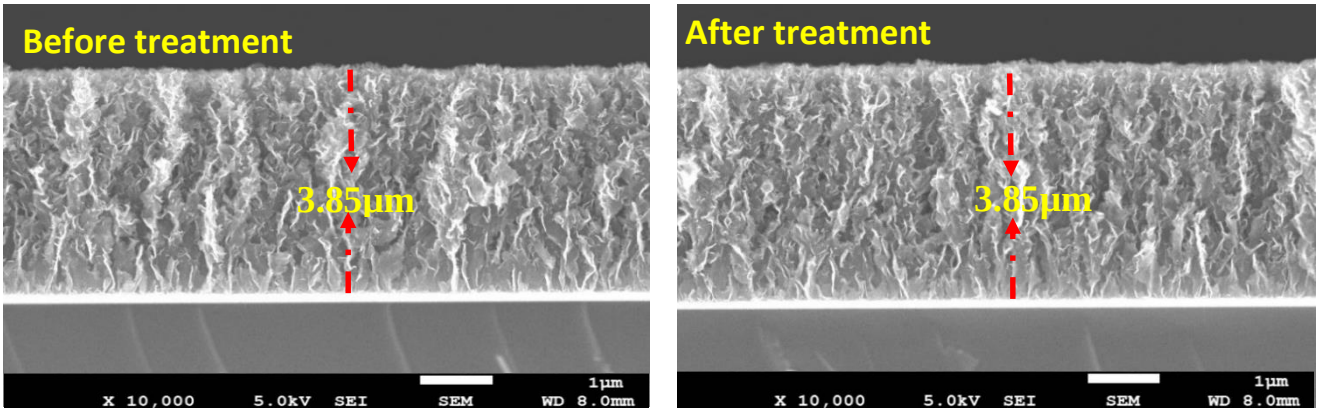

Figure 4.2. SEM images of CNW sample before and after treatment with O_2/Ar: 0.0/10sccm at low magnification (a), high magnification (b), and cross section (c)

(a)

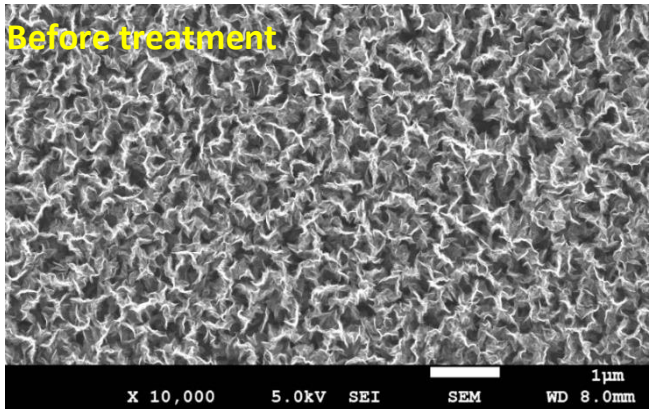

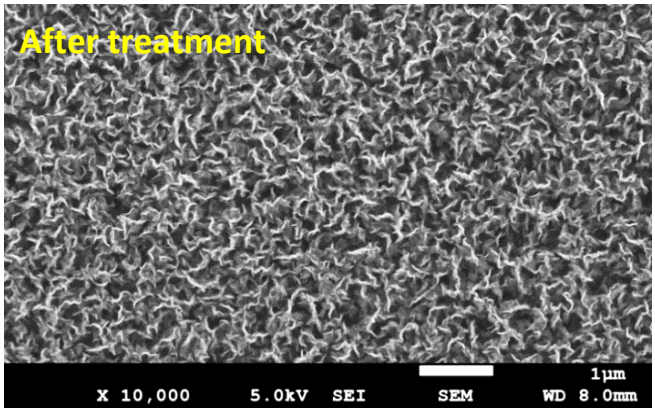

(b)

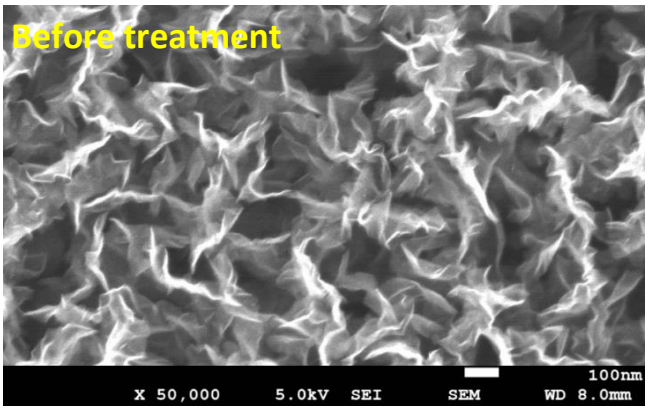

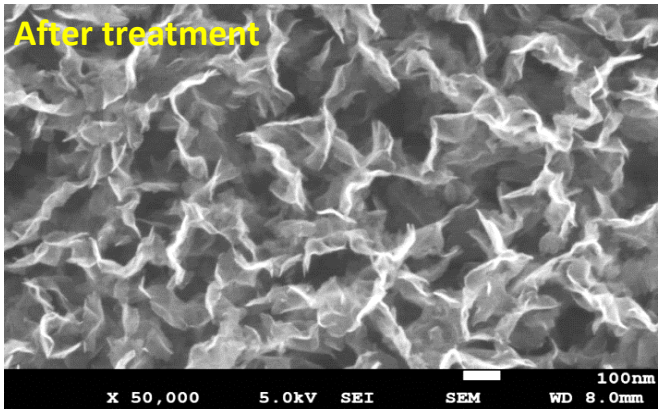

(c)

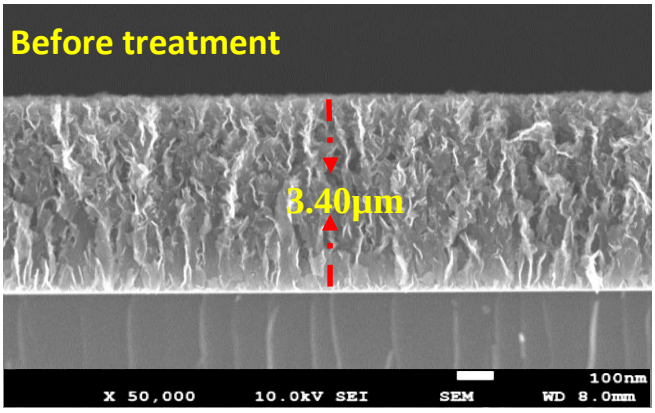

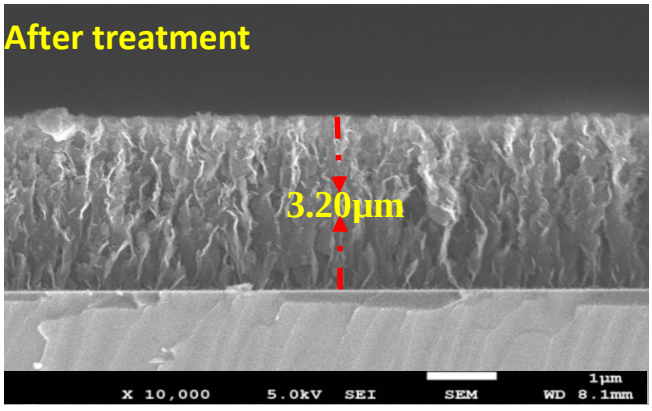

Figure 4.3. SEM image of CNW sample before and treatment with O_2/Ar: 0.1/10sccm at low magnification (a), high magnification (b), and cross section (c)

(a)

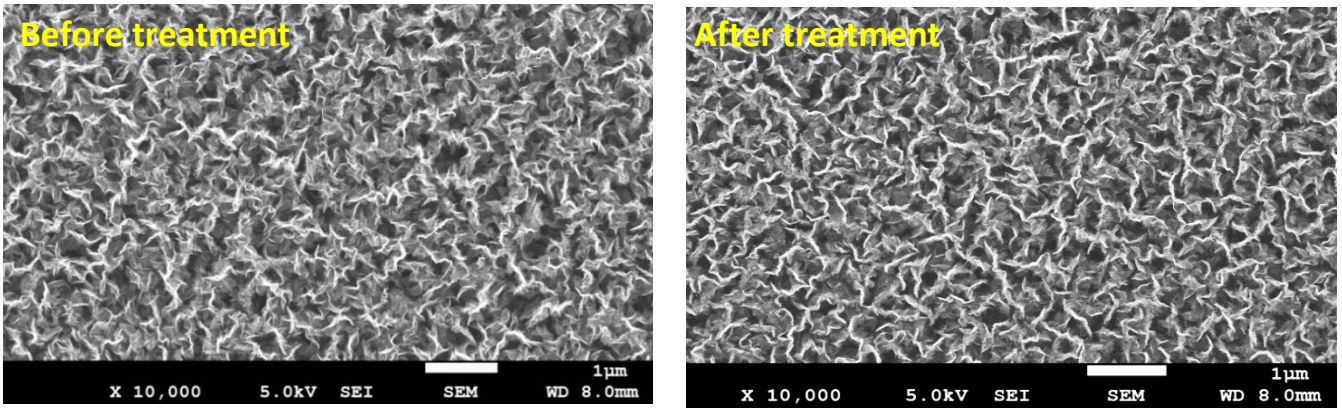

(b)

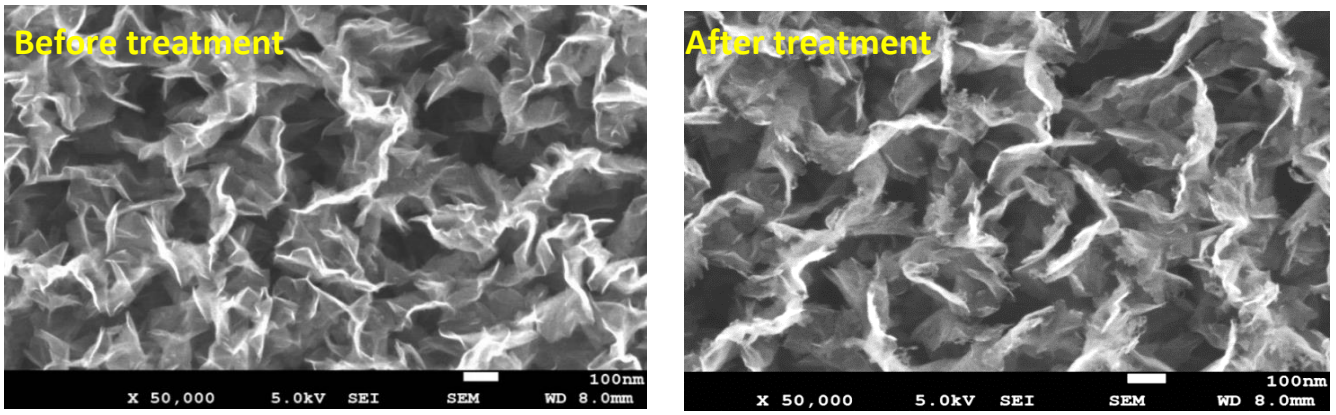

(c)

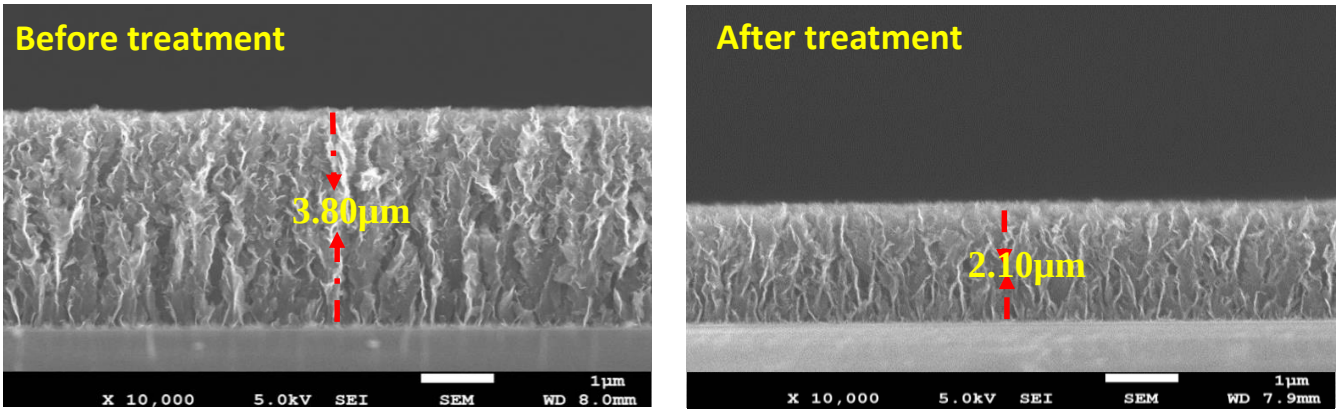

Figure 4.4. SEM image of CNW sample before and after treatment with O_2/Ar: 1.0/10sccm at low magnification (a), high magnification (b), and cross section (c)

(a)

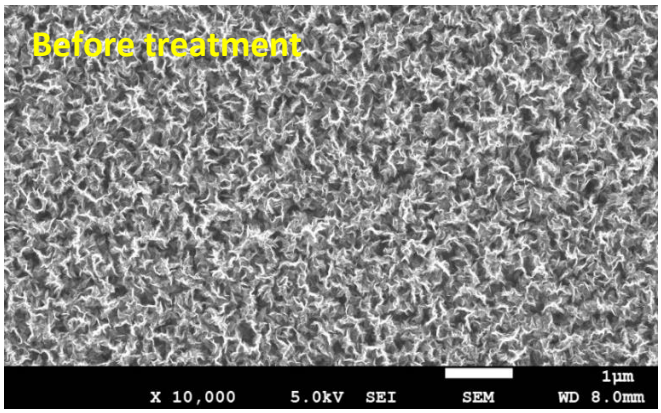
Before treatment
X 10,000 5.0kV SEI SEM 1µm WD 8.0mm

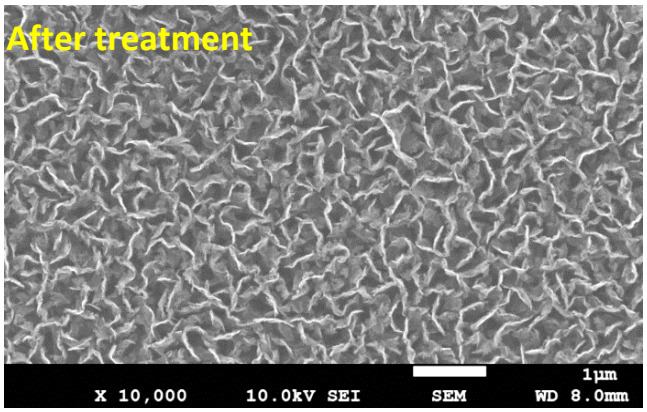
After treatment
X 10,000 10.0kV SEI SEM 1µm WD 8.0mm

(b)

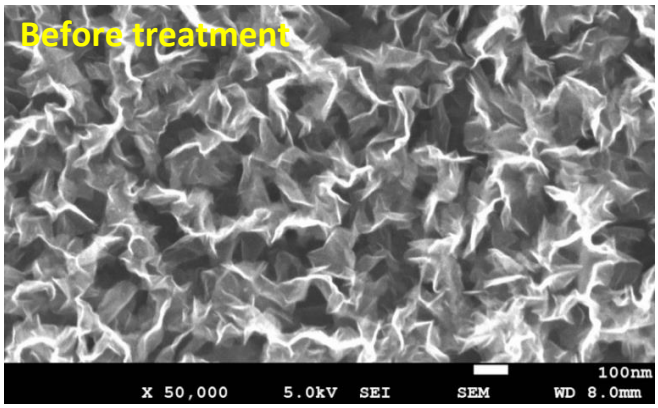
Before treatment
X 50,000 5.0kV SEI SEM 100nm WD 8.0mm

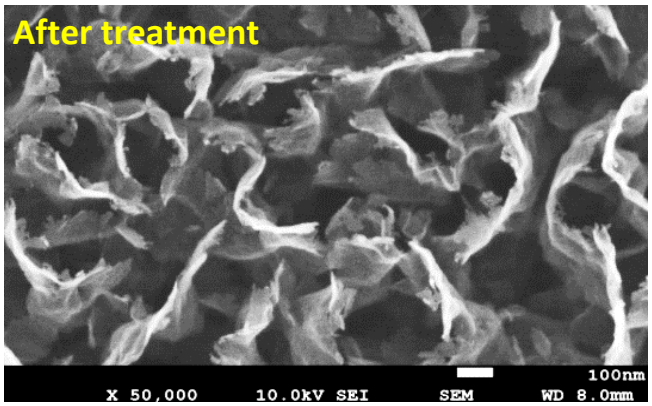
After treatment
X 50,000 10.0kV SEI SEM 100nm WD 8.0mm

(c)

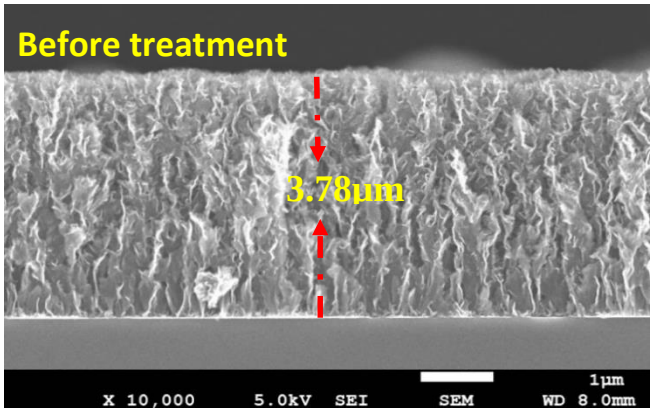
Before treatment
3.78µm
X 10,000 5.0kV SEI SEM 1µm WD 8.0mm

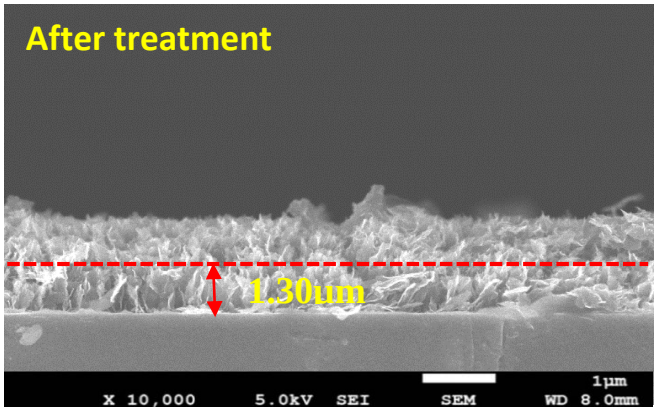
After treatment
1.30um
X 10,000 5.0kV SEI SEM 1µm WD 8.0mm

(d)

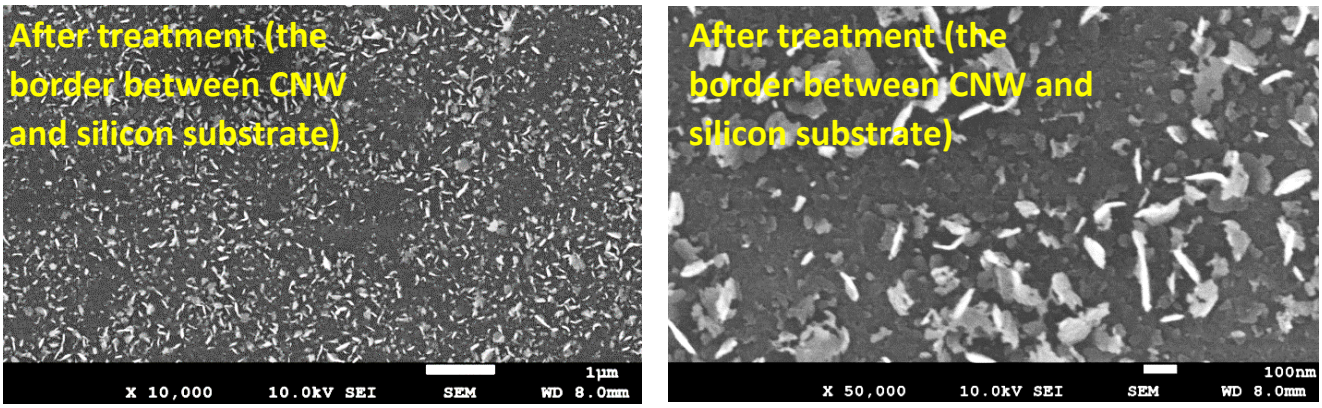

Figure 4.5. SEM image of CNW sample before and after treatment with O_2/Ar: 2.0/10sccm at low magnification (a), high magnification (b), cross section (c), and destroyed border between Si and left CNW in the middle of Si substrate (d)

4.3.2. Surface properties of as-grown CNW and plasma treated CNW samples

In order to determine the elemental composition and the type of oxygenated functional groups attached to the surface of CNW samples, XPS analysis was performed on the non-treated and plasma-treated surfaces. Figure 4.6a presents the XPS survey spectrum of as-grown CNW, CNW samples treated with O_2/Ar: 0.0/10sccm, O_2/Ar: 0.1/10sccm, and O_2/Ar: 1.0/10sccm. The CNW treated with O_2/Ar: 2.0/10sccm was not analyzed by XPS due to mainly destruction of its structure in this plasma treatment condition. As it observed, the XPS spectrum reveals the presence of C and O as main elements. The C1s and O1s peaks are observed at about 284.6 and 533.5eV, respectively. The relative percentage of O1s/C1s for untreated CNW, CNW treated with O_2/Ar: 0.0/10sccm, O_2/Ar: 0.1/10sccm, and O_2/Ar: 1.0/10sccm were <0.1%, 1.0%, 7.5%, and 1.8%, respectively (figure 4.6b). The result indicates that although the plasma condition of O_2/Ar: 1.0/10sccm has 10 times higher flow ratio of oxygen in comparison to the plasma condition of O_2/Ar: 0.1/10sccm, it contributes less oxygen on the CNW surface. One of the possible explanations for this can be related to this fact that at lower oxygen flow rate, the reactive oxygen species in the plasma can etch and remove the amorphous carbon selectively that exist on the as-grown CNW surface and simultaneously create oxygen functional groups on the defective positions and dangling bonds and stabilize them. On the other hand, further increase in oxygen

flow rate results in high density of excited species and radicals. This can consequently increase the etch rate from both amorphous and sp^2 structures and prevent the stabilization of oxygen in the defect positions, therefore contributing less oxygen functional groups on the CNW surface.

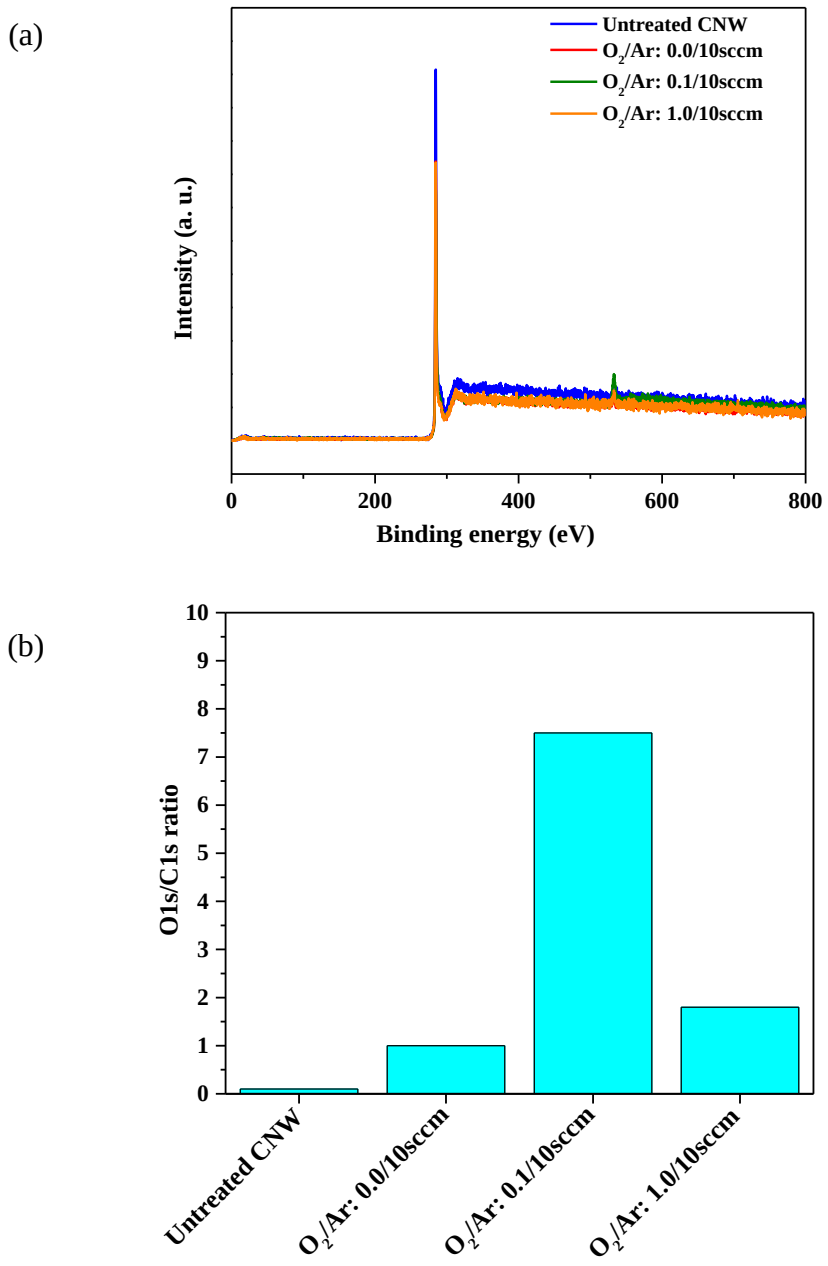

Figure 4.6. XPS survey spectrum for non-treated and treated CNW samples (a) and relative percentage of O1s/C1s (b)

For a detailed analysis of the surface chemistry of the samples, the XPS spectra in the region of the C1s peak (282-294eV) was recorded and displayed in figure 4.7a-d. The C1s spectrum was decomposed into 4 components for untreated CNW and 5 components for plasma treated CNW samples. The two major peaks at 284.4, and 285.0 corresponds to the sp^2 C=C and sp^3 C-C, respectively. The peak situated at 286.6 can be attributed to C-O (oxygen in alcohol or ether), while the peaks situated at 288.4eV and 291.8eV can be ascribed to C=O (carbonyl group), and π-π^* transition, respectively [145].

The quantitative analysis exhibits that plasma treatment causes a decrease in the graphitic fragment (figure 4.6e). The decay of sp^2 in plasma treated samples can be due to the high sputter yield of Ar and reactivity of oxygen species [146]. At the same time, the peak attributed to sp^3 C or disordered C (i.e. dangling bonds at the edges) increases after plasma treatment and has the greatest quantity for the CNW treated with only Ar.

An increase in contribution of C bonded to O is also evident after plasma treatment and it is found to have the highest quantity for the sample treated in low oxygen flow rate, hinting that oxygen radicals bind to the induced defective sites during plasma treatment process. Furthermore, despite the unreactive nature of Ar, oxidation takes place at the surface of CNW after treatment. This oxidation may occur due to exposure of the treated samples to the atmosphere upon extracting them from the plasma chamber. These changes suggest that highly energetic species can break C=C bonds and result in lower sp^2 fragment, while contributing new C-O_x groups on the treated surface as well as increasing the assigned sp^3 peak.

(a)

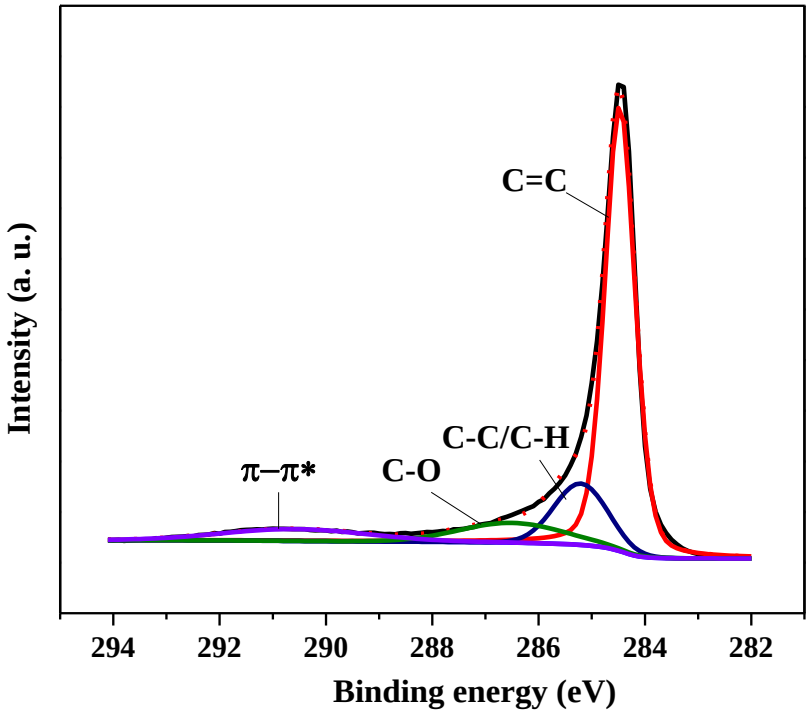
C=C
C-C/C-H
C-O
π–π*
Intensity (a. u.)
294
292
290
288
286
284
282
Binding energy (eV)

(b)

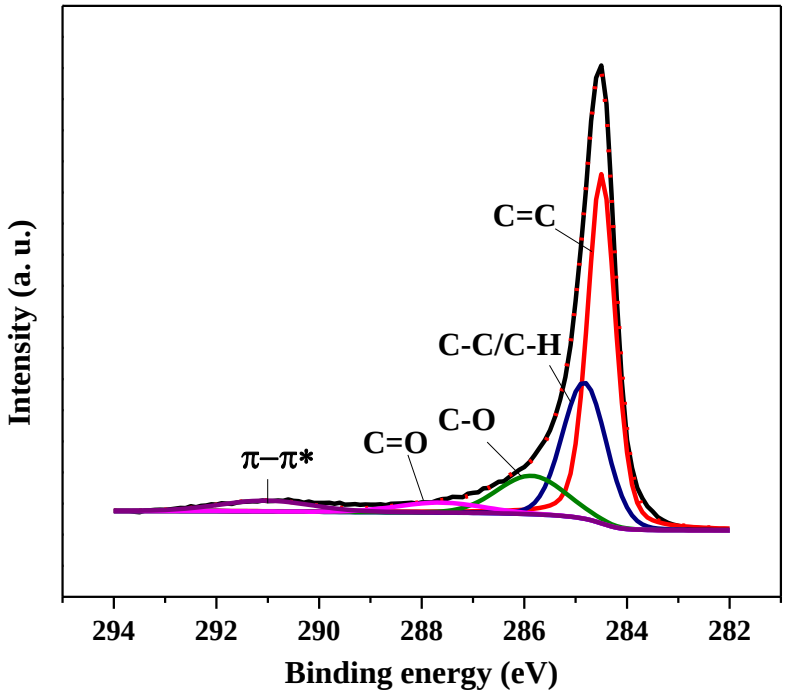
C=C
C-C/C-H
C-O
C=O
π–π*
Intensity (a. u.)
294
292
290
288
286
284
282
Binding energy (eV)

(c)

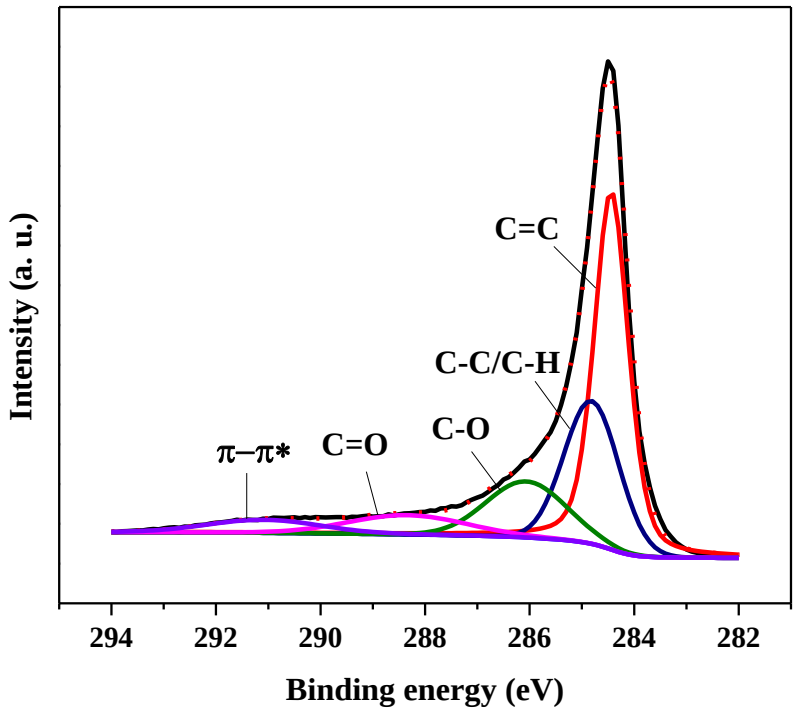
Intensity (a. u.)
C=C
C-C/C-H
C-O
C=O
π–π*
294
292
290
288
286
284
282
Binding energy (eV)

(d)

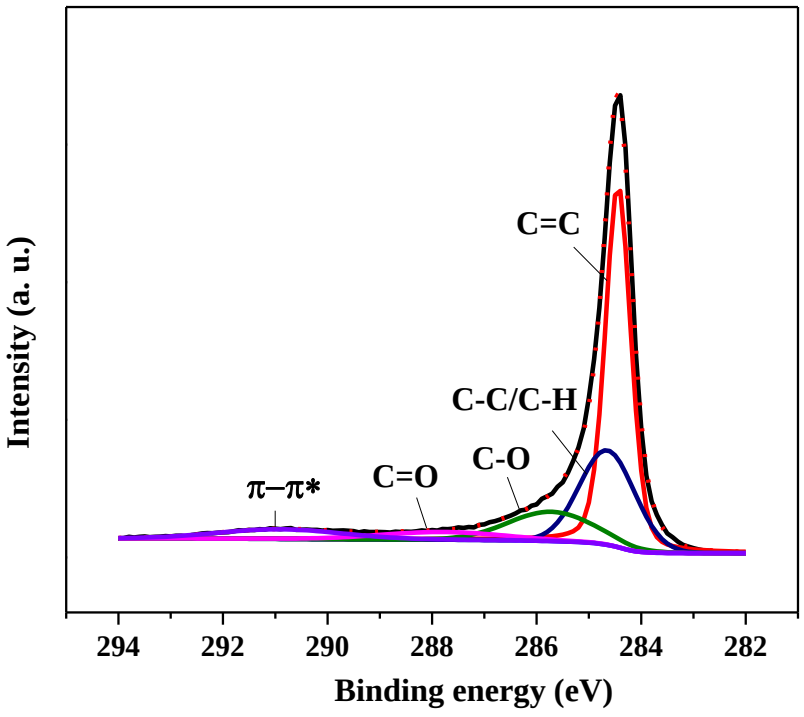
Intensity (a. u.)
C=C
C-C/C-H
C-O
C=O
π–π*
294
292
290
288
286
284
282
Binding energy (eV)

(e)

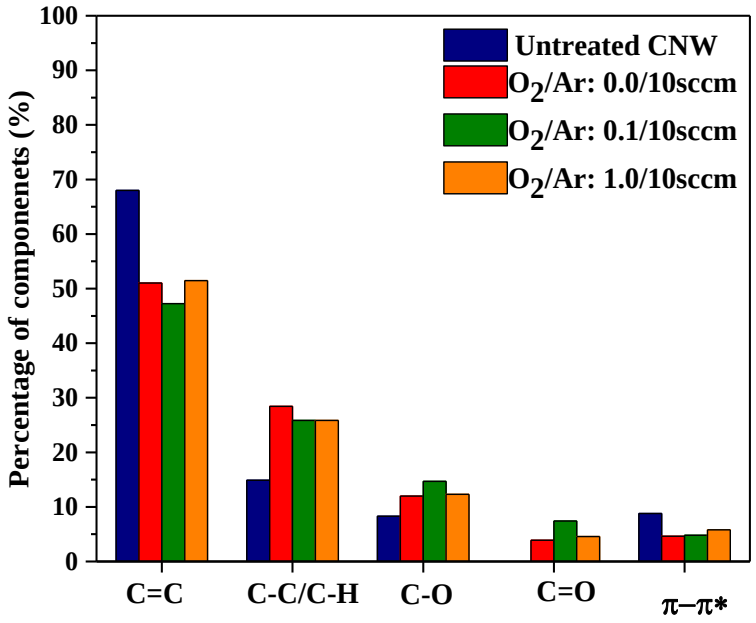

Figure 4.7. C1s spectra and their deconvolution for untreated CNW (a), CNW treated with O_2/Ar: 0.0/10sccm (b), CNW treated with O_2/Ar: 0.1/10sccm (c), CNW treated with O_2/Ar: 1.0/10sccm (d), and percentage of components (e).

In order to understand and compare the vibrational properties of untreated and treated CNW samples, FTIR measurement was performed on the CNW prepared on IR-transparent silicon as the substrate based on the previous reported literatures [52,147]. It was observed that our as-grown CNW sample is not transparent and the FTIR spectra did not reveal any information about functional group on our CNW samples (figure 4.8). The differences in height, density, and the thickness of the walls in the CNW samples prepared with different methods may be the reason for different FTIR results. The same result has been reported by Evlashin et al. that FTIR spectra do not reveal any functional groups on CNW surface [148].

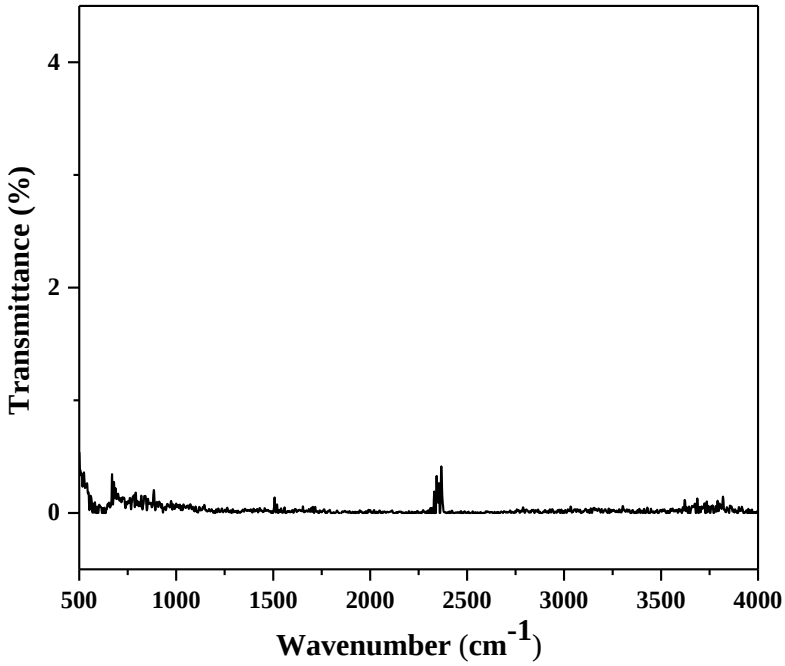

Figure 4.8. FTIR spectra for as-grown CNW

Raman spectroscopy was further applied to understand the structural characteristic of the CNW samples. As disclosed in figure 4.9, the samples show a typical spectrum for CNW with clear characteristic graphitic D, G, and D'. The D peak of the samples which is associated with the defects in sp^2 structures, was approximately shown at 1350cm^{-1}. The G band is related to the sp^2 structure, showing the degree of graphite-like domains in CNW was observed at 1580cm^{-1}. A weak band observed at around 1620cm^{-1} corresponds to D' that emerges with D band indicating disorder in the finite-sized sp^2 crystal and it is typical for graphene edges [119]. As observed, all these post synthesis plasma treatments do not induce significant differences in the Raman spectra of CNW, indicating preserving the basic structure of the material (the characterization of the CNW treated with O_2/Ar: 2.0/10sccm was done on the thin layer of left CNW on the middle of Si substrate). The ratio between the intensity of D and G bands (I_D/I_G) is used as the quantitative analysis technique to estimate the degree of disorder in graphene lattice [120]. The I_D/I_G ratios of CNW before and after plasma treatment was represented in figure 4.8b. It is seen that non-treated CNW has the I_D/I_G ratio of 1.65, which increases to 2.10 after Ar plasma treatment. Admixing a small amount of oxygen (0.1sccm) in Ar plasma gas mixture resulted in a decrease to a certain minimum

of I_D/I_G (1.5). However, further increase in oxygen flow rate from 0.1sccm to 1.0 and 2.0 sccm, causes the increase of I_D/I_G ratio to 1.76 and 1.99, respectively. It can be said that defect sites were heightened by Ar plasma treatment and lowered by admixing slight oxygen amount in plasm gas mixture. Moreover, further increase in oxygen flow rate, resulted in an increase in defect sites. These results indicate that low oxygen flow rate can lower the defect sites by selective etching and removing amorphous carbon on the surface of as-grown CNW and substitution of oxygen to the defect sites. However, further increase in oxygen flow rate can mainly result in etching and consequently producing more defect sites.

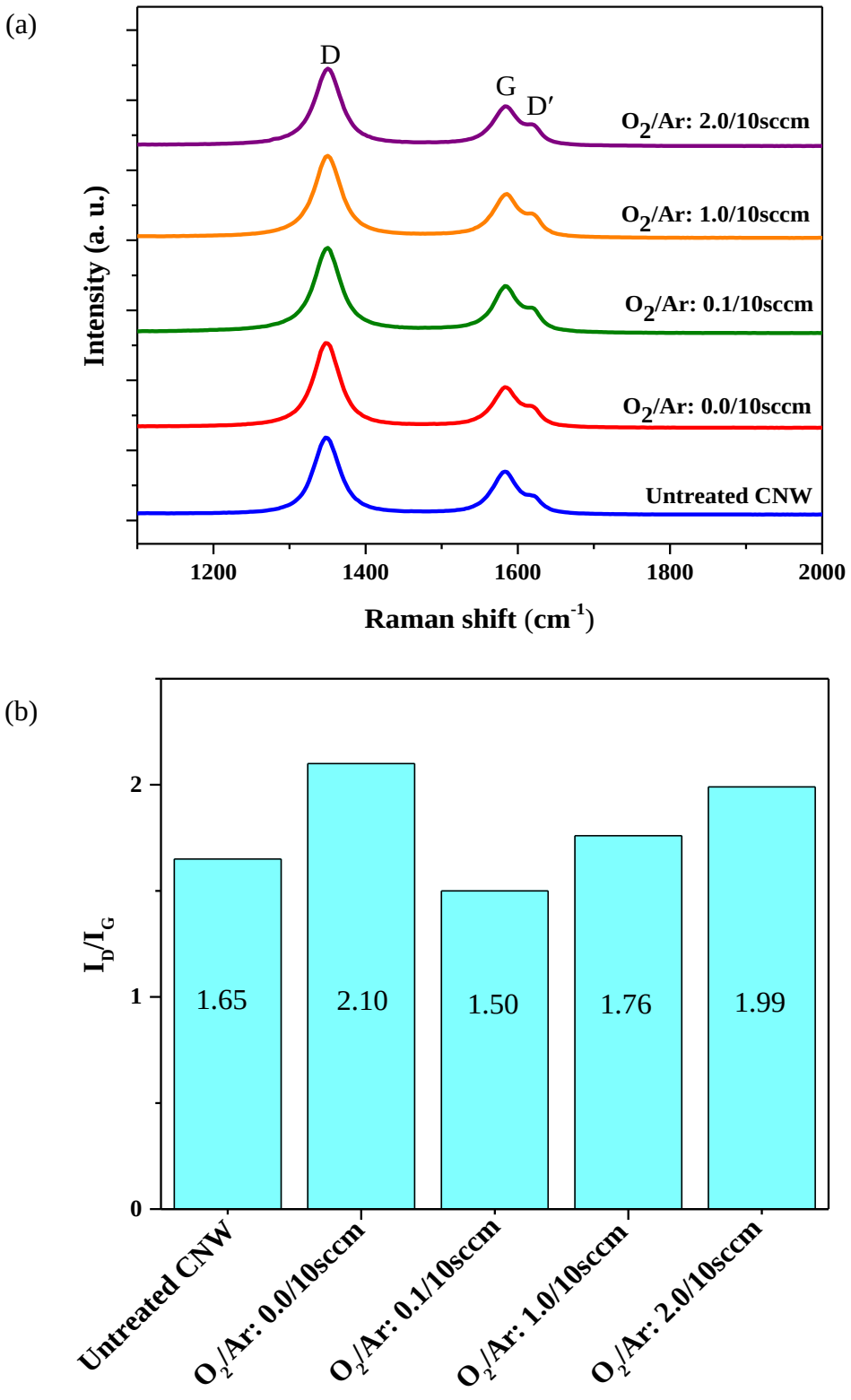

Figure 4.9. Raman spectra of CNW films before and after plasma treatment (a), I_D/I_G ratios of the samples (b)

As different oxygen flow rates lead to different morphology, chemical composition and structure modifications, revealed by SEM, XPS and Raman spectroscopy analyses, it is expected that plasma treatments may tune the wetting nature of CNW. To evaluate the wettability of the CNW samples, water contact angle measurement was performed. The variation of the contact angle as a function of oxygen flow rate in treatment gas mixture and the side-view photographic images of the water droplets on the CNW samples were shown in figure 4.10. As observed, before plasma treatment, the droplet on CNW surface remained in a spherical shape with the contact angle of 124.0^{o}, in which the CNW surface is almost super hydrophobic. After plasma exposure, the contact angle decreases from 124.0^{o} to 58.6^{o}, 10.2^{o}, 33.1^{o}, and 104.7^{o} for the CNW samples treated with O_2/Ar: 0.0/10sccm, O_2/Ar: 0.1/10sccm, O_2/Ar: 1.0/10sccm, and O_2/Ar: 2.0/10sccm, respectively. As the results display, the CNW treated with O_2/Ar: 0.1/10sccm shows the most hydrophilic surface among the samples. While further increase in oxygen flow rate in plasma treatment gas mixture lead to an increase in water contact angle. The water contact angle can be altered by changes in the surface roughness and the chemical properties of the surface.

Earlier, XPS analysis showed that CNW treated with O_2/Ar: 0.1/10sccm has the highest oxygen content on its surface, where by further increase in oxygen flow rate, the contribution of oxygen onto the CNW structure decreases. In addition, it was shown by SEM images that the CNW treated with O_2/Ar: 0.1/10sccm has almost similar morphology as the pristine CNW. This suggests that oxygenated functional groups attached to the CNW surface are responsible for the change in wetting properties, which has been reported by other research groups [55,145].

(a)

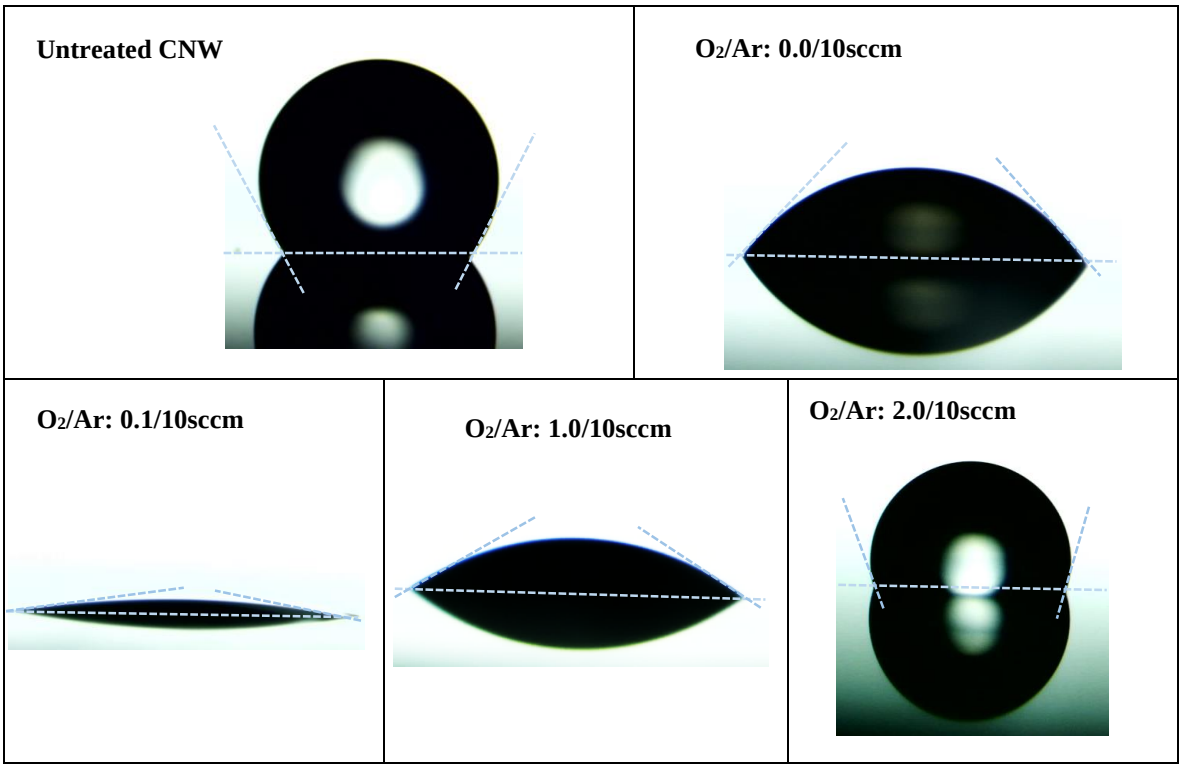

(b)

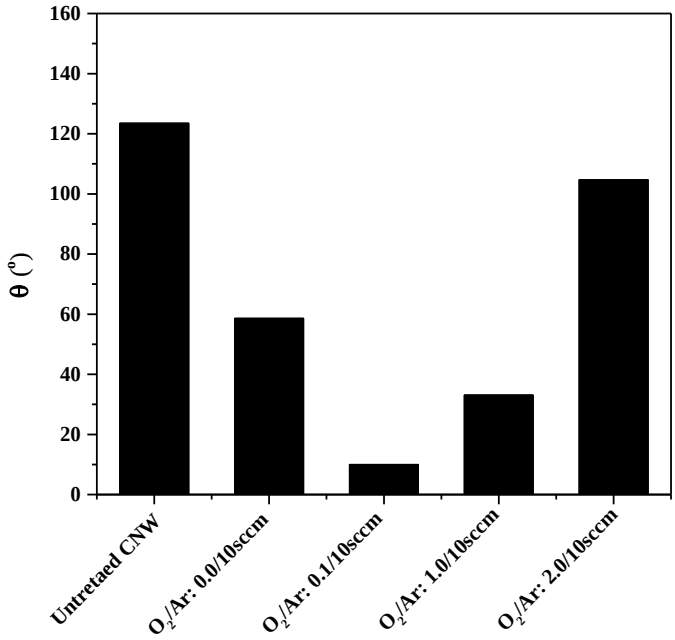

Figure 4.10. The side-view photographic images of water droplets on CNW samples (a), and contact angle of water droplet on CNW as a function of oxygen flow ratio in plasma treatment gas (b)

4.4. Introducing inter-synthesis sequential treatment method

In this section, we only introduce a novel inter-synthesis sequential treatment method in order to deposit CNW with conformal oxygen functional groups and more defective edge planes and its further optimization and characterization is proposed as the future work. In this technique, CNW is fabricated by the same method as reported in chapter 2 with this difference that total synthesis time of 60s was divided into 12 cycles, in which each cycle composed of 5s synthesis and 5s treatment with O_2/Ar: 0.1/10sccm. The plasma treatment condition of O_2/Ar: 0.1/10sccm was applied since it incorporates the highest quantity of oxygen functional groups in CNW structure which was discussed in previous section. Figure 4.11 illustrates the schematic representation of inter-synthesis sequential treatment method. The related SEM top-surface and cross-section images were displayed in figure 4.12 and compared with the CNW prepared with original method. Growing of CNW perpendicularly to the substrate can be revealed by cross section images. However, CNW earns layer by layer structure as synthesis is paused for 5secnods during the treatment time. In addition, more branched structure can be observed for the CNW prepared with sequential method.

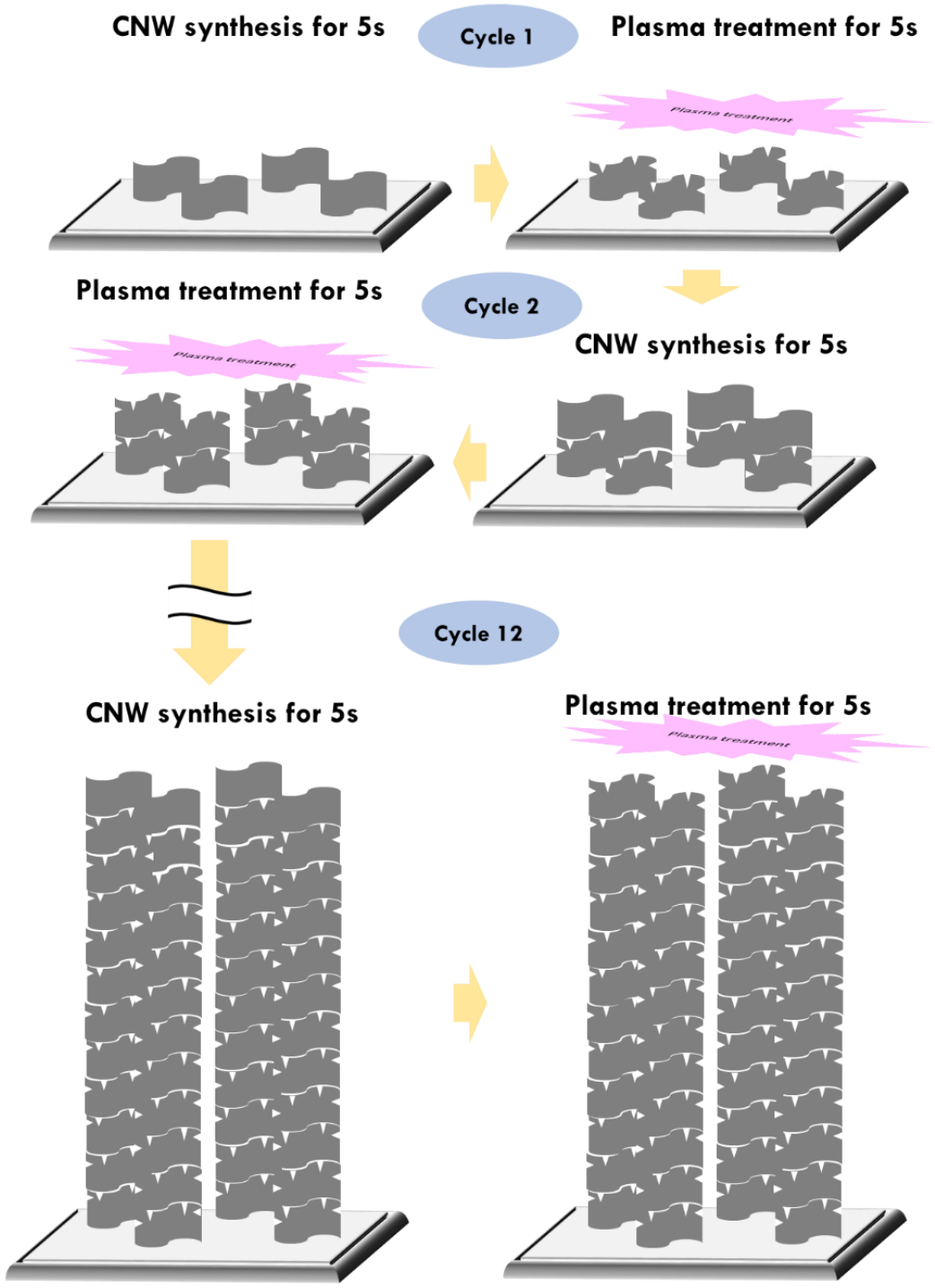

Figure 4.11. Schematic representation of depositing CNW by inter-synthesis sequential method (1 cycle: CNW synthesis for 5s, plasma treatment for 5s).

(Original CNW) (CNW prepared with sequential method)

(a)

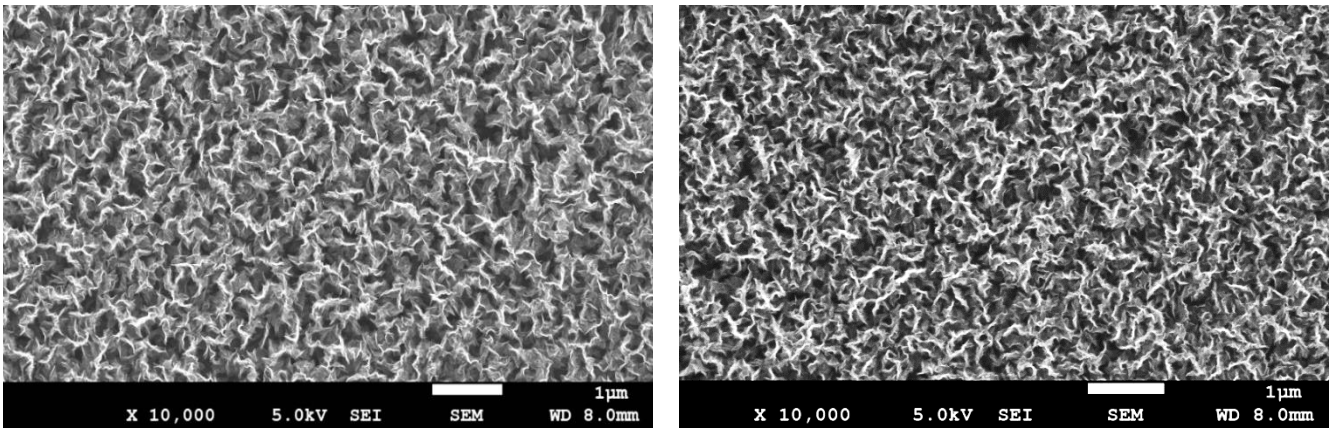

(b)

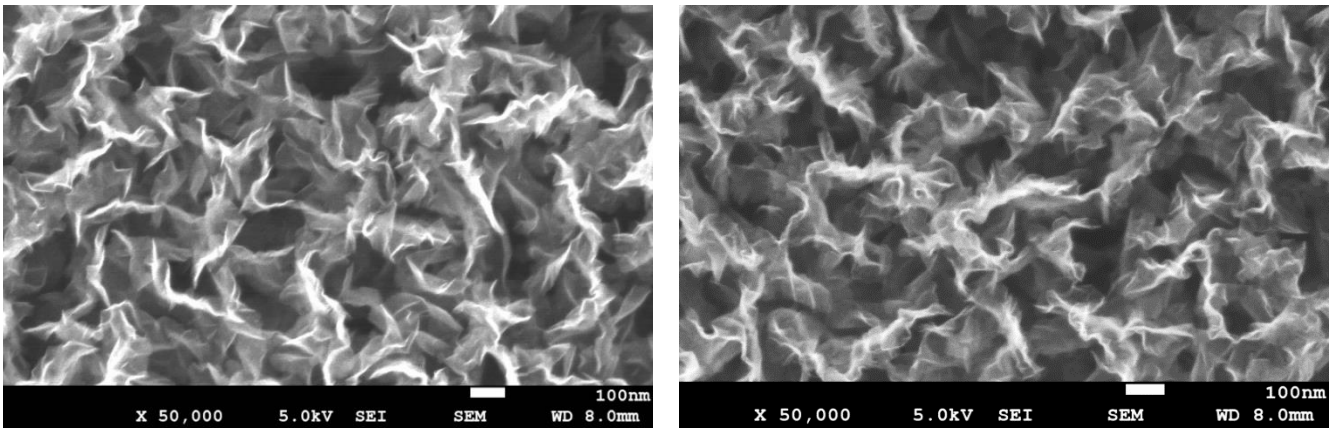

(c)

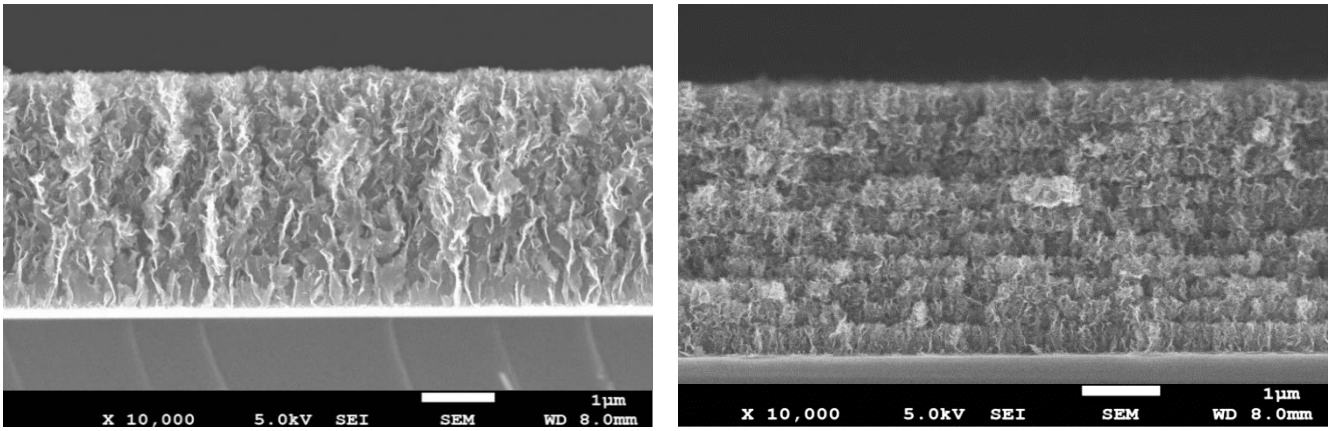

Figure 4.12. SEM image of CNW deposited by original method and inter-synthesis sequential method at low magnification (a), high magnification (b), and cross section (c)

To understand the structural characteristic of CNW synthesized by sequential method, Raman spectroscopy was applied (figure 4.13). As disclosed in figure 4.13, the sample shows a typical spectrum for CNW with clear characteristic graphitic D, G, and D'. It was found that I_D/I_G ratios of CNW increases to 2.2 to compare with original CNW which is at around 1.65. This increment can be related to the increase in defective graphitic edge planes.

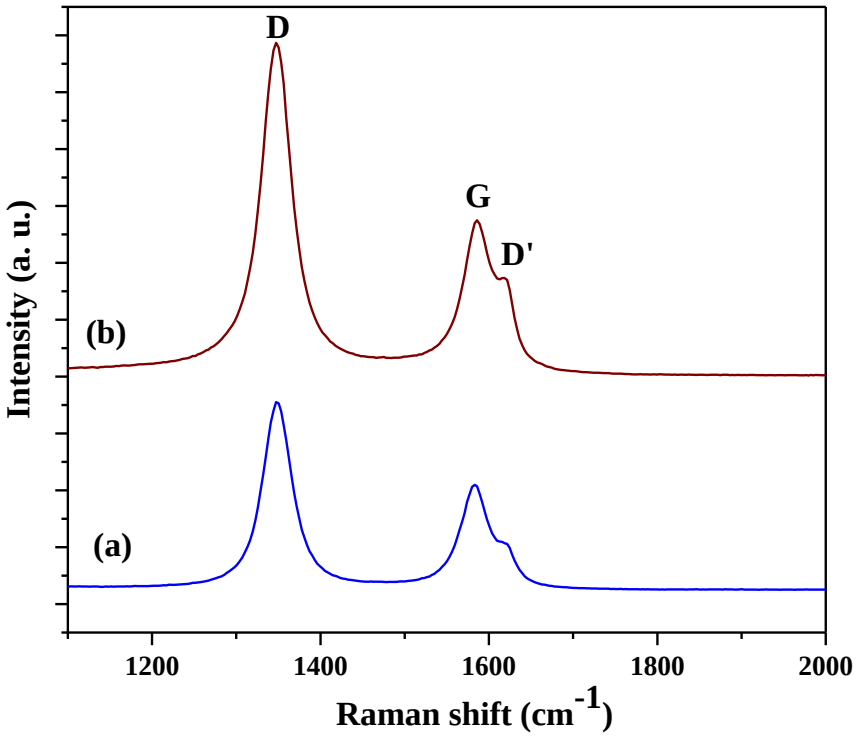

Figure 4.13. Raman spectra of CNW film prepared with original method (a) and inter-synthesis sequential method (b)

4.5. Summary of the chapter

Oxygen-incorporated CNW films were successfully produced by PECVD system using different concentration of oxygen plasma post treatments. An increase in the oxygen content of CNW structure after plasma exposure was confirmed by X-ray photo-electron spectroscopy. The CNW treated in low oxygen flow rate (O_2/Ar: 0.1/10sccm) displayed the highest concentration of incorporated oxygen (about 7.5%) among the samples, which in turn resulted in conversion of intrinsic hydrophobicity of CNW to hydrophilicity. While further increase in oxygen flow rate resulted in lower oxygen functional groups and also more structural and morphological defects. We assume that when low density of oxygen species exists in the plasma treatment gas mixture, the amorphous carbon structures that exist on the surface of as grown CNW are selectively etched and the potential active oxygen species are stabilized to the produced defect sites, therefore formation of oxygen functional groups occurs favorably. However, the higher density of reactive oxygen species can result in higher etching rate, which can consequently lead to increase the etch rate from both amorphous and sp^2 structures and prevent the stabilization of oxygen in the defect positions, hence contributing less oxygen functional groups on the CNW structure.

Subsequent to finding the surface properties of CNW samples after O_2/Ar plasma, novel inter-synthesis sequential treatment method was introduced to deposit CNW with conformal oxygen functional groups and more defective edge planes. Layer by layer structure with highly branched structure was observed by SEM images, and an increase in defective structure was confirmed by Raman spectroscopy.

Chapter 5. Electrochemical performance of plasma treated CNW samples towards H_2O_2 detecting

5.1. Background of the chapter

In chapter 3, we introduced a hybrid CNW structure combined with the transitional metal oxide MnO_x as an efficient non-enzymatic H_2O_2 sensor [138]. In this chapter, we aimed to enhance the electrochemical sensing performance of CNW by intrinsic modification, so that the optimum modified CNW can be utilized as a potential metal-free electrochemical sensor. This chapter discusses the electrochemical performance of CNW samples treated in different O_2/Ar plasma conditions and introduces a novel metal-free carbon based electrochemical sensor for detecting of H_2O_2 by surface modification of carbon nanowalls.

5.2. Experimental

The experimental method and equipment used in this chapter are similar to those in Chapter 3. Hydrogen peroxide (H_2O_2), Uric acid ($C_5H_4N_4O_3$), Citric acid ($C_6H_8O_7$), and Ascorbic acid ($C_6H_8O_6$) were purchased from FUJIFILM Wako Pure Chemical corporation. Phosphate buffer solution was purchased from Hayashi Pure Chemical Ind. Ltd. All chemicals were of analytical grade and deionized water was used throughout the experiment.

To evaluate the sensor performance of the CNW samples, cyclic voltammetry and amperometry measurements were carried out using a three-electrode system composed of CNW samples as working electrodes, Ag/AgCl (NaCl saturated) electrode as reference electrode and platinum wire as counter electrode. The potential range of 0.0 to 1.1V and a scan rate of 10.0mVs^{-1} were applied to perform CV measurements. 0.25M phosphate buffer solution (pH 7.2) was utilized as the supporting electrolyte. The phosphate buffer solution was pulsed with high purity nitrogen for 10min prior to the experiments. Amperometry measurements were done at an applied potential of +0.7V under the stirring and pulsing with N_2 throughout the experiment (Princeton Applied Research Versa STAT 3).

5.3. Result and discussion

5.3.1. Electrochemical characterization of as-grown CNW and plasma treated CNW samples

In order to evaluate the catalytic properties of untreated and treated CNW samples to oxidation of hydrogen peroxide (H_2O_2), cyclic voltammetry test was performed in N_2-saturated 0.25M phosphate buffer solution at a scan rate of 10.0mV/s. Figure 5.1 shows the CVs of untreated CNW,

CNW treated with O_2/Ar: 0.0/10sccm, O_2/Ar: 0.1/10sccm, O_2/Ar: 1.0/10sccm, and O_2/Ar: 2.0/10sccm in the absence of H_2O_2 (a), and in the presence of 5mM H_2O_2 (b). No redox peaks are observed for all the electrodes in the absence of H_2O_2. However, adding 5mM H_2O_2 in phosphate buffer solution showed a significant change in the voltametric behavior of the electrodes. It is notable from figure 5.1b and 5.1c that oxidation current significantly increases after plasma treatment of CNW surface. The CNW treated in 10sccm Ar showed an obvious increase in oxidation current to compare with untreated CNW. Admixing 0.1sccm O_2 with 10sccm Ar resulted in further increment in the current value. By increasing the oxygen flow rate from 0.1sccm to 1.0sccm, a small jump in the current response was observed. However, further increase in oxygen flow rate resulted in a decrease in the current. This can be attributed to the destruction of CNW at higher oxygen density of plasma treating gas as discussed in Chapter 4.

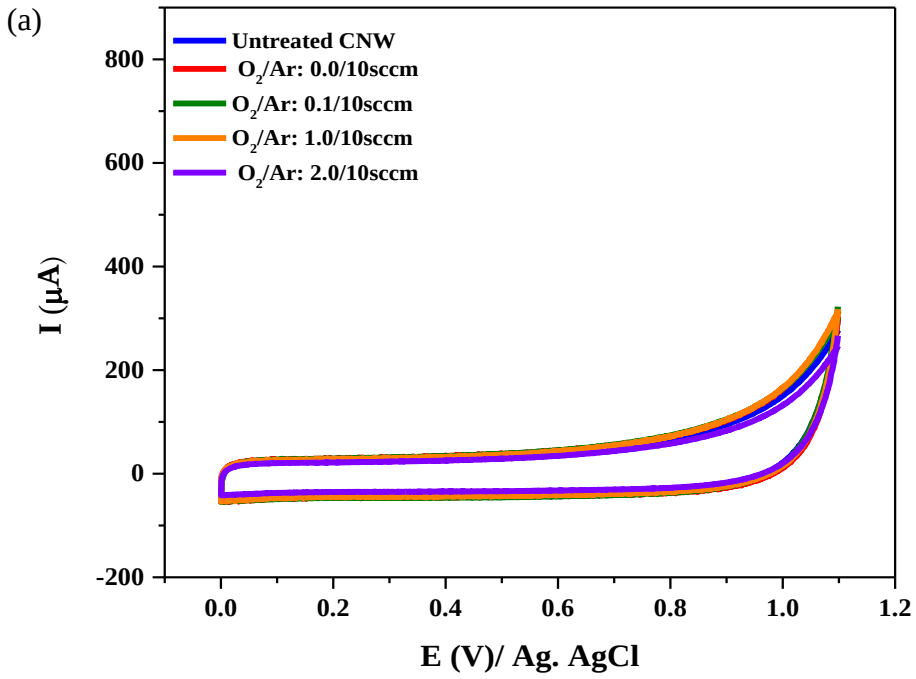

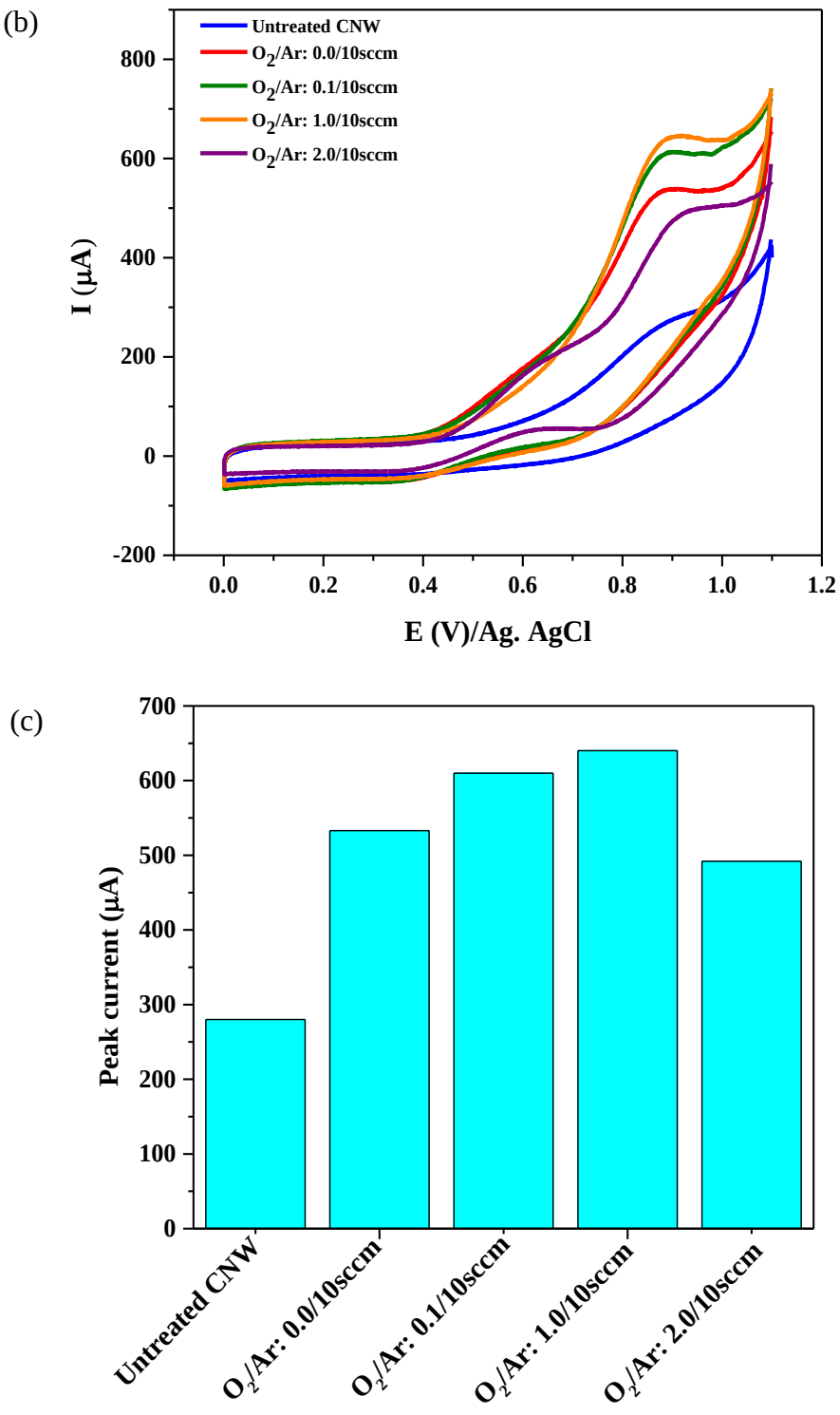

Figure 5.1. Cyclic voltammograms obtained using untreated CNW and treated CNW in different plasma condition in the absence of H_2O_2 (a), in the presence of 5mM H_2O_2 (b), and the peak current response for each electrode obtained in the presence of H_2O_2 (c)

To further confirm the electrocatalytic activity of CNW samples toward oxidation of H_2O_2, amperometric measurement was performed. Based on the cyclic voltammetry result, +0.7V was selected as an applied potential for the amperometric detection of H_2O_2 as response current increased sharply at this potential. Figure 5.2 shows the amperometric response for different samples at +0.7V by adding 0.5mM H_2O_2. As it can be seen, the highest amperometric response was observed for the CNW treated in O_2/Ar: 1.0/10sccm. The measured specific electrical conductivity of untreated and treated CNW samples by four-point probe system showed that the conductivity values for all the samples are roughly similar (figure 5.3). This indicates that conductivity is mainly determined by the bulk property of the samples which does not change due to the plasma surface treatment. Therefore, it can be said that different amperometric responses for CNW treated with different oxygen flow ratios in O_2/Ar plasma can be attributed to the changes in the surface of the CNW samples.

As it was earlier discussed in XPS and Raman spectroscopy sections in chapter 4, the treatment condition of O_2/Ar: 1.0/10sccm contributed lower oxygen content on CNW structure and in turn less hydrophilicity than the treatment condition of O_2/Ar: 0.1/10sccm, but also higher defect sites which can be potential active centers for chemical activity [14,149] . In addition, it was observed by SEM images that CNW treated with O_2/Ar: 1.0/10sccm possesses etched edges to compare with the CNW treated with O_2/Ar: 0.1/10sccm, which did not show any obvious changes on its surface morphology. Considering the water contact angle of the CNW treated with O_2/Ar: 1.0/10sccm ($\theta=33.1^0$), which assures enough hydrophilicity of the mentioned sample for enhanced electrochemical measurements and taking account of these structural and morphological defects, it can be suggested that both defects and hydrophilicity play important roles in the electrochemical behavior of the electrode. Defects can act as potential active sites for electrochemical reactions and hydrophilicity can enhance the surface area wetted by the electrolyte.

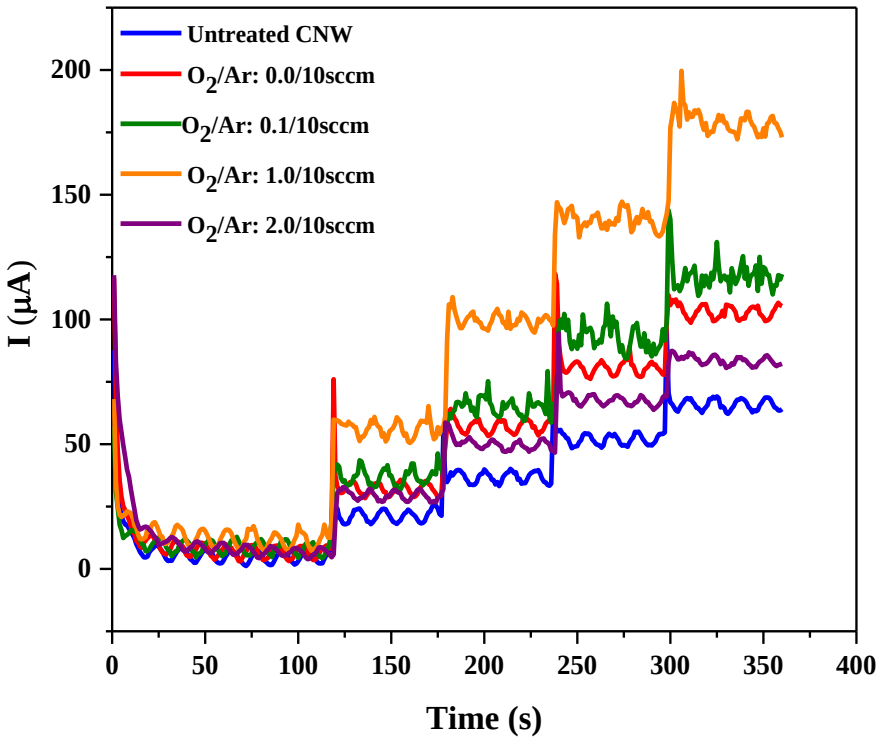

Figure 5.2. Amperometric response for non-treated and treated CNW samples at +0.7V

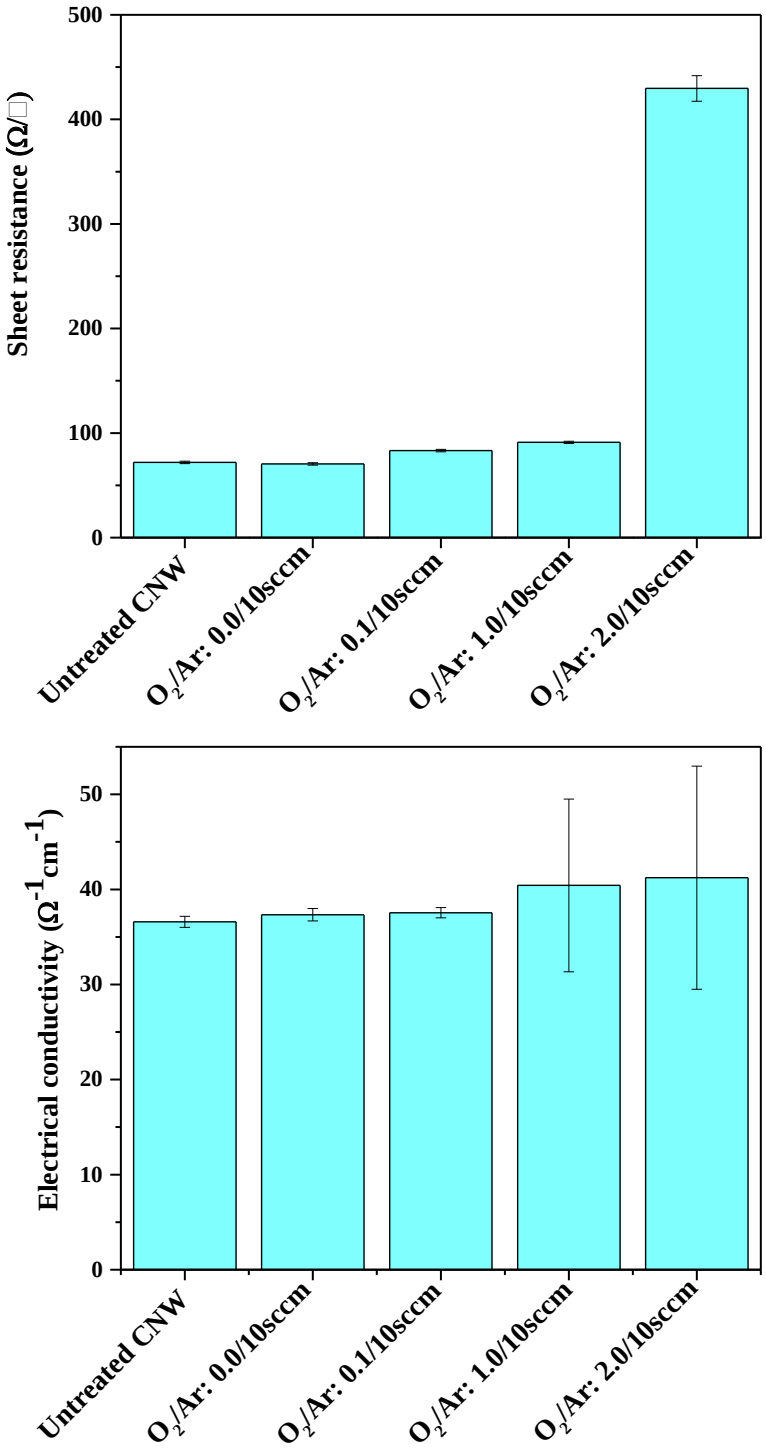

Figure 5.3. Sheet resistance (a) and electrical conductivity (b) of untreated and treated CNW samples

Owing to displaying the highest current response by CNW treated with O_2/Ar: 1.0/10sccm, the sensor performance measurements was applied for the same electrode. Figure 5.4a shows the typical amperometric response of the CNW treated with O_2/Ar: 1.0/10sccm upon the successive addition of H_2O_2 every 60s into phosphate buffer solution under stirring and pulsing N_2 at +0.7V. The related calibration plot of steady-state currents of CNW treated with O_2/Ar: 1.0/10sccm is depicted in figure 5.4b. The current increased linearly with increasing H_2O_2 concentration and exhibited a wide linear range from 50µM to 28000µM. The regression equation, I (µA)= 75.946CH_2O_2(mM) + 43.348 with correlation coefficient of 0.9977 was obtained. The limit of detection (LOD) for sensing H_2O_2 was estimated to be 0.91µM (S/N=3). The sensitivity was obtained to be 126.6µA/mM.cm^2, which is comparable to some previously reported electrodes applying carbon nanomaterials as the base conductive substrate[150–154]. Although, in most of the previous studies, the combination of transitional metal and/or a conductive polymer with carbon nanostructures have been reported as the electrodes for detecting H_2O_2, in this study we could succeed to utilize the only CNW structure for detecting H_2O_2.

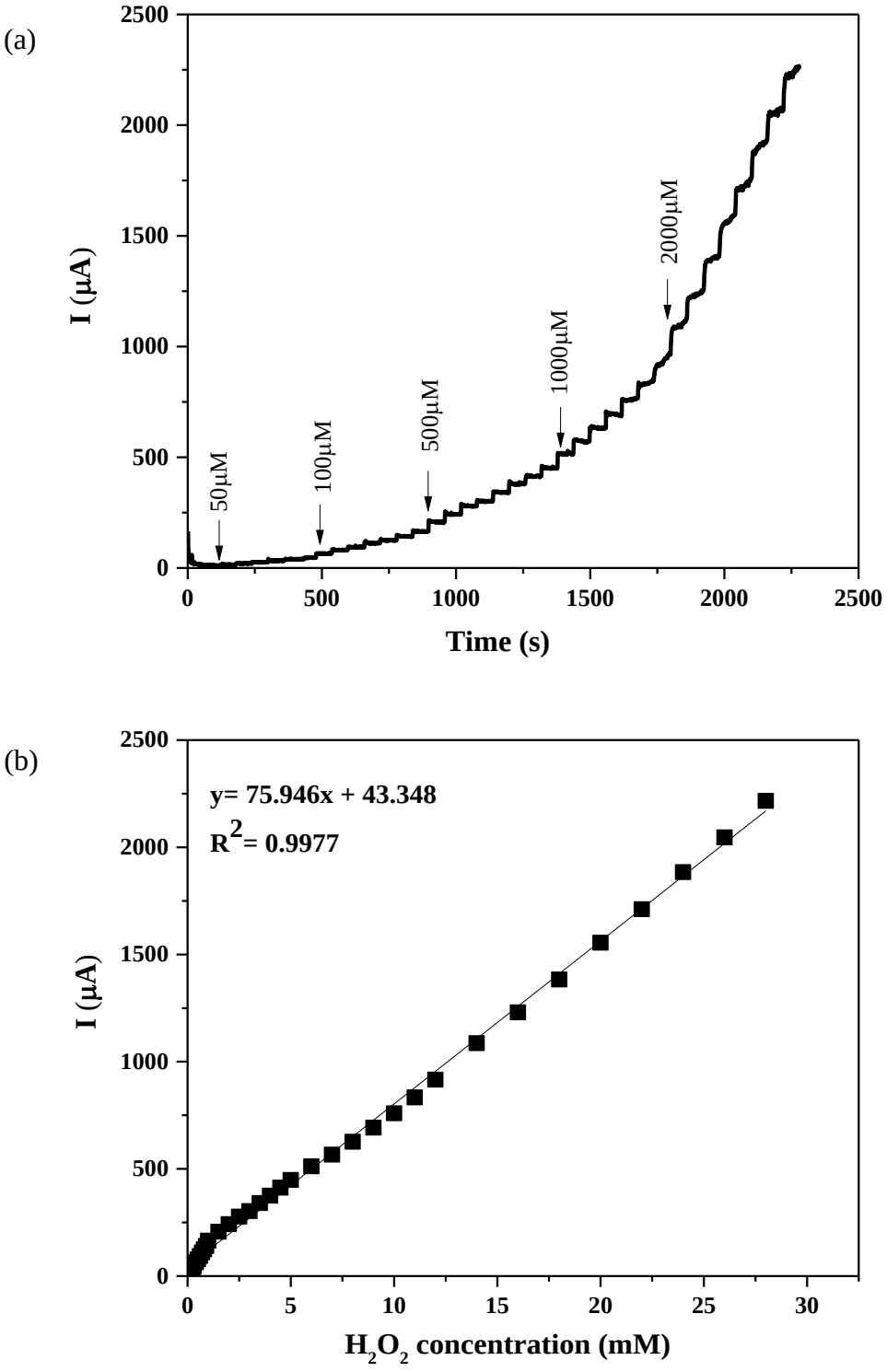

Figure 5.4. Amperometric responses of CNW treated in O_2/Ar: 1.0/10sccm with increasing H_2O_2 concentration in 0.25M phosphate buffer solution at an applied potential of +0.7V (a), the related calibration curve as a function of H_2O_2 concentration (b)

5.3.2. Selectivity, reproducibility and stability of CNW treated with O_2/Ar: 1.0/10sccm

The selectivity of the electrode was evaluated by an amperometric (i-t) curve upon successive addition of 0.5mM H_2O_2, and 1.0mM ascorbic acid (AA), uric acid (UA), and citric acid (CA), respectively. As shown in figure 5.5, CA did not interfere with determination of H_2O_2 and a slight interference of UA was observed. However, an equivalent concentration of AA showed significance interference. This may be ascribed to its strong reducibility [155].

The reproducibility and stability of the sensor was investigated by measuring the current response of the electrode upon 0.5mM of H_2O_2 in 0.25M phosphate buffer solution at +0.7V. In a series of 5 sensors prepared in a same way, the relative standard deviation (R.S.D) was 2.33%. For one electrode, the R.S.D. was found to be 1.94% for 5 successive measurements. These results indicate a good reproducibility for the proposed sensor. In order to understand the stability of the sensor, the current response to 0.5mM H_2O_2 was measured and the electrode was stored in an ambient condition. After three weeks storing, the same sensor was utilized to measure the current response to H_2O_2. The results displayed remaining of 95% of the sensor's initial current response. Although our result displayed the temporal stability of the fabricated sensor up to three weeks, the ambiguity on the long-term stability of the plasma modified carbon surfaces still exists. It has been reported by Mendez-Linan et al. and Ortiz-Ortega et al. that the plasma modified carbon surfaces can be influenced by aging effect or reorientation phenomenon, in which as the time progresses, the newly generated functional groups attempt to reorient themselves to occupy a lower state of energy, consequently leading to the loss of surface activity with time [146,156]. Furthermore, the effect of aging on CNW itself was reported by Vizireanu et al., stating that the CNW edges contains many defects initially, but those defects are passivated and become less chemically active after several days [157].To prevent the deactivation of plasma modified carbon surfaces, Kim et al. has proposed a new approach, in which applying second plasma treatment after two weeks from the first round of treatment can significantly enhance the degree and lifetime of plasma-induced functional groups on single-walled carbon nanotubes (SWCNTs) [158]. Considering the aging phenomena, further investigation of the long-term stability of the proposed sensor is necessary.

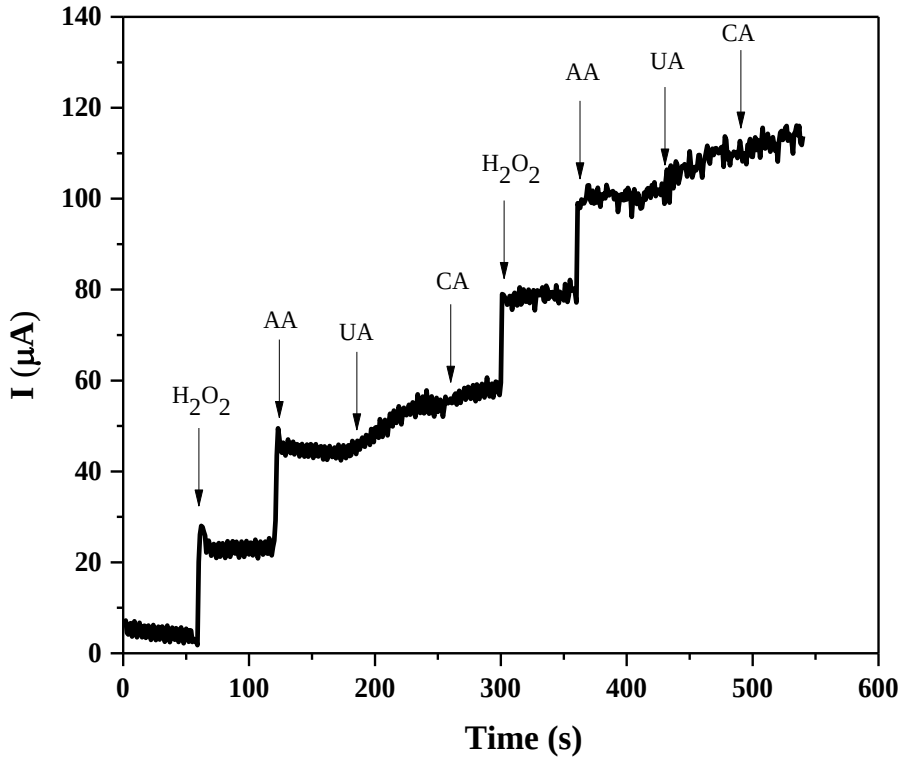

Figure 5.5. Amperimetric i-t curve for CNW treated with O_2/Ar: 1.0/10sccm towards the successive addition of 0.5mM H_2O_2 and 1.0mM interferential compounds

5.4. A possible reaction model

In order to get an insight into the reaction mechanism for the plasma treatment, optical emission spectroscopy for O_2/Ar plasma system was performed. The typical optical emission spectrum is indicated in figure 5.6 and the other spectrum for each condition were displayed in the Appendix. In figure 5.6, the intensity of atomic oxygen emission line at 777nm was plotted as a function of oxygen flow rates. The intensity increases with increasing oxygen flow rate up to 2.0 sccm monotonously and then decreases with increasing oxygen flow rate. This reduction of atomic oxygen line at high oxygen flow rate is mainly due to the reduction of atomic oxygen amount which is resulted in the electron energy reduction. From the OES results, it is safe to say that atomic oxygen increases with increasing molecular oxygen feed flow rate up to 2.0 sccm. However, interestingly, the highest oxygen amount and wettability of CNW surface was obtained with O_2/Ar: 0.1/1.0sccm plasma treatment and the highest electrocatalytic activity was obtained with O_2/Ar: 1.0/1.0sccm plasma treatment conditions.

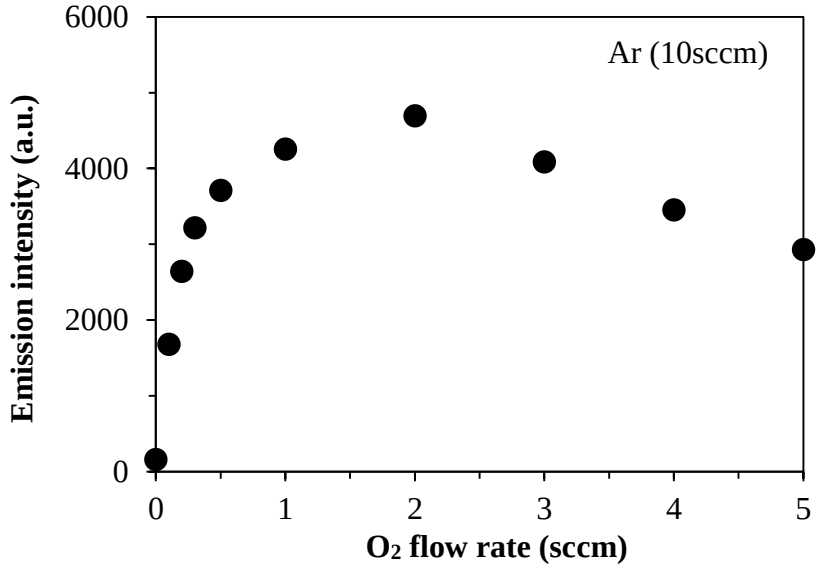

Figure 5.6. Emission intensity of atomic oxygen @ 777nm from O_2/Ar plasma

To illustrate the whole mechanism in a simple way, a schematic representation of the CNW treated in different oxygen plasma concentrations is displayed in figure 5.7. As it is seen, as-grown CNW has inherent hydrophobic nature which can hinder the interaction between the electrolyte and electrode and result in low performance of CNW in electrochemical system. Post plasma treatment of CNW with Ar increases the defect sites on CNW surface. The increment in defects after Ar

plasma treatment can lead to improving the electrochemical sensing performance due to acting as active sites for electrochemical reactions. Admixing slight amount of oxygen in Ar, results in attaching oxygen functional groups to the defect sites which consequently switch the hydrophobicity to hydrophilicity. The hydrophilic nature of CNW treated in O_2/Ar: 0.1/10sccm can further improve the performance of CNW in electrochemical systems due to increase the effective surface area accessible for the electrolyte. Further increase in oxygen flow rate from 0.1 to 1.0sccm displayed partial attaching functional groups to the defect sites, providing the CNW with some extend hydrophilicity and defective sites. This synergy effect between hydrophilicity and defects in the electrochemical behavior of the electrode resulted in the highest electrochemical activity of the CNW treated with O_2/Ar: 1.0/10sccm towards oxidation of H_2O_2. It can be said that insertion of oxygen functional groups to the C atom adjacent to defective carbon results in further reducing the aromaticity, generating unpaired sp electrons and forming localized high charge densities, which eventually facilitates H_2O_2 adsorption, dissociation, and consequently producing higher electrochemical response.

However, extra increase in oxygen flow rate from 1.0sccm to 2.0sccm resulted in destructing of CNW structure and consequently displaying weak electrochemical performance.

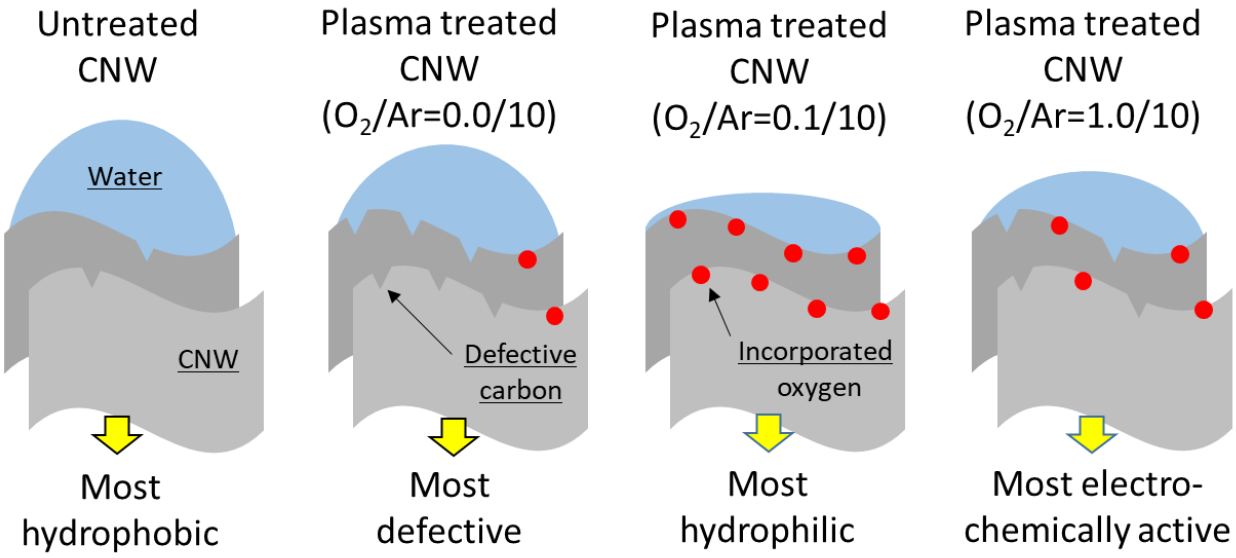

Figure. 5.7. Schematic representation of functionalization CNW with O_2/Ar plasma

5.5. Selective electrocatalysis properties of CNW

5.5.1. Selective electrocatalysis properties of CNW treated with O_2/Ar: 1.0/10sccm

In section 5.3.2, it was shown that CNW treated with O_2/Ar: 1.0/10sccm can detect H_2O_2 without any interference from citric acid (CA) and a slight interference from uric acid (UA). However, a significant interference from ascorbic acid (AA) was observed. In order to understand the potential range of interferential compounds and design a more selective electrode, the cyclic voltammetry measurement was performed in the presence of AA and UA at the potential range of -0.2V to 1.1V. Figure 5.8 illustrates the CV curves obtained from carbon rod, as-grown CNW, and CNW treated with O_2/Ar: 1.0/10sccm in the absence and presence of AA, UA, and their mixtures. Well-defined voltammetric peaks are seen for the direct oxidation of AA and UA in as-grown CNW and CNW treated with O_2/Ar: 1.0/10sccm in comparison to the carbon rod.

For the oxidation of AA, CV response with a pair of anodic peaks located at -0.063V and 0.643V from the CNW treated with O_2/Ar: 1.0/10sccm, anodic peaks situated at -0.028V and 0.630V from as-grown CNW, and only one oxidation peak at 0.164V from carbon rod can be observed. For the oxidation of UA, a redox pair with a ΔE_p of 28mV and an anodic peak at around 0.960V was observed at the CNW treated with O_2/Ar: 1.0/10sccm. The as-grown CNW showed a redox pair with a ΔE_p of 30mV, whereas only one anodic peak was observed at the carbon rod. For the binary mixture of AA and UA, four strong anodic peaks are observed at the CNW treated with O_2/Ar: 1.0/10sccm and three strong peaks for the as-grown CNW, while the carbon rod electrode presents only one wide anodic response.

Cyclic voltammetry results confirm that our CNW samples have strong electrocatalytic capability to simultaneously discriminate AA and UA. In addition, surface treatment of CNW with O_2/Ar: 1.0/10sccm results in enhancement of oxidation currents for AA and UA with compare to untreated CNW as depicted in figure 5.8d.

Electrochemical behavior of CNW treated with O_2/Ar: 1.0/10sccm was further evaluated in the presence of H_2O_2 and the ternary mixtures of AA + UA + H_2O_2 at the potential range of -0.2 to +1.1V (figure 5.9). Two oxidation peaks at around 0.680 and 0.900V were observed in the presence of H_2O_2, while there is no peak at negative potential side. The peak located at around

0.680V is assigned to the contamination with manganese oxide on counter electrode, which is very sensitive to decomposition of H_2O_2, therefore producing CV response only in the presence of H_2O_2.

When we compare the cyclic voltammetry curve for only H_2O_2 with the CV for ternary mixtures of AA, UA, and H_2O_2, it can be confirmed that CNW treated with O_2/Ar: 1.0/10sccm has the oxidation peak for both AA and H_2O_2 at potential of +0.7V. While there is no response for H_2O_2 at -0.063V and only AA can be detected at this potential. This can be considered as an advantage for detecting AA or H_2O_2 selectively by applying different potentials. Since there is a response for AA at potential of -0.063V, the concentration of AA can be estimated at this potential and its equivalent current response can be subtracted at potential of +0.7V, therefore H_2O_2 concentration can be determined from the residual current.

(a)

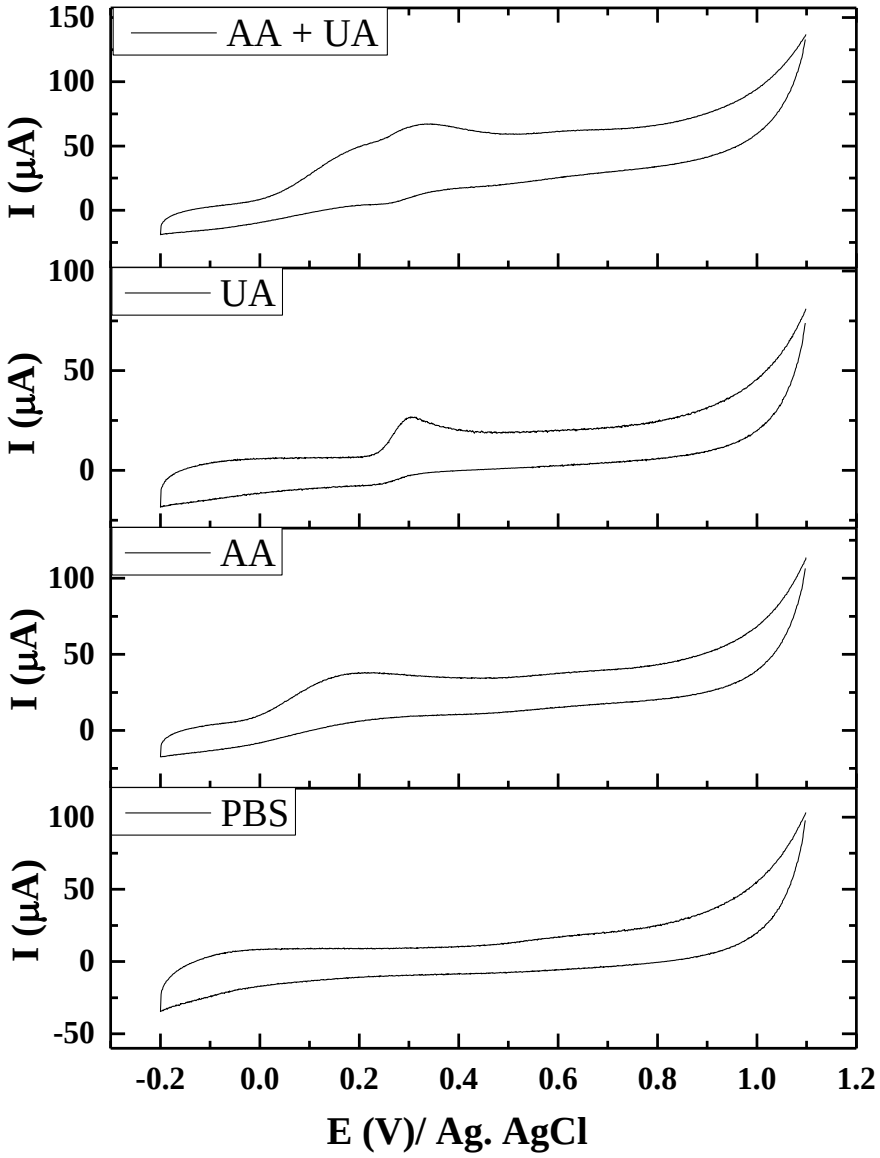

(b)

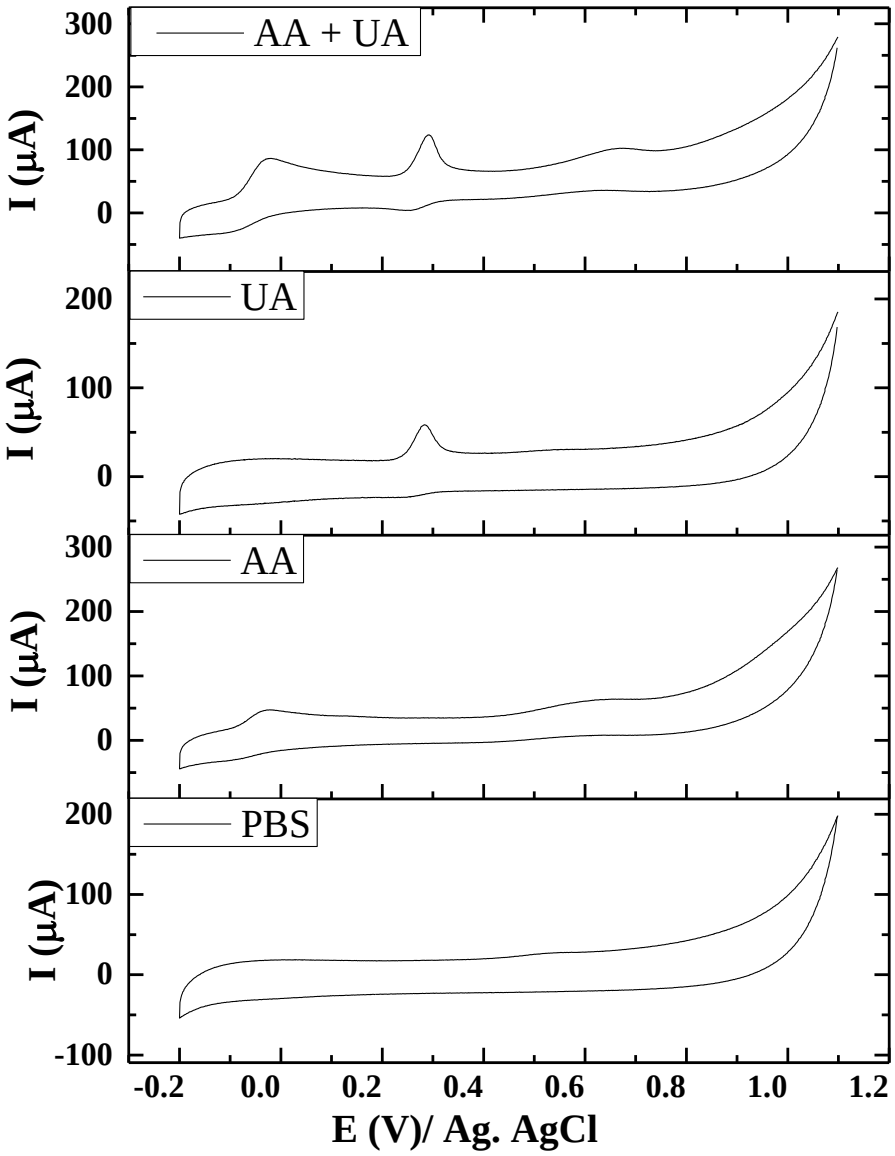
AA + UA
UA
AA
PBS
I (μA)
E (V)/ Ag. AgCl
300
200
100
0
-100
-0.2
0.0
0.2
0.4
0.6
0.8
1.0
1.2

(c)

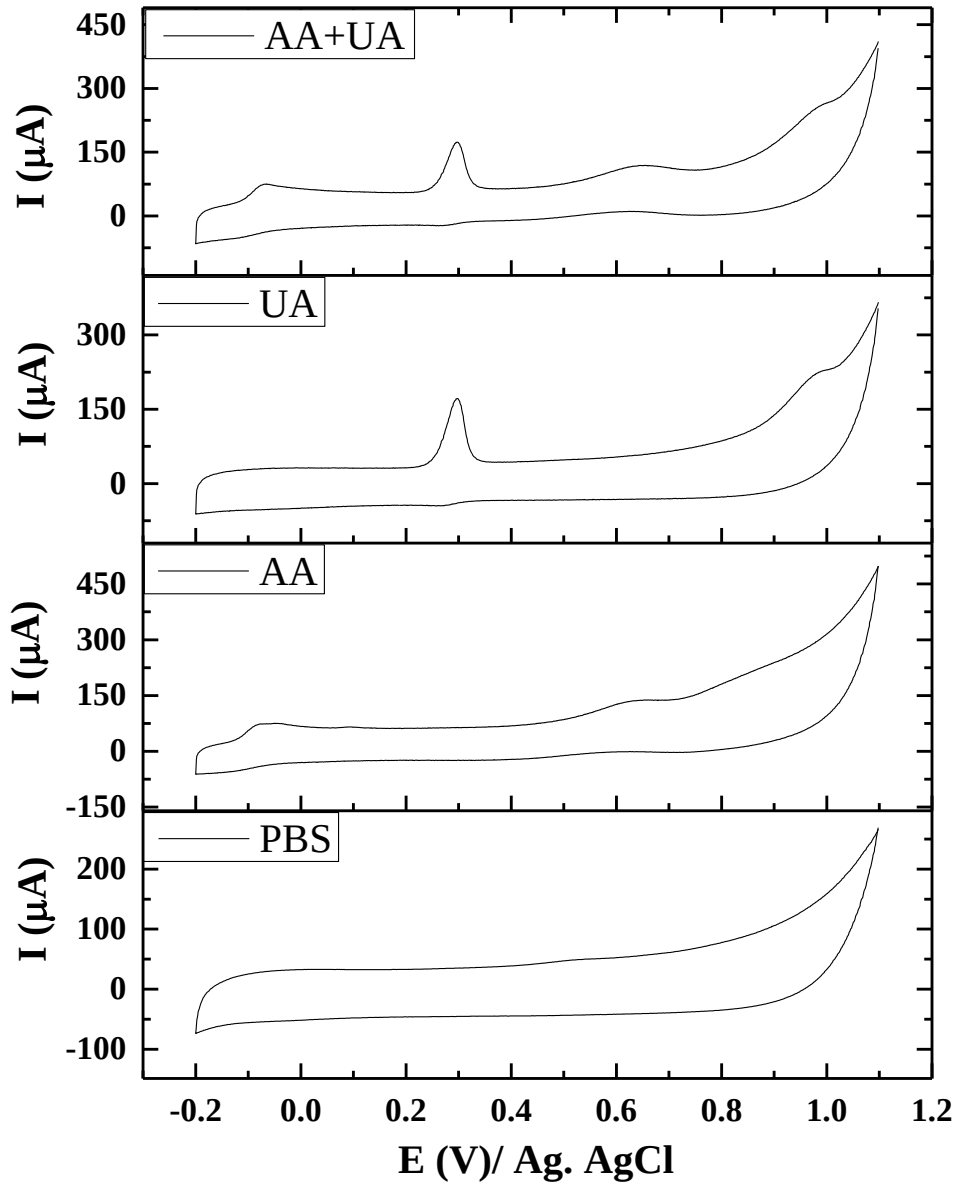
AA+UA
UA
AA
PBS
I (μA)
E (V)/ Ag. AgCl
450
300
150
0
-150
200
100
-100
-0.2
0.0
0.2
0.4
0.6
0.8
1.0
1.2

(d)

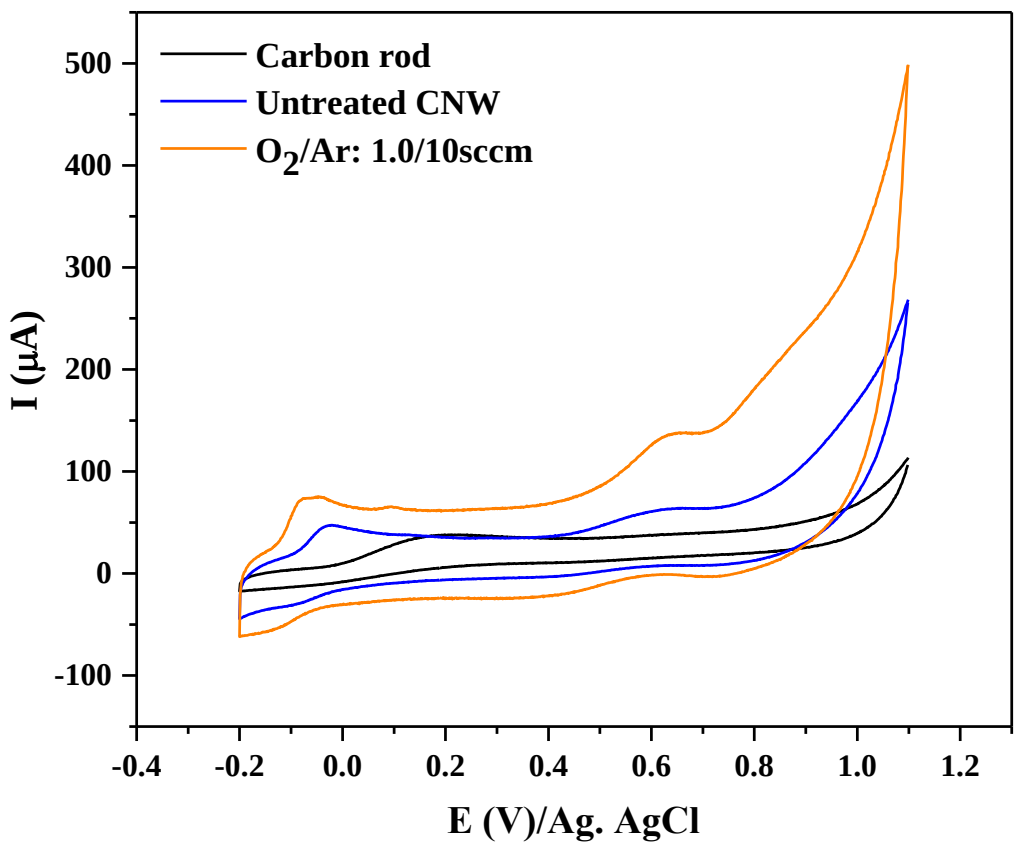

Figure. 5.8. CV profiles of (a) carbon rod, (b) untreated CNW, and (c) CNW treated with O_2/Ar: 1.0/10sccm in phosphate buffer solution, 1mM AA, 0.1mM UA, and binary mixture of 1mM AA + 0.1mM UA, and (d) their comparison for binary mixture of 1mM AA + 0.1mM UA

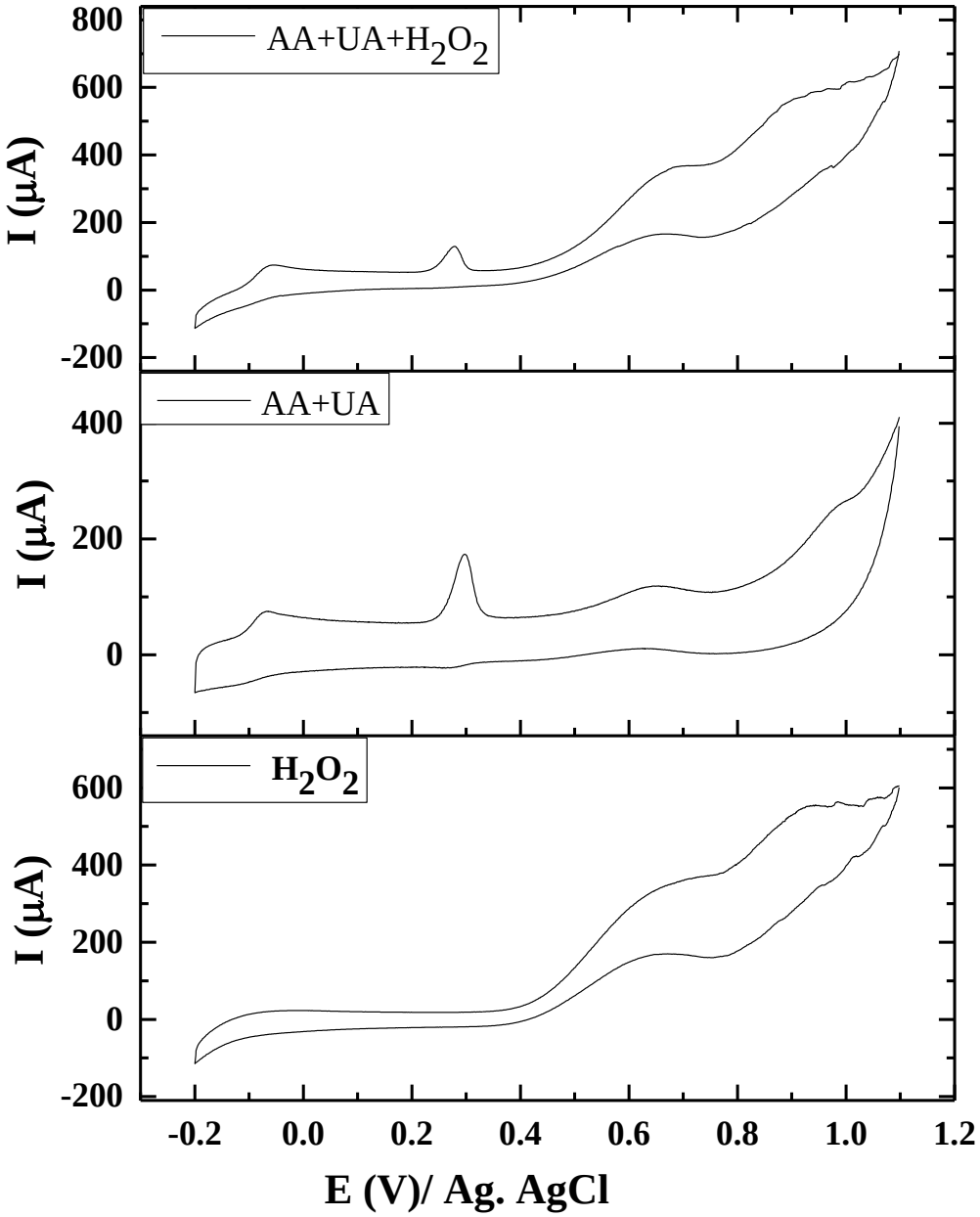

Figure 5.9. CVs of CNW treated with O_2/Ar: 1.0/10sccm in the presence of 5mMH_2O_2, 1mMAA +0.1mMUA, and ternary mixture of 1mMAA + 0.1mMUA + 5mMH_2O_2

5.5.2. Selective electrocatalysis properties of CNW prepared with inter-synthesis sequential treatment method

It was shown by SEM top surface and cross-section images (figure 4.12) that CNW prepared with sequential method has more branches and layer by layer structure. In addition, Raman spectroscopy (figure 4.13) revealed a noticeable increase in the defect density due to increase in the defective edge plane structure to compare with CNW prepared with original method. This noticeable increase in defect density and also possibility of formation oxygen in the deep parts of the pores for CNW prepared with sequential method can be considered as an advantage to detect the analytes that heterogeneous electron transfer (HET) rate at the edge planes are very fast for them and also electrochemically they are sensitive to oxygen functional groups (e.g. ascorbic acid and uric acid) [5]. Therefore, in this section we tried to evaluate the electrochemical performance of CNW prepared with sequential method towards detecting AA and UA and compare the result with CNW treated with O_2/Ar: 1.0/10sccm. As displayed in figure 5.10, the CV curves for the CNW synthesized with sequential method indicated an enhancement in oxidation current for AA and UA to compare with plasma surface treated CNW without decreasing its ability to simultaneously discriminate AA and UA.

In this thesis, we only introduced the inter-synthesis sequential method to prepare CNW with more edge planes and conformal oxygen functional group. However, its further characterization and in-depth analysis of its electrochemical performance is proposed as the future work.

(a)

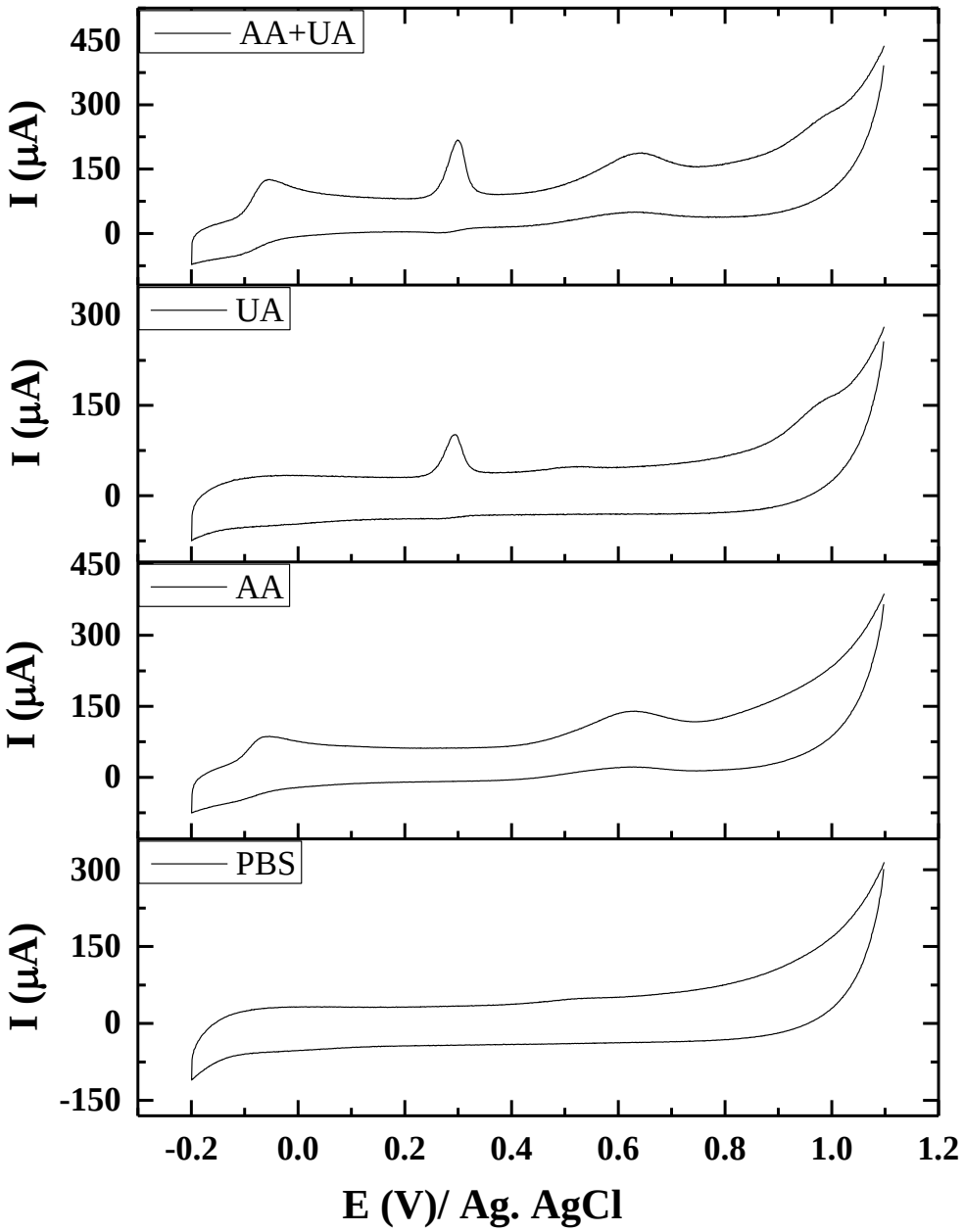
AA+UA
UA
AA
PBS
I (μA)
450
300
150
0
-150
-0.2
0.0
0.2
0.4
0.6
0.8
1.0
1.2
E (V)/ Ag. AgCl

(b)

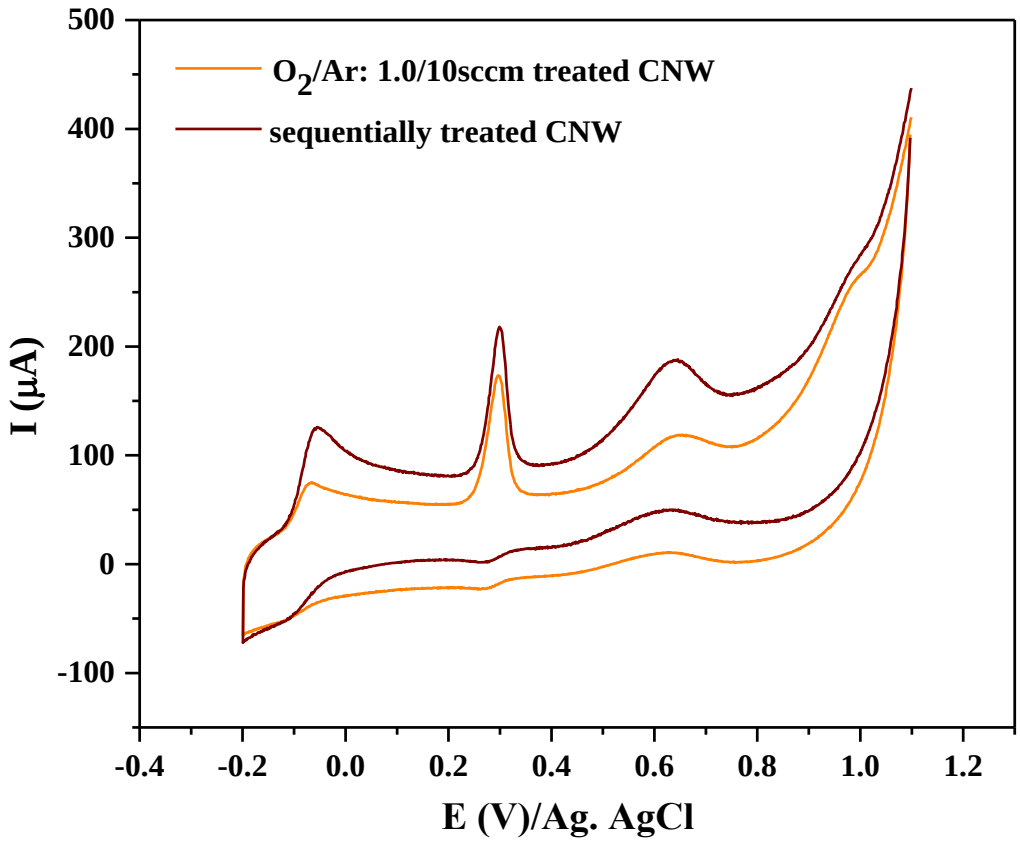

Figure. 5.10. CV profiles of (a) CNW prepared with inter-synthesis sequential treatment method in phosphate buffer solution, 1mM AA, 0.1mM UA, binary mixture of 1mM AA + 0.1mM UA, and (b) its comparison with CNW treated with O_2/Ar: 1.0/10 for binary mixture of 1mM AA + 0.1mM UA

5.6. Summary of the chapter

It was shown that the most hydrophilic CNW surface does not exhibit the highest electrochemical activity for the oxidation of H_2O_2. The highest amperometric response is observed for the CNW sample treated with O_2/Ar: 1.0/10sccm, which has lower oxygen content than CNW treated with O_2/Ar: 0.1/10sccm but still possessing hydrophilic characteristic and also owning more defective structure. These results can suggest the importance of both defects and oxygen-containing functional groups in electrochemical behavior of the electrodes as both defects and oxygen-containing functional groups can act as potential active sites for electrochemical reactions and

oxygen-containing functional groups can enhance the hydrophilicity and surface area wetted by the electrolyte. The modified CNW in O_2/Ar: 1.0/10sccm plasma displayed wide linear response range for oxidation H_2O_2 from 50µM to 28000µM, low LOD, and high sensitivity of 126.6µA/mM.cm^2. This study demonstrates that intrinsic modification of CNW by oxygen plasma can result in enhancing CNW performance in electrochemical sensing systems.

Chapter 6. Conclusions and future Work

6.1. Conclusions

In this study, the development of novel non-enzymatic H_2O_2 electrochemical sensors based on CNW was investigated. Two different approaches were considered to enhance electrochemical performance of CNW; Coating of CNW with transitional metal oxide MnO_x and surface plasma treatment of CNW in O_2/Ar system.

At first approach, synthesis of CNW films in different deposition times was performed and based on the obtained result from XPS and water contact angle analyses, the CNW prepared in 60s was selected for further investigations as it displayed same wettability and elemental concentrations as CNW prepared at 120s but having the advantage of shorter synthesis time. The following points can be concluded:

- Manganese oxides was electrodeposited on CNW at different deposition times (5s, 30s, and 60s). It was shown by SEM images that when deposition time is very short (5s), the film has mostly original CNW structure with some nucleation spots of MnO_x. By increasing deposition time to 30s, the accumulation of manganese oxides around the walls can be clearly confirmed. While, by further increase in deposition time (60s), it is difficult to distinguish the border between CNW and manganese oxide, which indicates that MnO_x can slightly infiltrate into the gaps between the walls.
- XPS analysis revealed that electrodeposited MnO_x coatings exhibit a mixed Mn valance states, where by increasing deposition time, the Mn oxidation state increases.
- Cyclic voltammetry (CV) measurement on MnO_x/CNW prepared in 60s showed an enhanced cathodic and anodic peak currents for MnO_x/CNW, indicating the excellent electrocatalytic activity of manganese oxides combined with high surface area and great electroconductivity of CNW.
- It was observed by amperometric responses that proposed electrode has high electrochemical activity for oxidation of hydrogen peroxide (H_2O_2) in phosphate buffer solution at an applied potential of +0.7V, showing a linear dependence on the concentration of H_2O_2 from 40µM to 10230µM, a high sensitivity (698.6 µA mM^{-1} cm^{-2}), and a detection limit of 0.55µM (signal/noise=3).

- The amperometric response for the reduction reaction at an applied potential of -0.5V showed a sensitivity of 21.03 μA mM^{-1} cm^{-2}, which is around 37 times less than the sensitivity obtained at the potential of +0.7V, suggesting MnO_x/CNW is highly sensitive to detect H_2O_2 at oxidation potential.

At second approach, further improvement in CNW performance as a metal-free electrochemical sensor through its intrinsic modification was evaluated. For this purpose, O_2/Ar plasma with different O_2 flow ratios were applied to modify the surfaces of CNW samples. The following points can be concluded:

- Our results revealed that CNW treated in low oxygen flow rate (O_2/Ar: 0.1/10sccm) exhibited the highest concentration of incorporated oxygen on its structure, which consequently resulted in conversion of intrinsic hydrophobicity of CNW to hydrophilicity.
- Interestingly, further increase in oxygen flow rate did not increase the oxygen content of CNW structure, but instead it resulted in an increment in the defect and contributing less oxygen on CNW surface.
- It is assumed that when low density of oxygen species exists in the plasma treatment gas mixture, the amorphous carbon that exists on the surface of as-grown CNW are selectively etched and the potential active oxygen species are stabilized to the produced defect sites, therefore formation of oxygen functional groups occurs favorably. However, the higher density of reactive oxygen species can result in higher etching rate, which can consequently lead to increase the etch rate from both amorphous and sp^2 structures and prevent the stabilization of oxygen in the defect positions, hence contributing less oxygen functional groups on the CNW structure.
- CV measurement confirmed that oxidation current significantly increases after plasma treatment of CNW surface, showing an obvious increase in oxidation current of CNW treated in 10sccm Ar, which further increased by adding and increasing O_2 (0.1sccm to 1.0sccm) in Ar plasma. However, further increase in oxygen flow rate (2.0sccm) resulted in a decrease in the current due to the destruction of CNW at higher oxygen density of plasma treating gas.
- Moreover, it was shown that the most hydrophilic CNW surface does not exhibit the highest electrochemical activity for the oxidation of H_2O_2. The highest amperometric

response is observed for the CNW sample treated with O_2/Ar: 1.0/10sccm, which has lower oxygen content than CNW treated with O_2/Ar: 0.1/10sccm but still possessing hydrophilic characteristic and also owning more defective structure.

- These results can suggest the importance of both defects and oxygen-containing functional groups in electrochemical behavior of the electrodes as both defects and oxygen-containing functional groups can act as potential active sites for electrochemical reactions and oxygen-containing functional groups can enhance the hydrophilicity and surface area wetted by the electrolyte.
- The modified CNW in O_2/Ar: 1.0/10sccm plasma displayed wide linear response range for oxidation H_2O_2 from 50µM to 28000µM, low LOD, and high sensitivity of 126.6µA/mM.cm^2. This study demonstrates that intrinsic modification of CNW by O_2/Ar plasma can result in enhancing CNW performance in electrochemical sensing systems as a metal-free electrode.
- The selective electrocatalysis properties of CNW treated with O_2/Ar: 1.0/10sccm was evaluated in the presence of ascorbic acid (AA), uric acid (UA), and H_2O_2. It was shown that by scanning different potentials, the effect of interference can be circumvented.

6.2. Future works

Based on the overall results presented in this thesis, future works can be considered as follows:

- In order to utilize the full advantage of CNW as a base conductive porous material in MnO_x/CNW nanocomposite's structure, depositing highly conformal coating on the deep parts of the pores shall be required. Optimization of electrochemical deposition condition or/ and atomic layer deposition (ALD) technique can be considered to design highly conformal thin coating.
- Considering the application of plasma modified CNW as a metal-free electrochemical sensor, it is required to consider the aging effect on plasma treated CNW samples and evaluate its effect on long-term stability of the sensor.

- The application of the modified CNW for detecting different biomarkers such as epinephrine, dopamine, and so on can be considered to further widen CNW application as electrochemical sensor.
- In depth analysis of characteristics and electrochemical performance of CNW prepared with inter-synthesis sequential treatment method is required to further take the advantage of highly defective edge plane structure and conformal oxygen functional groups in selectively detecting of different biomarkers.

Acknowledgment

There are several people, who without their help and support, this thesis and work done towards it would not have been possible. Hence, I would like to take this opportunity to show my gratitude to those who have assisted me to accomplish my study.

First of all, I would like to express my sincere gratitude to my supervisor, Professor Shinsuke Mori, who has been continuously providing the support throughout my PhD with his guidance, patience, enthusiasm and encouragement.

I would also like to thank Dr. Abdassedk Anagri. Your expertise and discussion have been invaluable. I would like to thank Nasrin and all my lab members for the friendship and the best time we had ever.

Many special thanks go to Takase scholarship foundation for financial support.

I am grateful to my family, who have consistently been a source of peace and inspiration throughout, without their love, support, and encouragement, this work could not have been achieved. I would like to present my sincere thankfulness to my late father, who passed away during my PhD study for his immense support and love in every step of my life.

Appendix (Supplementary data)

Chapter 2

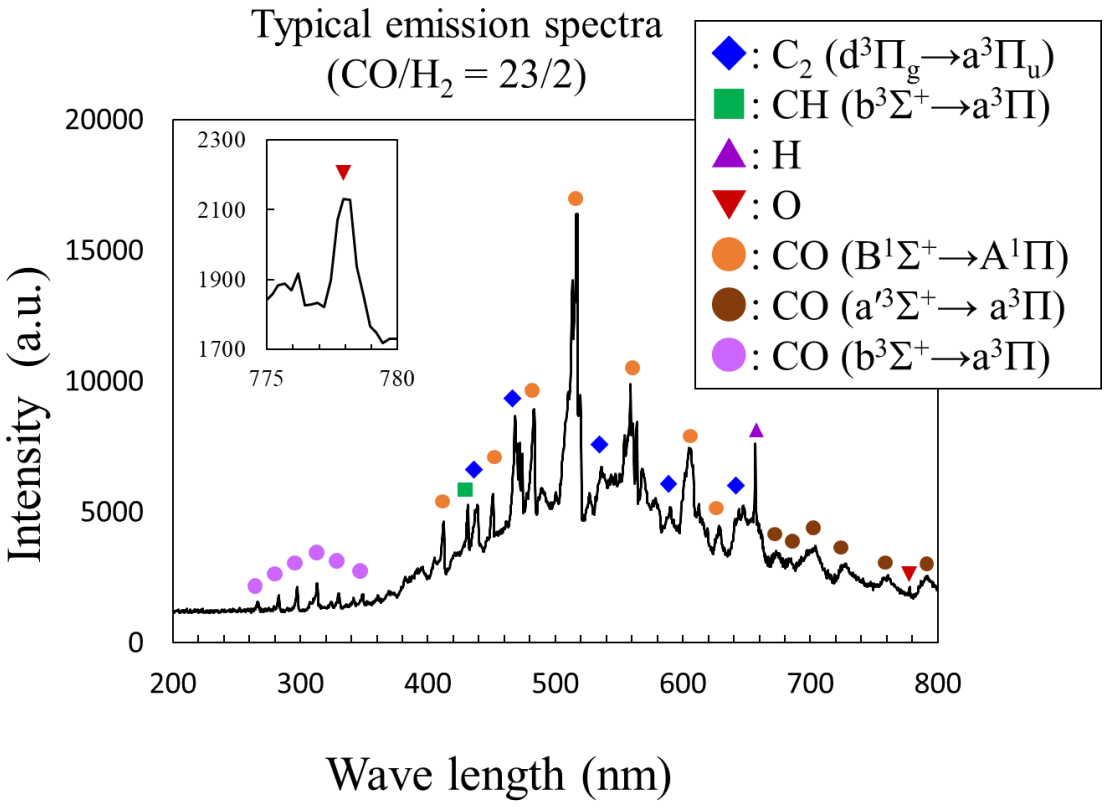

Figure S2-1. OES spectrum for CO/H_2 (23/2)sccm plasma

(a)

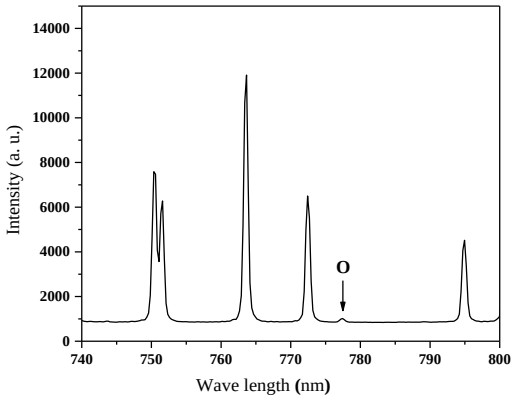
Intensity (a. u.)
Wave length (nm)
O

(b)

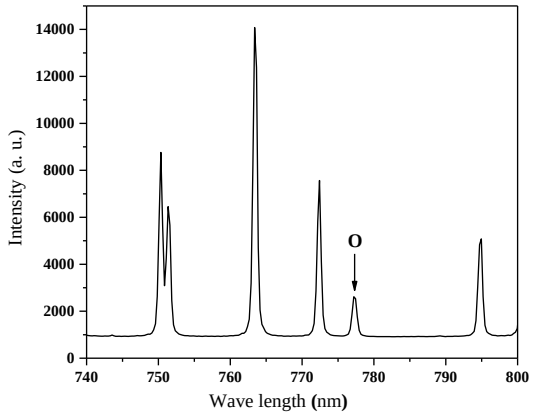
Intensity (a. u.)
Wave length (nm)
O

(c)

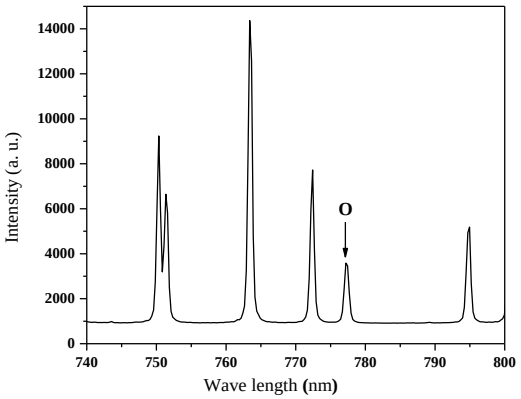
Intensity (a. u.)
Wave length (nm)
O

(d)

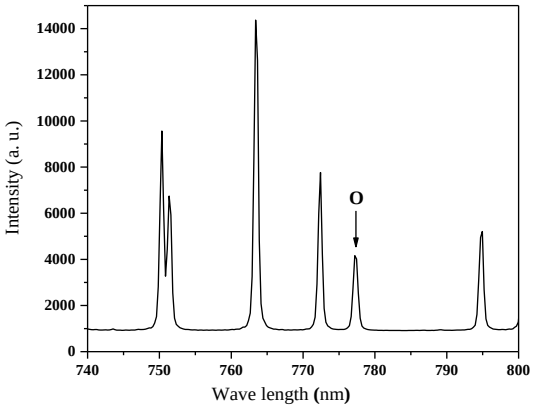
Intensity (a. u.)
Wave length (nm)
O

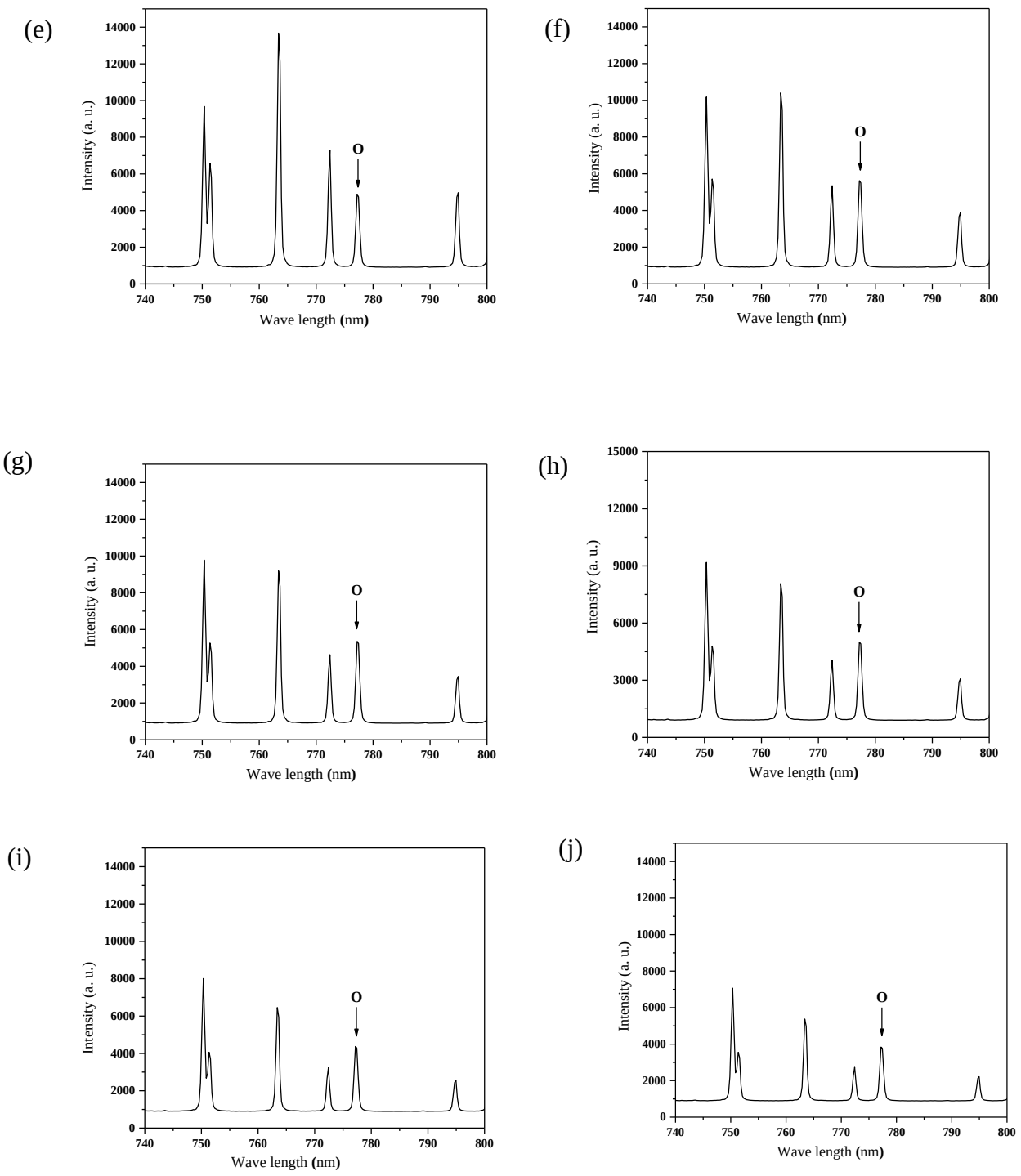

Figure S5-2. OES spectrum for plasma treatment condition of O_2/Ar: 0.0/10sccm (a), O_2/Ar: 0.1/10sccm (b), O_2/Ar: 0.2/10sccm (c), O_2/Ar: 0.3/10sccm (d), O_2/Ar: 0.5/10sccm (e), O_2/Ar: 1.0/10sccm (f), O_2/Ar: 2.0/10sccm (g), O_2/Ar: 3.0/10sccm (h), O_2/Ar: 4.0/10sccm (i), O_2/Ar: 5.0/10sccm (j)

Research achievements

Publications

1. F. Bohlooli, A. Yamatogi, S. Mori
   "Mangnaese oxides/carbon nanowall nanocomposite electrode as an efficient non-enzymatic electrochemical sensor for hydrogen peroxide", Sensing and Biosensing Research 31 (2021) 100392.
   https://doi.org/10.1016/j.sbsr.2020.100392

2. F. Bohlooli, A. Anagri, S. Mori
   "Development of carbon-based metal-free electrochemical sensor for hydrogen peroxide by surface modification of carbon nanowalls", Carbon 196 (2022) 327-336. https://doi.org/10.1016/j.carbon.2022.05.002

International conference

1. F. Bohlooli, A. Yamatogi, S. Mori
   "Electrochemical behavior of Manganese oxide/ Carbon nanowalls nanocomposite thin films", 11th Asian-European International Conference on Plasma Surface Engineering, Jeju Island (Korea), Sep 2017.

2. F. Bohlooli, S. Mori
   "Hydrogen peroxide sensor based on MnO_2/CNW nanocomposite electrode", 18th Asian Pacific Confederation of Chemical engineering congress, Sapporo (Japan), Sep 2019

3. F. Bohlooli, A. Anagri, S. Mori, J. Pulpytel, F. Arefi-Khonsari
   "Oxygen plasma treatment of carbon nanowalls and its effect on hydrogen peroxide detection", 18th International Conference on Plasma Surface Engineering, Erfurt (Germany), Sep 2022.

References

[1] D. Maiti, X. Tong, X. Mou, K. Yang, Carbon-based nanomaterials for biomedical applications: a recent study, Front. Pharmacol. 9 (2019) 1401.

[2] A. Hirsch, The era of carbon allotropes, Nat. Mater. 9 (2010) 868–871.

[3] A.K. Geim, K.S. Novoselov, The rise of graphene, in: Nanosci. Technol. Collect. Rev. Nat. J., World Scientific, 2010: pp. 11–19.

[4] S. Wu, Q. He, C. Tan, Y. Wang, H. Zhang, Graphene-based electrochemical sensors, Small. 9 (2013) 1160–1172.

[5] A. Ambrosi, C.K. Chua, A. Bonanni, M. Pumera, Electrochemistry of graphene and related materials, Chem. Rev. 114 (2014) 7150–7188.

[6] Z. González, S. Vizireanu, G. Dinescu, C. Blanco, R. Santamaría, Carbon nanowalls thin films as nanostructured electrode materials in vanadium redox flow batteries, Nano Energy. 1 (2012) 833–839.

[7] V.A. Krivchenko, D.M. Itkis, S.A. Evlashin, D.A. Semenenko, E.A. Goodilin, A.T. Rakhimov, A.S. Stepanov, N.V. Suetin, A.A. Pilevsky, P.V. Voronin, Carbon nanowalls decorated with silicon for lithium-ion batteries, Carbon. 50 (2012) 1438–1442.

[8] S. Hassan, M. Suzuki, S. Mori, A. Abd El-Moneim, MnO_2/carbon nanowalls composite electrode for supercapacitor application, J. Power Sources. 249 (2014) 21–27.

[9] S. Chul Shin, A. Yoshimura, T. Matsuo, M. Mori, M. Tanimura, A. Ishihara, K. Ota, M. Tachibana, Carbon nanowalls as platinum support for fuel cells, J. Appl. Phys. 110 (2011) 104308.

[10] K. Lehmann, O. Yurchenko, G. Urban, Carbon Nanowalls for oxygen reduction reaction in Bio Fuel Cells, in: J. Phys. Conf. Ser., IOP Publishing, 2014: p. 012008.

[11] A. Blout, J. Pulpytel, S. Mori, F. Arefi-Khonsari, C. Méthivier, A. Pailleret, C. Jolivalt, Carbon nanowalls functionalization for efficient O_2 reduction catalyzed by laccase using design of experiment, Appl. Surf. Sci. 547 (2021) 149112.

[12] M. Tomatsu, M. Hiramatsu, J.S. Foord, H. Kondo, K. Ishikawa, M. Sekine, K. Takeda, M. Hori, Hydrogen peroxide sensor based on carbon nanowalls grown by plasma-enhanced chemical vapor deposition, Jpn. J. Appl. Phys. 56 (2017) 06HF03.

[13] N.G. Shang, P. Papakonstantinou, M. McMullan, M. Chu, A. Stamboulis, A. Potenza, S.S. Dhesi, H. Marchetto, Catalyst-free efficient growth, orientation and biosensing properties of multilayer graphene nanoflake films with sharp edge planes, Adv. Funct. Mater. 18 (2008) 3506–3514.

[14] N.S. Komarova, A.G. Krivenko, E.V. Stenina, L.N. Sviridova, K.V. Mironovich, Y.M. Shulga, V.A. Krivchenko, Enhancement of the carbon nanowall film capacitance. Electron transfer kinetics on functionalized surfaces, Langmuir. 31 (2015) 7129–7137.

[15] M. Hiramatsu, H. Kondo, M. Hori, Graphene Nanowalls, in: J.R. Gong (Ed.), New Prog. Graphene Res., InTech, 2013. https://doi.org/10.5772/51528.

[16] V. Kumar, M.S. Mohamed, S. Veeranarayanan, T. Maekawa, D.S. Kumar, Functionalized carbon nanowalls as pro-angiogenic scaffolds for endothelial cell activation, ACS Appl. Bio Mater. 2 (2019) 1119–1130.

[17] Y. Wu, P. Qiao, T. Chong, Z. Shen, Carbon nanowalls grown by microwave plasma enhanced chemical vapor deposition, Adv. Mater. 14 (2002) 64–67.

[18] N. Santhosh, G. Filipič, E. Tatarova, O. Baranov, H. Kondo, M. Sekine, M. Hori, K. Ostrikov, U. Cvelbar, Oriented Carbon Nanostructures by Plasma Processing: Recent Advances and Future Challenges, Micromachines. 9 (2018) 565. https://doi.org/10.3390/mi9110565.

[19] R. Liu, Y. Chi, L. Fang, Z. Tang, X. Yi, Synthesis of carbon nanowall by plasma-enhanced chemical vapor deposition method, J. Nanosci. Nanotechnol. 14 (2014) 1647–1657.

[20] T. Yamada, J. Kim, M. Ishihara, M. Hasegawa, Low-temperature graphene synthesis using microwave plasma CVD, J. Phys. Appl. Phys. 46 (2013) 063001.

[21] K.B. Teo, D.B. Hash, R.G. Lacerda, N.L. Rupesinghe, M.S. Bell, S.H. Dalal, D. Bose, T.R. Govindan, B.A. Cruden, M. Chhowalla, The significance of plasma heating in carbon nanotube and nanofiber growth, Nano Lett. 4 (2004) 921–926.

[22] T. Terasawa, K. Saiki, Growth of graphene on Cu by plasma enhanced chemical vapor deposition, Carbon. 50 (2012) 869–874.

[23] S.K. Srivastava, A.K. Shukla, V.D. Vankar, V. Kumar, Growth, structure and field emission characteristics of petal like carbon nano-structured thin films, Thin Solid Films. 492 (2005) 124–130.

[24] R. Vitchev, A. Malesevic, R.H. Petrov, R. Kemps, M. Mertens, A. Vanhulsel, C. Van Haesendonck, Initial stages of few-layer graphene growth by microwave plasma-enhanced chemical vapour deposition, Nanotechnology. 21 (2010) 095602.

[25] A. Malesevic, R. Vitchev, K. Schouteden, A. Volodin, L. Zhang, G. Van Tendeloo, A. Vanhulsel, C. Van Haesendonck, Synthesis of few-layer graphene via microwave plasma-enhanced chemical vapour deposition, Nanotechnology. 19 (2008) 305604.

[26] A. Vesel, R. Zaplotnik, G. Primc, M. Mozetič, Synthesis of vertically oriented graphene sheets or carbon nanowalls—Review and challenges, Materials. 12 (2019) 2968.

[27] S. Kondo, S. Kawai, W. Takeuchi, K. Yamakawa, S. Den, H. Kano, M. Hiramatsu, M. Hori, Initial growth process of carbon nanowalls synthesized by radical injection plasma-enhanced chemical vapor deposition, J. Appl. Phys. 106 (2009) 094302. https://doi.org/10.1063/1.3253734.

[28] S. Mori, T. Ueno, M. Suzuki, Synthesis of carbon nanowalls by plasma-enhanced chemical vapor deposition in a CO/H_2 microwave discharge system, Diam. Relat. Mater. 20 (2011) 1129–1132.

[29] K. Yu, Z. Bo, G. Lu, S. Mao, S. Cui, Y. Zhu, X. Chen, R.S. Ruoff, J. Chen, Growth of carbon nanowalls at atmospheric pressure for one-step gas sensor fabrication, Nanoscale Res. Lett. 6 (2011) 1–9.

[30] M. Meško, V. Vretenár, P. Kotrusz, M. Hulman, J. Šoltỳs, V. Skákalová, Carbon nanowalls synthesis by means of atmospheric dcPECVD method, Phys. Status Solidi B. 249 (2012) 2625–2628.

[31] A. Giese, S. Schipporeit, V. Buck, N. Wöhrl, Synthesis of carbon nanowalls from a single-source metal-organic precursor, Beilstein J. Nanotechnol. 9 (2018) 1895–1905.

[32] J. Wang, M. Zhu, R.A. Outlaw, X. Zhao, D.M. Manos, B.C. Holloway, Synthesis of carbon nanosheets by inductively coupled radio-frequency plasma enhanced chemical vapor deposition, Carbon. 42 (2004) 2867–2872.

[33] Y. Wu, B. Yang, B. Zong, H. Sun, Z. Shen, Y. Feng, Carbon nanowalls and related materials, J. Mater. Chem. 14 (2004) 469–477.

[34] H. Kondo, M. Hori, M. Hiramatsu, Nucleation and Vertical Growth of Nano-Graphene Sheets, in: J. Gong (Ed.), Graphene - Synth. Charact. Prop. Appl., InTech, 2011. https://doi.org/10.5772/23703.

[35] M. Zhu, J. Wang, B.C. Holloway, R.A. Outlaw, X. Zhao, K. Hou, V. Shutthanandan, D.M. Manos, A mechanism for carbon nanosheet formation, Carbon. 45 (2007) 2229–2234.

[36] B. Dashtbozorg, X. Tao, H. Dong, Active-screen plasma surface multi-functionalisation of biopolymers and carbon-based materials–An overview, Surf. Coat. Technol. (2022) 128188.

[37] Y. Huang, Q. Yu, M. Li, S. Sun, H. Zhao, S. Jin, J. Fan, J. Wang, An overview of low-temperature plasma surface modification of carbon materials for removal of pollutants from liquid and gas phases, Plasma Process. Polym. 18 (2021) 2000171. https://doi.org/10.1002/ppap.202000171.

[38] K. Bazaka, M.V. Jacob, R.J. Crawford, E.P. Ivanova, Plasma-assisted surface modification of organic biopolymers to prevent bacterial attachment, Acta Biomater. 7 (2011) 2015–2028.

[39] G.Z. Qu, J. Li, D.L. Liang, D.L. Huang, D. Qu, Y.M. Huang, Surface modification of a granular activated carbon by dielectric barrier discharge plasma and its effects on pentachlorophenol adsorption, J. Electrost. 71 (2013) 689–694.

[40] H.C. Huang, D.Q. Ye, B.C. Huang, Nitrogen plasma modification of viscose-based activated carbon fibers, Surf. Coat. Technol. 201 (2007) 9533–9540.

[41] S. Duan, X. Liu, Y. Wang, Y. Meng, A. Alsaedi, T. Hayat, J. Li, Plasma surface modification of materials and their entrapment of water contaminant: A review, Plasma Process. Polym. 14 (2017) 1600218.

[42] O. González-Cordero, L.E. Cruz-Barba, S.A. Gómez-Torres, F.R. Carrillo-Pedroza, C. del R.A. del Rio, M.A. Sánchez-Castillo, Catalytic performance of oxygenated acid sites on activated carbon generated by non-isothermal plasma, Carbon. 126 (2018) 552–565.

[43] C. Chen, B. Liang, A. Ogino, X. Wang, M. Nagatsu, Oxygen functionalization of multiwall carbon nanotubes by microwave-excited surface-wave plasma treatment, J. Phys. Chem. C. 113 (2009) 7659–7665.

[44] C. Chen, B. Liang, D. Lu, A. Ogino, X. Wang, M. Nagatsu, Amino group introduction onto multiwall carbon nanotubes by NH3/Ar plasma treatment, Carbon. 48 (2010) 939–948.

[45] S. Tang, N. Lu, J.K. Wang, S.-K. Ryu, H.S. Choi, Novel effects of surface modification on activated carbon fibers using a low pressure plasma treatment, J. Phys. Chem. C. 111 (2007) 1820–1829.

[46] B. Eliasson, U. Kogelschatz, Nonequilibrium volume plasma chemical processing, IEEE Trans. Plasma Sci. 19 (1991) 1063–1077.

[47] W.H. Wang, B.C. Huang, L.S. Wang, D.Q. Ye, Oxidative treatment of multi-wall carbon nanotubes with oxygen dielectric barrier discharge plasma, Surf. Coat. Technol. 205 (2011) 4896–4901.

[48] R. Mohan, A. Modak, A. Schechter, NH_3-Plasma pre-treated carbon supported active iron–nitrogen catalyst for oxygen reduction in acid and alkaline electrolytes, Catal. Sci. Technol. 10 (2020) 1675–1687.

[49] M. Shi, G. Luo, Y. Xu, R. Zou, H. Zhu, J. Hu, X. Li, H. Yao, Using H_2S plasma to modify activated carbon for elemental mercury removal, Fuel. 254 (2019) 115549.

[50] B. Zhang, P. Xu, Y. Qiu, Q. Yu, J. Ma, H. Wu, G. Luo, M. Xu, H. Yao, Increasing oxygen functional groups of activated carbon with non-thermal plasma to enhance mercury removal efficiency for flue gases, Chem. Eng. J. 263 (2015) 1–8.

[51] H. Watanabe, H. Kondo, M. Hiramatsu, M. Sekine, S. Kumar, K. Ostrikov, M. Hori, Surface chemical modification of carbon nanowalls for wide-range control of surface wettability, Plasma Process. Polym. 10 (2013) 582–592.

[52] S. Vizireanu, M.D. Ionita, G. Dinescu, I. Enculescu, M. Baibarac, I. Baltog, Post-synthesis carbon nanowalls transformation under hydrogen, oxygen, nitrogen, tetrafluoroethane and sulfur hexafluoride plasma treatments, Plasma Process. Polym. 9 (2012) 363–370.

[53] N. Jiang, H.X. Wang, H. Zhang, H. Sasaoka, K. Nishimura, Characterization and surface modification of carbon nanowalls, J. Mater. Chem. 20 (2010) 5070–5073.

[54] D.C. Elias, R.R. Nair, T.M.G. Mohiuddin, S.V. Morozov, P. Blake, M.P. Halsall, A.C. Ferrari, D.W. Boukhvalov, M.I. Katsnelson, A.K. Geim, K.S. Novoselov, Control of Graphene's Properties by Reversible Hydrogenation: Evidence for Graphane, Science. (2009). https://doi.org/10.1126/science.1167130.

[55] S. Yamada, K. Tanabe, Y. Ieda, T. Suzuki, H. Sobue, T. Itoh, S. Nonomura, Changes in wettability of carbon nanowalls by oxygen plasma treatment, Jpn. J. Appl. Phys. 59 (2019) SAAB05.

[56] G. Sahoo, S.R. Polaki, S. Ghosh, N.G. Krishna, M. Kamruddin, K.K. Ostrikov, Plasma-tuneable oxygen functionalization of vertical graphenes enhance electrochemical capacitor performance, Energy Storage Mater. 14 (2018) 297–305.

[57] T. Gokus, R.R. Nair, A. Bonetti, M. Böhmler, A. Lombardo, K.S. Novoselov, A.K. Geim, A.C. Ferrari, A. Hartschuh, Making Graphene Luminescent by Oxygen Plasma Treatment, ACS Nano. 3 (2009) 3963–3968. https://doi.org/10.1021/nn9012753.

[58] Y. Wang, J. Li, K. Song, Study on formation and photoluminescence of carbon nanowalls grown on silicon substrates by hot filament chemical vapor deposition, J. Lumin. 149 (2014) 258–263.

[59] H.J. Cho, H. Kondo, K. Ishikawa, M. Sekine, M. Hiramatsu, M. Hori, Effects of nitrogen plasma post-treatment on electrical conduction of carbon nanowalls, Jpn. J. Appl. Phys. 53 (2014) 040307. https://doi.org/10.7567/JJAP.53.040307.

[60] Y.W. Chi, C.C. Hu, H.H. Shen, K.P. Huang, New Approach for High-Voltage Electrical Double-Layer Capacitors Using Vertical Graphene Nanowalls with and without Nitrogen Doping, Nano Lett. 16 (2016) 5719–5727. https://doi.org/10.1021/acs.nanolett.6b02401.

[61] H.F. Yen, Y.Y. Horng, M.S. Hu, W.H. Yang, J.R. Wen, A. Ganguly, Y. Tai, K.-H. Chen, L.C. Chen, Vertically aligned epitaxial graphene nanowalls with dominated nitrogen doping for superior supercapacitors, Carbon. 82 (2015) 124–134. https://doi.org/10.1016/j.carbon.2014.10.042.

[62] P. Hojati-Talemi, G.P. Simon, Field emission study of graphene nanowalls prepared by microwave-plasma method, Carbon. 49 (2011) 2875–2877.

[63] J.L. Qi, X. Wang, W.T. Zheng, H.W. Tian, C.Q. Hu, Y.S. Peng, Ar plasma treatment on few layer graphene sheets for enhancing their field emission properties, J. Phys. Appl. Phys. 43 (2010) 055302. https://doi.org/10.1088/0022-3727/43/5/055302.

[64] L. Cui, J. Chen, B. Yang, D. Sun, T. Jiao, RF-PECVD synthesis of carbon nanowalls and their field emission properties, Appl. Surf. Sci. 357 (2015) 1–7.

[65] H. Watanabe, H. Kondo, M. Sekine, M. Hiramatsu, M. Hori, Control of Super Hydrophobic and Super Hydrophilic Surfaces of Carbon Nanowalls Using Atmospheric Pressure Plasma Treatments, Jpn. J. Appl. Phys. 51 (2012) 01AJ07. https://doi.org/10.1143/JJAP.51.01AJ07.

[66] S.A. Evlashin, F.S. Fedorov, P.V. Dyakonov, Y.M. Maksimov, A.A. Pilevsky, K.I. Maslakov, Y.O. Kuzminova, Y.A. Mankelevich, E.N. Voronina, S.A. Dagesyan, Role of nitrogen and oxygen in capacitance formation of carbon nanowalls, J. Phys. Chem. Lett. 11 (2020) 4859–4865.

[67] J. Wang, Analytical electrochemistry, N. Y. USA Wiley. 10 (2006) 0471790303.

[68] A. lvarez-Lueje, M. Prez, C. Zapat, Electrochemical Methods for the In Vitro Assessment of Drug Metabolism, in: J. Paxton (Ed.), Top. Drug Metab., InTech, 2012. https://doi.org/10.5772/28647.

[69] N.J. Ronkainen, H.B. Halsall, W.R. Heineman, Electrochemical biosensors, Chem. Soc. Rev. 39 (2010) 1747. https://doi.org/10.1039/b714449k.

[70] J.N. Tiwari, V. Vij, K.C. Kemp, K.S. Kim, Engineered carbon-nanomaterial-based electrochemical sensors for biomolecules, ACS Nano. 10 (2016) 46–80.

[71] F. Zhao, R.C.T. Slade, J.R. Varcoe, Techniques for the study and development of microbial fuel cells: an electrochemical perspective, Chem. Soc. Rev. 38 (2009) 1926. https://doi.org/10.1039/b819866g.

[72] K. Dhara, D.R. Mahapatra, Recent advances in electrochemical nonenzymatic hydrogen peroxide sensors based on nanomaterials: a review, J. Mater. Sci. 54 (2019) 12319–12357.

[73] B. Xu, M.L. Ye, Y.X. Yu, W.D. Zhang, A highly sensitive hydrogen peroxide amperometric sensor based on MnO_2-modified vertically aligned multiwalled carbon nanotubes, Anal. Chim. Acta. 674 (2010) 20–26. https://doi.org/10.1016/j.aca.2010.06.004.

[74] H. Begum, M.S. Ahmed, S. Jeon, A novel δ-MnO_2 with carbon nanotubes nanocomposite as an enzyme-free sensor for hydrogen peroxide electrosensing, RSC Adv. 6 (2016) 50572–50580. https://doi.org/10.1039/C6RA08738H.

[75] W. Chen, S. Cai, Q.Q. Ren, W. Wen, Y.D. Zhao, Recent advances in electrochemical sensing for hydrogen peroxide: a review, Analyst. 137 (2012) 49–58.

[76] M. Giorgio, M. Trinei, E. Migliaccio, P.G. Pelicci, Hydrogen peroxide: a metabolic by-product or a common mediator of ageing signals?, Nat. Rev. Mol. Cell Biol. 8 (2007) 722–728.

[77] A. Buczyński, B. Wachowicz, K. Kędziora-Kornatowska, W. Tkaczewski, J. Kędziora, Changes in antioxidant enzymes activities, aggregability and malonyldialdehyde concentration in blood platelets from patients with coronary heart disease, Atherosclerosis. 100 (1993) 223–228.

[78] P. Jenner, P. Jenner, Oxidative stress as a cause of Parkinson's disease, Acta Neurol. Scand. 84 (1991) 6–15.

[79] J.W. Baynes, Role of oxidative stress in development of complications in diabetes, Diabetes. 40 (1991) 405–412.

[80] T.P. Szatrowski, C.F. Nathan, Production of large amounts of hydrogen peroxide by human tumor cells, Cancer Res. 51 (1991) 794–798.

[81] R. Wilson, A.P.F. Turner, Glucose oxidase: an ideal enzyme, Biosens. Bioelectron. 7 (1992) 165–185.

[82] M. Seki, K. Iida, M. Saito, H. Nakayama, S. Yoshida, Hydrogen peroxide production in Streptococcus pyogenes: involvement of lactate oxidase and coupling with aerobic utilization of lactate, J. Bacteriol. 186 (2004) 2046–2051.

[83] N.V. Klassen, David. Marchington, H.C.E. McGowan, H_2O_2 Determination by the I3-Method and by $KMnO_4$ Titration, Anal. Chem. 66 (1994) 2921–2925. https://doi.org/10.1021/ac00090a020.

[84] E.C. Hurdis, Hendrik. Romeyn, Accuracy of Determination of Hydrogen Peroxide by Cerate Oxidimetry, Anal. Chem. 26 (1954) 320–325. https://doi.org/10.1021/ac60086a016.

[85] U. Pinkernell, S. Effkemann, U. Karst, Simultaneous HPLC Determination of Peroxyacetic Acid and Hydrogen Peroxide, Anal. Chem. 69 (1997) 3623–3627. https://doi.org/10.1021/ac9701750.

[86] G. Eisenberg, Colorimetric determination of hydrogen peroxide, Ind. Eng. Chem. Anal. Ed. 15 (1943) 327–328.

[87] S. Hanaoka, J.-M. Lin, M. Yamada, Chemiluminescent flow sensor for H_2O_2 based on the decomposition of H_2O_2 catalyzed by cobalt (II)-ethanolamine complex immobilized on resin, Anal. Chim. Acta. 426 (2001) 57–64.

[88] R.F. Beers, I.W. Sizer, A spectrophotometric method for measuring the breakdown of hydrogen peroxide by catalase, J. Biol. Chem. 195 (1952) 133–140.

[89] Z. Jiang, L. Kun, H. Ouyang, A. Liang, H. Jiang, A Simple and Sensitive Fluorescence Quenching Method for the Determination of H_2O_2 Using Rhodamine B and Fe3O4 Nanocatalyst, J. Fluoresc. 21 (2011) 2015–2020. https://doi.org/10.1007/s10895-011-0902-7.

[90] Y. Shu, J. Xu, J. Chen, Q. Xu, X. Xiao, D. Jin, H. Pang, X. Hu, Ultrasensitive electrochemical detection of H_2O_2 in living cells based on ultrathin MnO_2 nanosheets, Sens. Actuators B Chem. 252 (2017) 72–78. https://doi.org/10.1016/j.snb.2017.05.124.

[91] C. Batchelor-McAuley, Y. Du, G.G. Wildgoose, R.G. Compton, The use of copper (II) oxide nanorod bundles for the non-enzymatic voltammetric sensing of carbohydrates and hydrogen peroxide, Sens. Actuators B Chem. 135 (2008) 230–235.

[92] Y. Xiao, H.X. Ju, H.Y. Chen, Hydrogen peroxide sensor based on horseradish peroxidase-labeled Au colloids immobilized on gold electrode surface by cysteamine monolayer, Anal. Chim. Acta. 391 (1999) 73–82.

[93] S. Guo, D. Wen, S. Dong, E. Wang, Gold nanowire assembling architecture for H_2O_2 electrochemical sensor, Talanta. 77 (2009) 1510–1517. https://doi.org/10.1016/j.talanta.2008.09.042.

[94] S. Guo, D. Wen, Y. Zhai, S. Dong, E. Wang, Platinum Nanoparticle Ensemble-on-Graphene Hybrid Nanosheet: One-Pot, Rapid Synthesis, and Used as New Electrode Material for Electrochemical Sensing, ACS Nano. 4 (2010) 3959–3968. https://doi.org/10.1021/nn100852h.

[95] M.Y. Wang, T. Shen, M. Wang, D.E. Zhang, Z. Tong, J. Chen, One-pot synthesis of α-Fe_2O_3 nanoparticles-decorated reduced graphene oxide for efficient nonenzymatic H_2O_2 biosensor, Sens. Actuators B Chem. 190 (2014) 645–650. https://doi.org/10.1016/j.snb.2013.08.091.

[96] C.Y. Lin, Y.H. Lai, A. Balamurugan, R. Vittal, C.W. Lin, K.-C. Ho, Electrode modified with a composite film of ZnO nanorods and Ag nanoparticles as a sensor for hydrogen peroxide, Talanta. 82 (2010) 340–347.

[97] H.L. Xu, W.D. Zhang, Graphene oxide–MnO_2 nanocomposite-modified glassy carbon electrode as an efficient sensor for H_2O_2, Chin. Chem. Lett. 28 (2017) 143–148.

[98] D. Ye, H. Li, G. Liang, J. Luo, X. Zhang, S. Zhang, H. Chen, J. Kong, A three-dimensional hybrid of MnO_2/graphene/carbon nanotubes based sensor for determination of hydrogen-peroxide in milk, Electrochimica Acta. 109 (2013) 195–200. https://doi.org/10.1016/j.electacta.2013.06.119.

[99] R. Zhang, W. Chen, Recent advances in graphene-based nanomaterials for fabricating electrochemical hydrogen peroxide sensors, Biosens. Bioelectron. 89 (2017) 249–268.

[100] Z.L. Wu, C.K. Li, J.G. Yu, X.Q. Chen, MnO_2/reduced graphene oxide nanoribbons: Facile hydrothermal preparation and their application in amperometric detection of hydrogen peroxide, Sens. Actuators B Chem. 239 (2017) 544–552. https://doi.org/10.1016/j.snb.2016.08.062.

[101] K.J. Babu, A. Zahoor, K.S. Nahm, R. Ramachandran, M.A.J. Rajan, G. Gnana Kumar, The influences of shape and structure of MnO_2 nanomaterials over the non-enzymatic sensing ability of hydrogen peroxide, J. Nanoparticle Res. 16 (2014). https://doi.org/10.1007/s11051-014-2250-4.

[102] X. Jia, G. Hu, F. Nitze, H.R. Barzegar, T. Sharifi, C.W. Tai, T. Wågberg, Synthesis of palladium/helical carbon nanofiber hybrid nanostructures and their application for hydrogen peroxide and glucose detection, ACS Appl. Mater. Interfaces. 5 (2013) 12017–12022.

[103] X. Gan, T. Liu, J. Zhong, X. Liu, G. Li, Effect of silver nanoparticles on the electron transfer reactivity and the catalytic activity of myoglobin, ChemBioChem. 5 (2004) 1686–1691.

[104] C. Ray, S. Dutta, A. Roy, R. Sahoo, T. Pal, Redox mediated synthesis of hierarchical Bi_2O_3/MnO_2 nanoflowers: a non-enzymatic hydrogen peroxide electrochemical sensor, Dalton Trans. 45 (2016) 4780–4790. https://doi.org/10.1039/C6DT00062B.

[105] A. Salimi, R. Hallaj, S. Soltanian, H. Mamkhezri, Nanomolar detection of hydrogen peroxide on glassy carbon electrode modified with electrodeposited cobalt oxide nanoparticles, Anal. Chim. Acta. 594 (2007) 24–31.

[106] X.M. Miao, R. Yuan, Y.Q. Chai, Y.T. Shi, Y.Y. Yuan, Direct electrocatalytic reduction of hydrogen peroxide based on Nafion and copper oxide nanoparticles modified Pt electrode, J. Electroanal. Chem. 612 (2008) 157–163.

[107] P. Salazar, V. Rico, A.R. González-Elipe, Non-enzymatic hydrogen peroxide detection at NiO nanoporous thin film-electrodes prepared by physical vapor deposition at oblique angles, Electrochimica Acta. 235 (2017) 534–542.

[108] L. Wang, M. Deng, G. Ding, S. Chen, F. Xu, Manganese dioxide based ternary nanocomposite for catalytic reduction and nonenzymatic sensing of hydrogen peroxide, Electrochimica Acta. 114 (2013) 416–423. https://doi.org/10.1016/j.electacta.2013.10.074.

[109] S. He, B. Zhang, M. Liu, W. Chen, Non-enzymatic hydrogen peroxide electrochemical sensor based on a three-dimensional MnO_2 nanosheets/carbon foam composite, RSC Adv. 4 (2014) 49315–49323. https://doi.org/10.1039/C4RA09007A.

[110] C. Yang, M.E. Denno, P. Pyakurel, B.J. Venton, Recent trends in carbon nanomaterial-based electrochemical sensors for biomolecules: A review, Anal. Chim. Acta. 887 (2015) 17–37.

[111] Y. Han, J. Zheng, S. Dong, A novel nonenzymatic hydrogen peroxide sensor based on Ag–MnO_2–MWCNTs nanocomposites, Electrochimica Acta. 90 (2013) 35–43.

[112] K. Vijayalakshmi, S.D. Jereil, K. Alagusundaram, Electron beam and spray technologies fabrication of hybrid MnO_2/CNT/Ta nanocomposite for the electrochemical detection of H_2O_2, Ceram. Int. 43 (2017) 14464–14472.

[113] W. Liu, G. Speranza, Functionalization of Carbon Nanomaterials for Biomedical Applications, C. 5 (2019) 72. https://doi.org/10.3390/c5040072.

[114] L. Li, Z. Du, S. Liu, Q. Hao, Y. Wang, Q. Li, T. Wang, A novel nonenzymatic hydrogen peroxide sensor based on MnO_2/graphene oxide nanocomposite, Talanta. 82 (2010) 1637–1641. https://doi.org/10.1016/j.talanta.2010.07.020.

[115] F. Zeng, Y. Pan, Y. Yang, Q. Li, G. Li, Z. Hou, G. Gu, Facile construction of Mn_3O_4-MnO_2 hetero-nanorods/graphene nanocomposite for highly sensitive electrochemical detection of hydrogen peroxide, Electrochimica Acta. 196 (2016) 587–596.

[116] Y. Pan, Z. Hou, H. Yang, Y.N. Liu, Hierarchical architecture of nanographene-coated rice-like manganese dioxide nanorods/graphene for enhanced electrocatalytic activity toward hydrogen peroxide reduction, Mater. Sci. Semicond. Process. 40 (2015) 176–182.

[117] J. Zhang, D. Rao, J. Zheng, Synthesis of Ag nanoparticle doped MnO_2/GO nanocomposites at a gas/liquid interface and its application in H_2O_2 detection, Electroanalysis. 28 (2016) 588–595.

[118] S. Hassan, M. Suzuki, S. Mori, A. Abd El-Moneim, MnO_2/carbon nanowalls composite electrode for supercapacitor application, J. Power Sources. 249 (2014) 21–27.

[119] Y. Yerlanuly, R. Zhumadilov, R. Nemkayeva, B. Uzakbaiuly, A.R. Beisenbayev, Z. Bakenov, T. Ramazanov, M. Gabdullin, A. Ng, V.V. Brus, Physical properties of carbon nanowalls synthesized by the ICP-PECVD method vs. the growth time, Sci. Rep. 11 (2021) 1–12.

[120] N. M Santhosh, G. Filipič, E. Kovacevic, A. Jagodar, J. Berndt, T. Strunskus, H. Kondo, M. Hori, E. Tatarova, U. Cvelbar, N-graphene nanowalls via plasma nitrogen incorporation and substitution: The experimental evidence, Nano-Micro Lett. 12 (2020) 1–17.

[121] M. Toupin, T. Brousse, D. Bélanger, Charge storage mechanism of MnO_2 electrode used in aqueous electrochemical capacitor, Chem. Mater. 16 (2004) 3184–3190.

[122] M. Chigane, M. Ishikawa, Manganese oxide thin film preparation by potentiostatic electrolyses and electrochromism, J. Electrochem. Soc. 147 (2000) 2246.

[123] M. Toupin, T. Brousse, D. Bélanger, Influence of microstucture on the charge storage properties of chemically synthesized manganese dioxide, Chem. Mater. 14 (2002) 3946–3952.

[124] M. Huynh, D.K. Bediako, Y. Liu, D.G. Nocera, Nucleation and growth mechanisms of an electrodeposited manganese oxide oxygen evolution catalyst, J. Phys. Chem. C. 118 (2014) 17142–17152.

[125] K. Schachl, H. Alemu, K. Kalcher, J. Ježkova, I. Švancara, K. Vytřas, Amperometric Determination of Hydrogen Peroxide With a ManganeseDioxide-modified Carbon Paste Electrode Using Flow InjectionAnalysis, Analyst. 122 (1997) 985–989.

[126] L. Qi, C. YingXu, W. ZhaoWei, W. YuanPeng, Study on the possibility of hydrogen peroxide pretreatment and plant system to remediate soil pollution, Chemosphere. 57 (2004) 1439–1447.

[127] E. Ludwig, P. Eyer, Reactivity of glutathione adducts of 4-(dimethylamino) phenol. Involvement of reactive oxygen species during the interaction with oxyhemoglobin, Chem. Res. Toxicol. 8 (1995) 363–368.

[128] E. Zapp, V. Nascimento, D. Dambrowski, A.L. Braga, I.C. Vieira, Bio-inspired sensor based on glutathione peroxidase mimetic for hydrogen peroxide detection, Sens. Actuators B Chem. 176 (2013) 782–788.

[129] Y. Li, A. Townshend, Evaluation of the adsorptive immobilisation of horseradish peroxidase on PTFE tubing in flow systems for hydrogen peroxide determination using fluorescence detection, Anal. Chim. Acta. 359 (1998) 149–156.

[130] C. Guo, H. Li, X. Zhang, H. Huo, C. Xu, 3D porous CNT/MnO_2 composite electrode for high-performance enzymeless glucose detection and supercapacitor application, Sens. Actuators B Chem. 206 (2015) 407–414.

[131] L. Hu, W. Chen, X. Xie, N. Liu, Y. Yang, H. Wu, Y. Yao, M. Pasta, H.N. Alshareef, Y. Cui, Symmetrical MnO_2–Carbon Nanotube–Textile Nanostructures for Wearable Pseudocapacitors with High Mass Loading, ACS Nano. 5 (2011) 8904–8913. https://doi.org/10.1021/nn203085j.

[132] C. Zhang, Y. Zhang, Z. Miao, M. Ma, X. Du, J. Lin, B. Han, S. Takahashi, J. Anzai, Q. Chen, Dual-function amperometric sensors based on poly (diallydimethylammoniun

chloride)-functionalized reduced graphene oxide/manganese dioxide/gold nanoparticles nanocomposite, Sens. Actuators B Chem. 222 (2016) 663–673.

[133] X. Xiao, Y. Song, H. Liu, M. Xie, H. Hou, L. Wang, Z. Li, Electrospun carbon nanofibers with manganese dioxide nanoparticles for nonenzymatic hydrogen peroxide sensing, J. Mater. Sci. 48 (2013) 4843–4850.

[134] X. Feng, Y. Zhang, J. Song, N. Chen, J. Zhou, Z. Huang, Y. Ma, L. Zhang, L. Wang, MnO2/graphene nanocomposites for nonenzymatic electrochemical detection of hydrogen peroxide, Electroanalysis. 27 (2015) 353–359.

[135] J.H. Lee, H.G. Hong, Nonenzymatic electrochemical sensing of hydrogen peroxide based on a polyaniline-MnO_2 nanofiber-modified glassy carbon electrode, J. Appl. Electrochem. 45 (2015) 1153–1162.

[136] L. Luo, F. Li, L. Zhu, Z. Zhang, Y. Ding, D. Deng, Non-enzymatic hydrogen peroxide sensor based on MnO_2-ordered mesoporous carbon composite modified electrode, Electrochimica Acta. 77 (2012) 179–183.

[137] S. Cui, Y. Li, D. Deng, L. Zeng, X. Yan, J. Qian, L. Luo, Photo-reduction assisted synthesis of MnO_2/reduced graphene oxide/P25 for electrochemical detection of hydrogen peroxide, RSC Adv. 6 (2016) 2632–2640.

[138] F. Bohlooli, A. Yamatogi, S. Mori, Manganese oxides/carbon nanowall nanocomposite electrode as an efficient non-enzymatic electrochemical sensor for hydrogen peroxide, Sens. Bio-Sens. Res. 31 (2021) 100392.

[139] L. Zeng, D. Lei, W. Wang, J. Liang, Z. Wang, N. Yao, B. Zhang, Preparation of carbon nanosheets deposited on carbon nanotubes by microwave plasma-enhanced chemical vapor deposition method, Appl. Surf. Sci. 254 (2008) 1700–1704.

[140] N. Jiang, H.X. Wang, H. Zhang, H. Sasaoka, K. Nishimura, Characterization and surface modification of carbon nanowalls, J. Mater. Chem. 20 (2010) 5070–5073.

[141] K. Teii, S. Shimada, M. Nakashima, A.T. Chuang, Synthesis and electrical characterization of n-type carbon nanowalls, J. Appl. Phys. 106 (2009) 084303.

[142] E.C. Stancu, A.-M. Stanciuc, S. Vizireanu, C. Luculescu, L. Moldovan, A. Achour, G. Dinescu, Plasma functionalization of carbon nanowalls and its effect on attachment of fibroblast-like cells, J. Phys. Appl. Phys. 47 (2014) 265203.

[143] T. Xu, J. Yang, J. Liu, Q. Fu, Surface modification of multi-walled carbon nanotubes by O_2 plasma, Appl. Surf. Sci. 253 (2007) 8945–8951.

[144] H. Shimoeda, H. Kondo, K. Ishikawa, M. Hiramatsu, M. Sekine, M. Hori, Atomic oxygen etching from the top edges of carbon nanowalls, Appl. Phys. Express. 6 (2013) 095201.

[145] H. Choi, S.H. Kwon, H. Kang, J.H. Kim, W. Choi, Analysis of plasma-grown carbon oxide and reduced-carbon-oxide nanowalls, RSC Adv. 10 (2020) 9761–9767.

[146] J.I. Mendez-Linan, E. Ortiz-Ortega, M.F. Jimenez-Moreno, M.I. Mendivil-Palma, E. Martínez-Guerra, F.S. Aguirre-Tostado, S.O. Martinez-Chapa, S. Hosseini, M.J. Madou, Aging effect of plasma-treated carbon surfaces: An overlooked phenomenon, Carbon. 169 (2020) 32–44.

[147] V. Mărăscu, S. Vizireanu, S. Stoica, V. Barna, A. Lazeastoyanova, G. Dinescu, FTIR investigation of the ageing process of carbon nanowalls, Rom Rep Phys. 68 (2016) 1108–1114.

[148] S. Evlashin, S. Svyakhovskiy, N. Suetin, A. Pilevsky, T. Murzina, N. Novikova, A. Stepanov, A. Egorov, A. Rakhimov, Optical and IR absorption of multilayer carbon nanowalls, Carbon. 70 (2014) 111–118.

[149] D.W. Boukhvalov, M.I. Katsnelson, Chemical functionalization of graphene with defects, Nano Lett. 8 (2008) 4373–4379.

[150] L. Zhao, Y. Wang, X. Zhao, Y. Deng, Q. Li, Y. Xia, Green preparation of ag-Au bimetallic nanoparticles supported on graphene with alginate for non-enzymatic hydrogen peroxide detection, Nanomaterials. 8 (2018) 507.

[151] B. Wu, N. Zhao, S. Hou, C. Zhang, Electrochemical synthesis of polypyrrole, reduced graphene oxide, and gold nanoparticles composite and its application to hydrogen peroxide biosensor, Nanomaterials. 6 (2016) 220.

[152] X. Zhang, Y. Bao, Y. Bai, Z. Chen, J. Li, F. Feng, In situ electrochemical reduction assisted assembly of a graphene-gold nanoparticles@ polyoxometalate nanocomposite film and its high response current for detection of hydrogen peroxide, Electrochimica Acta. 300 (2019) 380–388.

[153] Y. Ni, Y. Liao, M. Zheng, S. Shao, In-situ growth of Co_3O_4 nanoparticles on mesoporous carbon nanofibers: a new nanocomposite for nonenzymatic amperometric sensing of H_2O_2, Microchim. Acta. 184 (2017) 3689–3695.

[154] Y. Qin, Y. Sun, Y. Li, C. Li, L. Wang, S. Guo, MOF derived Co_3O_4/N-doped carbon nanotubes hybrids as efficient catalysts for sensitive detection of H_2O_2 and glucose, Chin. Chem. Lett. 31 (2020) 774–778.

[155] S. Yao, S. Yuan, J. Xu, J. Luo, S. Hu, A hydrogen peroxide sensor based on colloidal MnO2/Na-montmorillonite, Appl. Clay Sci. 33 (2006) 35–42.

[156] E. Ortiz-Ortega, S. Hosseini, S.O. Martinez-Chapa, M.J. Madou, Aging of plasma-activated carbon surfaces: Challenges and opportunities, Appl. Surf. Sci. 565 (2021) 150362.

[157] S. Vizireanu, M.D. Ionita, R.E. Ionita, S.D. Stoica, C.M. Teodorescu, M.A. Husanu, N.G. Apostol, M. Baibarac, D. Panaitescu, G. Dinescu, Aging phenomena and wettability control of plasma deposited carbon nanowall layers, Plasma Process. Polym. 14 (2017) 1700023.

[158] J.H. Kim, J.-H. Jin, N.K. Min, Enhanced Stability and Amplified Signal Output of Single-Wall Carbon Nanotube-Based NH_3-Sensitive Electrode after Dual Plasma Treatment, Nanomaterials. 10 (2020) 1026.